CSI Drive Induction Motor by Vector Approximation

Kozo Ide

Department of Electrical Engineering
Faculty of Engineering
Kyushu Institute of Technology
Kitakyushu, Japan

January, 1996

Preface and Acknowledgements

"The field oriented control" was proposed about 25 years ago to realize simple ac drives control like dc ones, using moving frames of reference determined by the angular position of flux waves, and made it possible to transform the complex structure of ac machines to that of an equivalent separately excited dc machine. The method has been accepted widely because it has proved to be well adaptable to all types of power converters and ac machines, furthermore it has been developed with the microprocessors, which showed that most of complex control functions could be implemented by software in recent years. Nowadays since most of the signal processing is done in software, original field oriented control can be extended, improved, and modified.

This dissertation concerns with a microcomputer-controlled current source inverter (CSI) drive induction motor by vector approximation. "The vector approximation" in the title means shaping inverter output current wave so as to realize the desirable wave form using vectorial approximation, and this is different idea from the conventional pulse width modulation (PWM) method on the same purpose. Moreover, parameter adaptation and robust control for the induction motor drives are proposed in this dissertation. The author wishes that this dissertation would contribute to the further development of the precise torque and speed control technique for the induction motor drives.

This dissertation has grown out of this research for the doctoral degree of engnieering at the Kyushu Institute of Technology, Japan under Prof. Teruo Tsuji, in the Electrical Engineering Department since 1993.

I would like to express my sincere appreciation to Prof. Teruo Tsuji, who introduced me to the subject, and his serious attitude to research has always shown a correct direction to

orient myself to achieve my purpose.

Special thanks are due to Prof. Takuro Mochizuki, Prof. Gyoichi Nogami, and Prof. Toshihiro Kobayashi, who provided valuable comments and advices on this dissertation.

Several colleagues gave me the benefit of their helpful comments. Of these, I would like to mention: Kazuhiko Yonekura, Hideaki Iura, and Zhi Guo Bai, who have done research for their master degrees with me since 1990; Run De Qi, Tomohiro Hachino, Shang Hui Hao, Ryuichi Oguro, Zi Jiang Yang, and Prof. Yoshiaki Tanaka, who also provided many useful comments.

From November 1991 to November 1992 I had the honour of being Visiting Researcher supported by the Italian government at L'Aquila University, Italy, and I had good fortune to research with Prof. Enzo Chiricozzi, Prof. Francesco Parasiliti, Prof. Carlo Cecati, Dr. Marco Tursini, and Dr. Da Qing Zhang who gave me some fundamental idea concerning a part of this dissertation. I am also indebted to them.

Finally, I want to thank my parents Takeyuki and Eiko for their strong support over the years.

January 1996 Kozo Ide

Contents

Notations and Abbreviations

Notations

N_s	number of turns of a stator windings
k_{ws}	winding factor of a stator winding
$\Im_s$	resultant MMF distribution produced by stator [AT]
$\boldsymbol{\Phi}_s$	space vector of the stator flux linkages expressed in the stator or stationary reference frame [Wb]
$\boldsymbol{\Phi}_r$	space vector of the rotor flux linkages expressed in the rotor reference frame [Wb]
$\boldsymbol{\Phi}'_s$	space vector of the stator flux linkagesexpressed in the rotor reference frame [Wb]
$\boldsymbol{\Phi}'_r$	space vector of the rotor flux linkages expressed in the stator or stationary reference frame [Wb]
Φ_{ru}, Φ_{rv}, Φ_{rw}	instantaneous values of the rotor flux linkages in the rotor phases ru, rv, and rw respectively [Wb]
$\Phi_{s\alpha}$, $\Phi_{s\beta}$	instantaneous values of the direct- and quadrature-axis stator flux linkage components expressed in the stator or stationary reference frame [Wb]
$\Phi_{r\alpha}$, $\Phi_{r\beta}$	instantaneous values of the direct- and quadrature-axis rotor flux linkage components expressed in the rotor or stationary reference frame [Wb]
Φ_{rd}, Φ_{rq}	instantaneous values of the direct- and quadrature-axis rotor flux linkage components expressed in the stator or rotating reference frame [Wb]
Φ_{sd}, Φ_{sq}	instantaneous values of the direct- and quadrature-axis stator flux linkage components expressed in the rotor or rotating reference frame [Wb]

$\boldsymbol{\Phi}_{r\Phi r}$	rotor flux-linkage space vector in the field oriented reference frame [Wb]
$\boldsymbol{\Phi}_{s\Phi r}$	stator flux-linkage space vector in the field oriented reference frame [Wb]
Φ_r, $\lvert\boldsymbol{\Phi}_r\rvert$	magnitude of the rotor flux-linkage space vector [Wb]
u_{sU}, u_{sV}, u_{sW}	instantaneous values of the stator phase voltages respectively [V]
u_{ru}, u_{rv}, u_{rw}	instantaneous values of the rotor phase voltages respectively [V]
$\boldsymbol{u}_s$	space vector of the stator voltage expressed in the stator or stationary reference frame [V]
$\boldsymbol{u}_r$	space vector of the rotor voltage expressed in the rotor reference frame [V]
$\boldsymbol{u}'_s$	space vector of the stator voltage expressed in the rotor reference frame [V]
$\boldsymbol{u}'_r$	space vector of the rotor voltage expressed in the stator or stationary reference frame [V]
$u_{s\alpha}$, $u_{s\beta}$	instantaneous values of direct- and quadrature-axis rotor voltages respectively expressed in the stator or stationary reference frame [V]
$u_{r\alpha}$, $u_{r\beta}$	instantaneous values of direct- and quadrature-axis rotor voltages respectively expressed in the rotor or stationary reference frame [V]
u_{sd}, u_{sq}	instantaneous values of direct- and quadrature-axis rotor voltages respectively expressed in the rotor or rotating reference frame [V]
u_{rd}, u_{rq}	instantaneous values of direct- and quadrature-axis rotor voltages respectively expressed in the stator reference frame [V]

i_{sU}, i_{sV}, i_{sW}	instantaneous values of the stator phase currents respectively [A]
$\boldsymbol{i}_s$	space vector of the stator current expressed in the stator or stationary reference frame [A]
$\boldsymbol{i}_r$	space vector of the rotor current expressed in the rotor reference frame [A]
$\boldsymbol{i}'_s$	space vector of the stator current expressed in the rotor reference frame [A]
$\boldsymbol{i}'_r$	space vector of the rotor current expressed in the stator or stationary reference frame [A]
$\boldsymbol{i}_{mr}$	space vector of rotor magnetizing current [A]
$i_{s\alpha}$, $i_{s\beta}$	instantaneous values of direct- and quadrature-axis rotor currents respectively expressed in the stator or stationary reference frame [A]
$i_{r\alpha}$, $i_{r\beta}$	instantaneous values of direct- and quadrature-axis rotor currents respectively expressed in the rotor or stationary reference frame [A]
i_{sd}, i_{sq}	instantaneous values of direct- and quadrature-axis rotor currents respectively expressed in the rotor or rotating reference frame [A]
i_{rd}, i_{rq}	instantaneous values of direct- and quadrature-axis rotor currents respectively expressed in the stator reference frame [A]
$i_{mr\alpha}$, $i_{mr\beta}$	instantaneous values of direct- and quadrature-axis rotor magnetizing currents respectively expressed in the stationary reference frame [A]
i_{mr}, $\lvert\boldsymbol{i}_{mr}\rvert$	magnitude of the rotor magnetizing space vector [A]
$\boldsymbol{i}_{r\Phi r}$	rotor current space vector in the field oriented reference frame [A]
$\boldsymbol{i}_{s\Phi r}$	stator current space vector in the field oriented reference frame [A]

ω_{mr}	angular velocity of the field oriented reference frame [rad/s]
ω_i	stator angular velocity [rad/s]
ω_r	rotor angular velocity [rad/s]
ω_{sl}	slip angular velocity [rad/s]
θ	angle around the periphery with reference to the axis of stator windings sU [rad]
θ_r	rotor angle [rad]
α_μ	phase angle of the rotor flux linkage space phasor with respect to the direct-axis of the stationary reference frame [rad]
T_e	instantaneous value of the electromagnetic torque [N m]
T_L	load torque [N m]
V_{DC}	inverter input voltage [V]
E_d	output voltage of the converter [V]
I_{DC}	dc link current [A]
f_v	viscous friction
J	polar moment of ineretia [kgm^2]
P	number of pole-pairs
$\bar{L}_r$	self-inductance of a rotor winding [H]
$\bar{M}_r$	mutual inductance between two rotor phases [H]
L_r, L_{rl}	self- and leakage inductance of rotor respectively [H]
L_s, L_{sl}	self- and leakage inductance of stator respectively [H]
L_m	magnetizing inductance [H]
R_s	stator resistance [Ω]
R_r	rotor resistance [Ω]
σ	resultant leakage constant
σ_s	stator leakage constant
σ_r	rotor leakage constant
T_s, T_r	stator and rotor time constants respectively [s]
σT_s	stator and rotor transient time constants respectively [s]
γ	inverse rotor time constant [1/s]

k_t	torque coefficient
$Re,\ Im$	the real- and imaginary- component
$p,\ (\dot{})$	differential operator
$R^{n\times m}$	the set of $n \times m$ proper real-rational matrices
$\left[\begin{array}{c\|c} A & B \\ \hline C & D \end{array}\right]$	$= C(sI - A)^{-1}B + D$

Abbreviations

CSI	current source inverter
VSI	voltage source inverter
$MRAS$	model reference adaptive system
SAC	simplified adaptive control

Chapter 1

Introduction

In the past, dc machines have been used to stand for the high performance of variable speed drives and is still used for the same purpose, since their flux and torque could be controlled easily by the field and armature currents. In recent years ac machines, however, got to be popular on the variable speed drives by the development of power electronics, frequency transformation technology in virtue of semiconductor technology emerged. The advantages of ac machines against dc ones are as follows:

—— no brush and commutator, and then maintenance free,

and especially squirrel-cage induction motor is well-known as

—— small size, solidity, comparatively cheap, reliability

and these feature causes good circumstances for the motor installation.

Furthermore VVVF control (variable–voltage variable–frequency control) made it possible to control speed for the wide range of the induction motor with the good performances of response and also realized four-quadrant operation as well as dc motor drive systems.

The ac motor drives with VVVF control showed good features; however, the torque response at the transient has been inferior to that of dc motor drives because it could not control the instantaneous torque. This obstacle came into next focus.

The separately excited dc machine has a very simple control structure based on orthogonal axes, where the magnetic flux and torque are decoupled so that it is easy to design controlled

drives with high dynamic performance, field weakening, torque limit and so on. When many researchers attempted to transplant this simple control feature to ac machines, they met unexpected difficulties because their dynamic interactions are far more complex than those of dc motors.

Many control schemes have been proposed based on steady state models of the ac machines but it has taken a lot of time to realize the dynamic performance of the ac machines as well as the dc machines. About 25 years ago, Hasse and Blaschke showed how to decouple the current vector of the ac machines by vectorial control, that is, the new control methods based on the moving frames of reference determined by angular position of flux waves, hence this vectorial control is called "the field oriented control". Field oriented control techniques incorporating fast microprocessors have made possible the application of induction motor and synchronous motor drives to high performance drives instead of the dc drives. In the past, such control techniques would have not been possible because of the complexity of hardware and software required to solve the complexity control problem. The torque control in ac machines as well as dc ones is achieved by controlling the motor currents. In contrast to the dc machines, however, in the ac machines not only the phase angle but also the magnitude of the current has to be controlled, hence the field oriented control is also called "the vector control". With the field oriented control of the ac machines the torque– and flux–producing current components are decoupled, and the transient response characteristics are similar to those of the separately excited dc machines. The system would adapt to any load disturbances and reference value variations as fast as the dc machines. As next development, the field oriented control of various types of ac machines with rapid developments in the field of microelectronics can be applied to servo-drives.

For the ac drives there are much greater varieties than for dc ones, according to the different types of inverters (voltage source, current source, cycloconverter, and so on) which can be combined with various types of the ac machines.

In recent years, voltage source inverters (VSI) are more popular than current source inverters (CSI) for ac drives, perhaps because the VSI has faster current response to supply and can be applied to a PWM system in the high frequency region more easily. This is why the field oriented control (vector control) is often applied to control VSI-fed ac motor drive

systems [1]. The CSI, however, still has better features, such as capability of four-quadrant operation without any extra power circuit for regeneration, ruggedness and reliability, no shoot-through fault, and high precision of current control with the CSI is possible. Thus, the CSI seem to be appropriate for large capacity drive systems such as steel mills, elevator motors, and so on. However, the CSI-fed ac motor has problems in the low frequency region, where torque pulsation and harmonic heating occur because of a rectangular current wave with 120° conduction. In order to cope with these problems, a vector approximation method was proposed [2], which would not only decrease torque ripple but also control the instantaneous torque of an induction motor driven by the CSI even in transient state. Although the PWM−type CSI drive induction motor system has been proposed in [3][4] and the design of the PWM signal was considered to decrease the higher harmonic components of current waveforms, our method is different from the PWM methods. In this dissertation, a modified vector approximation method with dc link current control is shown. The vector approximation method approximates the desirable stator current vector by two of six realizable current vectors which are adjacent to the desirable one. The magnitude of the desirable current is adjusted by the control of the dc link current for each instant. Thus, the modified vector approximation method can produce any current vector so that a sinusoidal phase current is realizable, if necessary. On the other hand, the phase angle of the desirable stator current is determined by utilizing the rotor flux angle, which is computed by the on-line simulation. If the rotor flux angle is estimated correctly, the so-called magnetizing current and torque producing current can be decoupled precisely and so controlled independently by the field oriented control [5]. However, the field oriented control is influenced by the rotor parameter variation, that is, the rotor resistance varies with temperature and the inductance is a function of main flux saturation. To solve this problem, many identification or adaptation schemes have already been proposed [6]~[13]. An off-line automated identification scheme [6] and an adaptation scheme with using the reactive power transferred to the rotor [7] have been evaluated as effective methods. With different approaches, model reference adaptive systems (MRAS) [8], [9] have been presented. The adaptive system estimates the error between the motor outputs and that of reference model, and tunes the adaptive gains or parameters to decrease the error to zero. As a result, the degradation of torque control by the rotor resistance variation is observed in [8] and [9]. On the other hand, the selection of flux level with regard to magnetic saturation effects was discussed in [10]. Saturated dynamic

models of the induction motor with the vector control have been proposed in [11]~[13].

The purpose of this dissertation is to realize the ideal vector approximation system for the CSI drive induction motor; therefore, both resistance and inductance variation problems also have to be solved.

The remainder of this dissertation is organized as follows:

- In Chapter **2**, the dynamic model of the induction machine using space vectors are reviewed and the mathematical model of the induction machine is shown. The foundation of every control design is explained by the mathematical model of the plant.
- Chapter **3** shows the principle of the field oriented control. The field oriented control requires the information of the magnitude values and the phase angle of the rotor flux space vector, and then the rotor flux estimation is needed because the direct measurement of the rotor flux is undesirable due to the high cost and the complex hardware setting. Four kinds of the flux estimation models are shown in this chapter, and the comparison of these models are discussed in the last section.
- Chapter **4** shows the vector approximation method. The principle and the algorithm of the vector approximation are described. The system configuration for the implement is shown. The performance of the vector approximation is verified by the simulation and the experiments.
- Chapter **5** shows the parameter adaptation and the torque control technique. In order to adapt both resistance and inductance variation, the vector approximation system newly includes a magnetic saturation model which is obtained by a novel off-line identification method. Thus, on-line compensation of magnetizing inductance variation becomes possible. This system also includes MRAS using the model reference error of torque to compensate rotor resistance variation. Consequently, this method makes it possible to asymptotically track the actual torque and estimate the accurate rotor resistance without the influence of inductance variation, which occurs at the field weakening or the optimal efficiency control. The effectiveness of the parameter adaptation system is verified by the simulation and the experiments.

- Chapter 6 shows the applications of robust control. Conventional linear control methods such as PI control have been widely used in industry electrical drives; however, dynamic performance of the control system is often limited due to the conflict between overshoot and long setting time of the system response. The conventional linear control methods have inadequate rejections against external disturbance as well as the sensitivity in performance to the system parameter variation and nonlinearity. Thus, robust stable drive systems are required for any applications. This chapter concerns with the applications of robust control, an H_∞ control and a simplified adaptive control. In order to design the robust speed control system, first, the nonlinear dynamical model of the rotor angular velocity and the dc link current is linearized by exact linearization. Then the linearized system is applied to design the H_∞ controller and the simplified adaptive controller, respectively. The robustness of these systems compared with PI control system based on the conventional control theory are verified by the simulation and the experiments.

- Finally, Chapter 7 provides conclusions.

Chapter 2

Dynamic machine model using space vectors

2.1 Introduction

The foundation of every control design is explained by the mathematical model of the plant. In order to understand and design field oriented controlled drives, it is necessary to know the dynamic machine model to be controlled. The control designs are approximated roughly, since every schemes cannot help containing the machine parameters which change due to the changes in the temperature, supply, non-linearity and so on. The error may be considered as acceptable within even a ten percent. In order to design the control system, however, an adequate model of the electrical machine must preferably incorporate all the important dynamic effects during steady state and transient operation, and also should be useful for any instantaneous variation of voltage and current generated by converter which supplies the machine.

Space vector theory can realize such a model and it is related to the two-axis theory of electrical machines.

This chapter, introduces the dynamic model of smooth air gap induction machines which are delivered at several references described in the references section of this dissertation. Here space vector quantities (voltages, currents, MMFs, flux densities, flux linkages, etc.) will be introduced on the mathematical and physical considerations.

2.2 Space vector of the stator MMFs and stator currents

Assume a smooth air gap symmetrical ac machine with two-pole, three phase windings. Fig. 2.1 shows the cross section of a symmetrical three phase ac machine. Here it is assumed that the effects of slotting have been neglected, the permeability of the iron parts is infinite and the flux density is radial in the air-gap, and the effects of iron losses and end- effects are also neglected. In Fig. 2.1 the stator and rotor windings are shown as single, multiple-turn full pitch coils situated on the two sides of the air-gap; these, however, represent distributed windings, which at every instant produce sinusoidal MMF waves centered on the magnetic axes of the respective phases. The phase windings are displaced by 120 electrical degrees from each other. In Fig. 2.1 θ_r is the rotor angle, the angle between the magnetic axes of stator winding sU and rotor winding ru. In general, the electrical instantaneous angular velocity of the rotor is $\omega_r = d\theta_r/dt$, and its positive direction is also shown in Fig. 2.1.

Assume that the stator windings have an equal number of effective turns $N_{se}(= N_s k_{ws})$, where N_s and k_{ws} are the number of turns and the winding factor respectively of a stator winding.

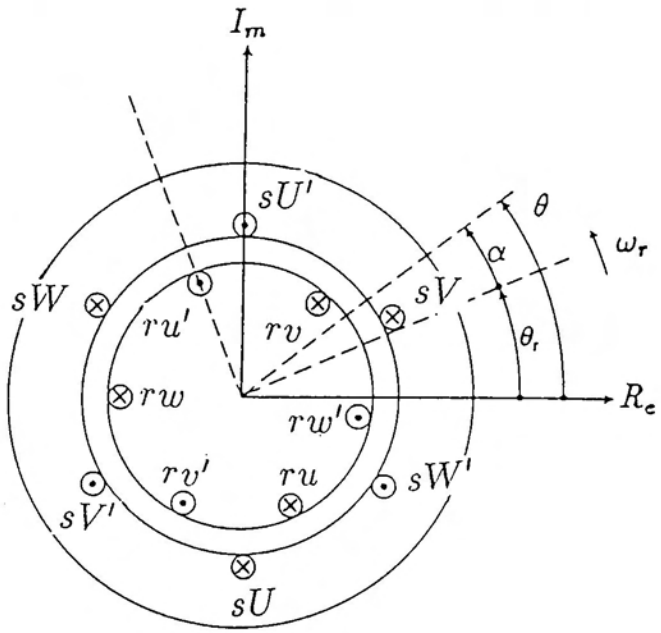

Fig. 2.1. Cross section of a symmetrical three phase ac machine.

The resultant MMF distribution produced by stator is described as follows:

$$\Im_s(\theta,t) = N_{se}\left[i_{sU}(t)\cos\theta + i_{sV}(t)\cos(\theta - 2\pi/3) + i_{sW}(t)\cos(\theta - 4\pi/3)\right] \tag{2.1}$$

where θ is the angle around the periphery with reference to the axis of stator windings sU, which coincides with real axis of the stator denoted as Re, and i_{sU}, i_{sV}, and i_{sW} are three phase currents. The complex notation of (2.1) shows as follows:

$$\Im_s(\theta,t) = \frac{3}{2}N_{se}Re\left\{\frac{2}{3}\left[i_{sU}(t) + ai_{sV}(t) + a^2 i_{sW}(t)\right]e^{-j\theta}\right\} \tag{2.2}$$

By using complex expressions, a time dependent complex current vector in the stationary reference frame fixed to the stator is defined as

$$\boldsymbol{i}_s(t) = \frac{2}{3}\left[i_{sU}(t) + ai_{sV}(t) + a^2 i_{sW}(t)\right] = |\boldsymbol{i}_s|e^{j\alpha_s} \tag{2.3}$$

where $a = e^{j2\pi/3}$, $|\boldsymbol{i}_s|$ is the magnitude of the stator current space vector and α_s is the phase angle with respect to the real axis of the stationary reference frame fixed to the stator. Thus the space vector of the stator MMFs is defined as follows:

$$\mathfrak{S}_s(t) = N_{se}\boldsymbol{i}_s(t) = \mathfrak{S}_{sU}(t) + \mathfrak{S}_{sV}(t) + \mathfrak{S}_{sW}(t) \tag{2.4}$$

where $\mathfrak{S}_{sU}(t), \mathfrak{S}_{sV}(t)$, and $\mathfrak{S}_{sW}(t)$ are the space vectors of the individual phase MMFs.

Next the space vectors by utilizing two-axis theory is introduced here and this method was followed by Park. The space vector of the stator currents can be defined that it has two vector components of which are the instantaneous value of the direct-axis stator current ($i_{s\alpha}$) and the quadrature- axis stator current ($i_{s\beta}$). Thus, the stator current space vector in the stationary reference frame fixed to the stator can be expressed as

$$\boldsymbol{i}_s(t) = i_{s\alpha}(t) + ji_{s\beta}(t). \tag{2.5}$$

In symmetrical three phase machines, the direct- and quadrature- axis stator currents ($i_{s\alpha}$, $i_{s\beta}$) are fictitious and quadrature-two-phase current components. The relationships between these components and actual three-phase stator currents are shown as follows:

$$\begin{bmatrix} i_{s\alpha} \\ i_{s\beta} \end{bmatrix} = c\begin{bmatrix} 1 & -1/2 & -1/2 \\ 0 & \sqrt{3}/2 & -\sqrt{3}/2 \end{bmatrix}\begin{bmatrix} i_{sU} \\ i_{sV} \\ i_{sW} \end{bmatrix} \tag{2.6}$$

where c is a constant, 2/3 or $\sqrt{2/3}$. The non-power invariant form of the phase transformation from three- to two- (quadrature) phase components utilizes $c = 2/3$ while the power invariant form utilizes $c = \sqrt{2/3}$. It depends on the definition of the space vector of the stator current.

If the non-power invariant form is utilized, the real- and imaginary- component yields as follows:

$$Re(\boldsymbol{i}_s) = Re\left[\frac{2}{3}\left(i_{sU} + a i_{sV} + a^2 i_{sW}\right)\right] = \frac{2}{3}\left(i_{sU} - \frac{1}{2}i_{sV} - \frac{1}{2}i_{sW}\right) = i_{s\alpha} \qquad (2.7)$$

$$Im(\boldsymbol{i}_s) = Im\left[\frac{2}{3}\left(i_{sU} + a i_{sV} + a^2 i_{sW}\right)\right] = \left(i_{sV} - i_{sW}\right)/\sqrt{3} = i_{s\beta} \qquad (2.8)$$

If the non-power-invariant form of the transformations is used, it may be a useful consequence that if there are no zero-sequence components, the projections of a space vector quantity on the corresponding phase axes directly yield the instantaneous values phase variables of the same quantity. This is shown in Fig. 2.2 for the case of the space vector of the stator currents.

From the mathematical point of view, this means that, by utilizing

$$i_{sU} + i_{sV} + i_{sW} = 0 \ , \qquad (2.9)$$

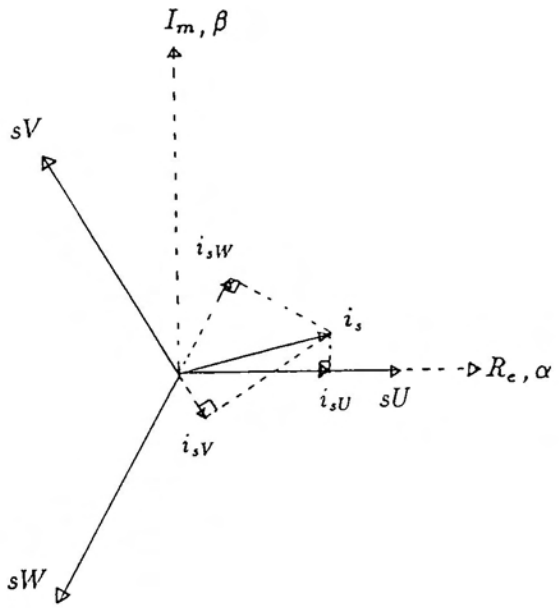

Fig. 2.2. Projections of the stator current space vector.

and by using the non-power invariant forms of the zero-sequence current component and the space vector of the stator currents, the following equations are obtained:

$$Re(\boldsymbol{i}_s) = \frac{2}{3}\left(i_{sU} - \frac{1}{2}i_{sV} - \frac{1}{2}i_{sW}\right) = i_{sU} \tag{2.10}$$

$$Re(a^2\boldsymbol{i}_s) = Re\left[\frac{2}{3}\left(a^2 i_{sU} + i_{sV} + a i_{sW}\right)\right] = i_{sV} \tag{2.11}$$

$$Re(a\boldsymbol{i}_s) = Re\left[\frac{2}{3}\left(a i_{sU} + a^2 i_{sV} + i_{sW}\right)\right] = i_{sW} \tag{2.12}$$

2.3 Rotor flux-linkage space vector in the rotating reference frame fixed to the rotor

The space vector of the rotor flux linkages expressed in its own reference frame, that is, in the reference frame fixed to the rotor, and rotating at the angular velocity ω_r, is defined as follows:

$$\boldsymbol{\Phi}_r = \frac{2}{3}\left[\Phi_{ru}(t) + \Phi_{rv}(t) + \Phi_{rw}(t)\right] \tag{2.13}$$

where $\Phi_{ru}(t), \Phi_{rv}(t)$, and $\Phi_{rw}(t)$ are instantaneous values of the rotor flux linkages in the rotor phases ru, rv, and rw respectively. In terms of the instantaneous values of the stator and rotor currents they can be expressed as follows:

$$\begin{aligned}\Phi_{ru} = {} & \bar{L}_r i_{ru} + \bar{M}_r i_{rv} + \bar{M}_r i_{rw} \\ & + \bar{M}_{sr}\cos\theta_r i_{sU} + \bar{M}_{sr}\cos(\theta_r + 4\pi/3) i_{sV} + \bar{M}_{sr}\cos(\theta_r + 2\pi/3) i_{sW} \qquad (2.14)\\ \Phi_{rv} = {} & \bar{L}_r i_{rv} + \bar{M}_r i_{ru} + \bar{M}_r i_{rw} \\ & + \bar{M}_{sr}\cos(\theta_r + 2\pi/3) i_{sU} + \bar{M}_{sr}\cos\theta_r i_{sV} + \bar{M}_{sr}\cos(\theta_r + 4\pi/3) i_{sW} \qquad (2.15)\\ \Phi_{rw} = {} & \bar{L}_r i_{rw} + \bar{M}_r i_{ru} + \bar{M}_r i_{rv} \\ & + \bar{M}_{sr}\cos(\theta_r + 4\pi/3) i_{sU} + \bar{M}_{sr}\cos(\theta_r + 2\pi/3) i_{sV} + \bar{M}_{sr}\cos\theta_r i_{sW} \qquad (2.16)\end{aligned}$$

where $\bar{L}_r$ is the self-inductance of a rotor winding, $\bar{M}_r$ is the mutual inductance between two rotor phases. It can be seen that all three rotor flux-linkage components contain three flux-linkage components produced by the rotor currents and three mutual flux-linkage components produced by the stator currents. For simplification, (2.14), (2.15), and (2.16) are substituted

into (2.13) and thus the space vector of rotor flux linkages in the rotor reference frame is obtained as

$$\boldsymbol{\Phi}_r = L_r \boldsymbol{i}_r + L_m \boldsymbol{i}'_s \tag{2.17}$$

where $L_r (= \bar{L}_r - \bar{M}_r)$ is the total three-phase rotor inductance and $\boldsymbol{i}'_s$ is the space vector of the stator currents expressed in the reference frame fixed to the rotor. In (2.17), $(L_r \boldsymbol{i}_r)$ is the rotor self-flux linkage space vector expressed in the rotor reference frame and is occurred due to the rotor currents and $(L_m \boldsymbol{i}'_s)$ is a mutual flux- linkage space vector, produced by the stator currents and expressed in the same reference frame.

Here it is also possible to define the rotor flux-linkage space vector in terms of its two-axis components as follows:

$$\boldsymbol{\Phi}_r = \Phi_{r\alpha} + j\Phi_{r\beta} \tag{2.18}$$

From (2.17), the direct- and the quadrature-axis rotor flux- linkage components can be defined respectively as follows:

$$\Phi_{r\alpha} = L_r i_{r\alpha} + L_m i_{sd} \tag{2.19}$$

$$\Phi_{r\beta} = L_r i_{r\beta} + L_m i_{sq} \tag{2.20}$$

In (2.19) and (2.20), $i_{r\alpha}$, $i_{r\beta}$, i_{sd} and i_{sq} are direct- and quadrature-axis rotor and stator current components respectively, and all the current components are expressed in the reference frame fixed to the rotor. The relationship of the stator current components (i_{sd}, i_{sq}) and stator current components ($i_{s\alpha}$, $i_{s\beta}$) will be shown in the next section.

2.4 Rotor flux-linkage space vector in the stationary reference frame

The rotor flux-linkage components in the reference frame fixed to the rotor ($\Phi_{r\alpha}$, $\Phi_{r\beta}$) are related to the rotor flux-linkage components expressed in the stationary reference frame (Φ_{rd}, Φ_{rq}) by the transformation ($e^{j\theta_r}$). Thus the following equation holds:

$$\boldsymbol{\Phi}'_r = \Phi_{rd} + j\Phi_{rq} = \boldsymbol{\Phi}_r e^{j\theta_r} = (\Phi_{r\alpha} + j\Phi_{r\beta})\, e^{j\theta_r} \tag{2.21}$$

and this can be reformed as follows:

$$\begin{bmatrix} \Phi_{rd} \\ \Phi_{rq} \end{bmatrix} = \begin{bmatrix} \cos\theta_r & -\sin\theta_r \\ \sin\theta_r & \cos\theta_r \end{bmatrix} \begin{bmatrix} \Phi_{r\alpha} \\ \Phi_{r\beta} \end{bmatrix} \tag{2.22}$$

By the substitution of (2.17) into (2.21), the space vector of the rotor flux linkages in the stationary reference frame can be expressed as

$$\boldsymbol{\Phi}'_r = \left(L_r \boldsymbol{i}'_r + L_m \boldsymbol{i}'_s e^{j\theta_r}\right) = L_r \boldsymbol{i}'_r + L_m \boldsymbol{i}_s. \tag{2.23}$$

This contains two flux-linkage components, a self flux linkage produced by the rotor currents but expressed in the stationary reference frame ($L_r \boldsymbol{i}'_r$) and a mutual flux-linkage component produced by the stator currents and also expressed in the stationary reference frame ($L_m \boldsymbol{i}_s = L_m \boldsymbol{i}'_s e^{j\theta_r}$). Thus the stator currents in the stationary reference frame are related to the stator current components in the rotating reference frame fixed to the rotor by the following complex transformation

$$\boldsymbol{i}_s = \boldsymbol{i}'_s e^{j\theta_r} \tag{2.24}$$

where $\boldsymbol{i}_s$ and $\boldsymbol{i}'_s$ are expressed in terms of their two-axis components as follows:

$$\begin{aligned} \boldsymbol{i}_s &= i_{s\alpha} + j i_{s\beta} \\ \boldsymbol{i}'_s &= i_{sd} + j i_{sq} \end{aligned} \tag{2.25}$$

It follows from (2.24) that the transformed stator current space vector in the rotating reference frame fixed to the rotor can be obtained from the space vector of the stator currents, expressed in the stationary reference frame, as

$$\boldsymbol{i}'_s = \boldsymbol{i}_s e^{-j\theta_r}. \tag{2.26}$$

The corresponding two-axis form can be obtained by the substitution of (2.25) into (2.26),

$$\begin{bmatrix} i_{sd} \\ i_{sq} \end{bmatrix} = \begin{bmatrix} \cos\theta_r & \sin\theta_r \\ -\sin\theta_r & \cos\theta_r \end{bmatrix} \begin{bmatrix} i_{s\alpha} \\ i_{s\beta} \end{bmatrix} \tag{2.27}$$

and these are the stator currents used in (2.19) and (2.20). The transformation described by (2.26) can also be obtained by considering Fig. 2.3.

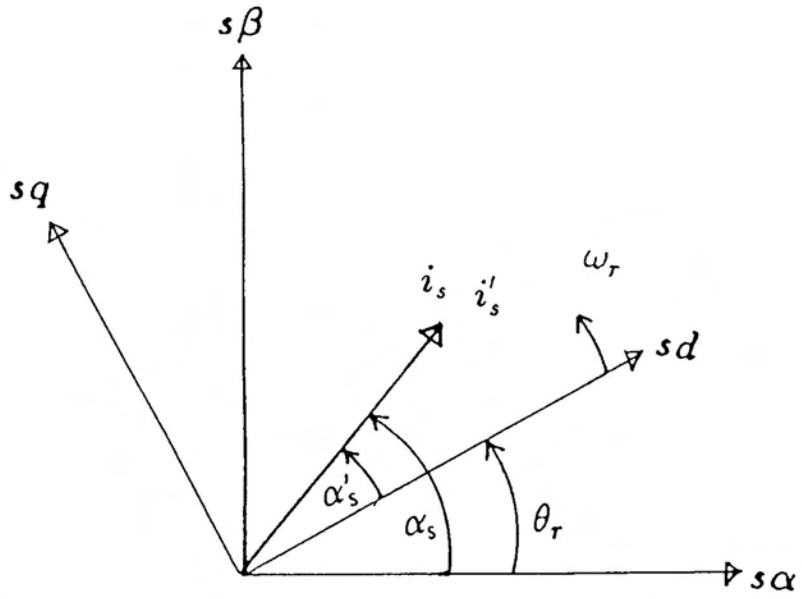

Fig. 2.3. Transformation of the stator current space vector.

2.5 Space vectors of the stator and rotor voltages

The space vector of the stator voltage can be defined in the stationary reference frame as follows:

$$\boldsymbol{u}_s = \frac{2}{3}\left[u_{sU}(t) + a u_{sV}(t) + a^2 u_{sW}(t)\right] = u_{s\alpha} + j u_{s\beta} \tag{2.28}$$

and the space vector of the rotor voltage in the reference frame fixed to the moving rotor is

$$\boldsymbol{u}_r = \frac{2}{3}\left[u_{ru}(t) + a u_{rv}(t) + a^2 u_{rw}(t)\right] = u_{r\alpha} + j u_{r\beta}. \tag{2.29}$$

In (2.28) and (2.29), $u_{sU}(t)$, $u_{sV}(t)$, $u_{sW}(t)$, $u_{ru}(t)$, $u_{rv}(t)$, and $u_{rw}(t)$ are the instantaneous values of the stator and rotor phase voltages respectively and $u_{s\alpha}$, $u_{s\beta}$, $u_{r\alpha}$, $u_{r\beta}$ are the corresponding direct- and quadrature-axis components. The relationship between the three-phase and quadrature-phase voltages are

$$\begin{aligned} u_{s\alpha} &= Re\left\{\frac{2}{3}\left[u_{sU}(t) + a u_{sV}(t) + a^2 u_{sW}(t)\right]\right\} \\ &= \frac{2}{3}\left(u_{sU} - \frac{1}{2}u_{sV} - \frac{1}{2}u_{sW}\right) \end{aligned} \tag{2.30}$$

$$\begin{aligned} u_{s\beta} &= Im\left\{\frac{2}{3}\left[u_{sU}(t) + a u_{sV}(t) + a^2 u_{sW}(t)\right]\right\} \\ &= \left(u_{sV} - u_{sW}\right)/\sqrt{3}. \end{aligned} \tag{2.31}$$

Similarly, the rotor voltage components are

$$u_{r\alpha} = \frac{2}{3}\left(u_{ru} - \frac{1}{2}u_{rv} - \frac{1}{2}u_{rw}\right) \tag{2.32}$$

$$u_{r\beta} = \left(u_{rv} - u_{rw}\right)/\sqrt{3}. \tag{2.33}$$

Eqs. (2.30) and (2.31) are expressed by a matrix form as follows:

$$\begin{bmatrix} u_{s\alpha} \\ u_{s\beta} \end{bmatrix} = \frac{2}{3}\begin{bmatrix} 1 & -1/2 & -1/2 \\ 0 & \sqrt{3}/2 & -\sqrt{3}/2 \end{bmatrix}\begin{bmatrix} u_{sU} \\ u_{sV} \\ u_{sW} \end{bmatrix} \tag{2.34}$$

A similar transformation can apply for the rotor voltages. The projections of the space vector of voltages on the corresponding axes yield the phase voltages,

$$u_{sU} = Re(\boldsymbol{u}_s) \tag{2.35}$$

$$u_{sV} = Re(a^2\boldsymbol{u}_s) \tag{2.36}$$

$$u_{sW} = Re(a\boldsymbol{u}_s). \tag{2.37}$$

The stator voltage space vector expressed in the stationary reference frame ($\boldsymbol{u}_s$) can be transformed into the stator space vector expressed in the reference frame fixed to the rotor ($\boldsymbol{u}'_s$),

$$\boldsymbol{u}'_s = \boldsymbol{u}_s e^{-j\theta_r} = u_{sd} + j u_{sq}. \tag{2.38}$$

If this is resolved into real- and imaginary-axis components, the same transformation matrix will appear as in (2.27).

The rotor voltage space vector expressed in the reference frame fixed to the rotor ($\boldsymbol{u}_r$) can be expressed in the reference frame fixed to the stator ($\boldsymbol{u}'_r$),

$$\boldsymbol{u}'_r = \boldsymbol{u}_r e^{j\theta_r} = u_{rd} + j u_{rq}\ , \tag{2.39}$$

and this is equivalent to the matrix:

$$\begin{bmatrix} u_{rd} \\ u_{rq} \end{bmatrix} = \begin{bmatrix} \cos\theta_r & -\sin\theta_r \\ \sin\theta_r & \cos\theta_r \end{bmatrix}\begin{bmatrix} u_{r\alpha} \\ u_{r\beta} \end{bmatrix} \tag{2.40}$$

If the relationship between u_{sU}, u_{sV}, u_{sW} and u_{sd}, u_{sq} is required, it follows from (2.38) and (2.28) that

$$u_{sd} + ju_{sq} = \frac{2}{3}\left[u_{sU}(t) + au_{sV}(t) + a^2u_{sW}(t)\right](\cos\theta_r - j\sin\theta_r). \tag{2.41}$$

This is equivalent to the matrix:

$$\begin{bmatrix} u_{sd} \\ u_{sq} \end{bmatrix} = \frac{2}{3}\begin{bmatrix} \cos\theta_r & \cos(\theta_r - 2\pi/3) & \cos(\theta_r - 4\pi/3) \\ -\sin\theta_r & -\sin(\theta_r - 2\pi/3) & -\sin(\theta_r - 4\pi/3) \end{bmatrix}\begin{bmatrix} u_{sU} \\ u_{sV} \\ u_{sW} \end{bmatrix} \tag{2.42}$$

which define the so-called Park transformation.

2.6 Space vector voltage equations in the stationary reference frame

In the present section, the space vector forms of the voltage equations is presented. The equations is expressed in the stationary reference frames. The relationship between the space vector and matrix forms will be shown. The stator and rotor voltage equations of the space vector form are expressed as follows:

$$\boldsymbol{u}_s = R_s\boldsymbol{i}_s + \frac{d\boldsymbol{\Phi}_s}{dt} \tag{2.43}$$

$$\boldsymbol{u}'_r = R_r\boldsymbol{i}'_r + \frac{d\boldsymbol{\Phi}'_r}{dt} - j\omega_r\boldsymbol{\Phi}'_r \tag{2.44}$$

where $\boldsymbol{\Phi}_s$ is the space vector of the stator flux linkages in the stationary reference frame fixed to the stator. In (2.43) and (2.44), the first term on the right-hand side of these equations is the space vector form of the ohmic losses, the second term is a transformer EMF, which is the first derivative of the flux-linkage space vector of the stator and rotor respectively. The term $(-j\omega_r\boldsymbol{\Phi}'_r)$ represents a rotational EMF, which is due to the rotation of the rotor and contributes to electromechanical energy conversion.

Now the definition of all the space vector quantities are repeated below using the definitions of the space vectors of the three-phase quantities. The space vectors of the stator voltages, currents and flux linkages in the stationary reference frame fixed to the stator are

expressed as follows:

$$\boldsymbol{u}_s = \frac{2}{3}\left[u_{sU}(t) + a u_{sV}(t) + a^2 u_{sW}(t)\right] = u_{s\alpha} + j u_{s\beta} \tag{2.45}$$

$$\boldsymbol{i}_s = \frac{2}{3}\left[i_{sU}(t) + a i_{sV}(t) + a^2 i_{sW}(t)\right] = i_{s\alpha} + j i_{s\beta} \tag{2.46}$$

$$\boldsymbol{\Phi}_s = \frac{2}{3}\left[\Phi_{sU}(t) + a\Phi_{sV}(t) + a^2\Phi_{sW}(t)\right] = \Phi_{s\alpha} + j\Phi_{s\beta} = L_s \boldsymbol{i}_s + L_m \boldsymbol{i}'_r \tag{2.47}$$

and similarly the space vectors of the rotor voltages, current, and flux linkages in the reference frame fixed to the rotor are expressed as follows:

$$\boldsymbol{u}_r = \frac{2}{3}\left[u_{ru}(t) + a u_{rv}(t) + a^2 u_{rw}(t)\right] = u_{r\alpha} + j u_{r\beta} \tag{2.48}$$

$$\boldsymbol{i}_r = \frac{2}{3}\left[i_{ru}(t) + a i_{rv}(t) + a^2 i_{rw}(t)\right] = i_{r\alpha} + j i_{r\beta} \tag{2.49}$$

$$\begin{aligned} \boldsymbol{\Phi}_r &= \frac{2}{3}\left[\Phi_{ru}(t) + a\Phi_{rv}(t) + a^2\Phi_{rw}(t)\right] = L_r \boldsymbol{i}_r + L_m \boldsymbol{i}'_s \\ &= L_r \boldsymbol{i}_r + L_m \boldsymbol{i}_s e^{j\theta_r} = \Phi_{r\alpha} + j\Phi_{r\beta} \end{aligned} \tag{2.50}$$

The rotor quantities defined above are, in the reference frame fixed to the stator,

$$\boldsymbol{u}'_r = \boldsymbol{u}_r e^{j\theta_r} = u_{rd} + j u_{rq} \tag{2.51}$$

$$\boldsymbol{i}'_r = \boldsymbol{i}_r e^{j\theta_r} = i_{rd} + j i_{rq} \tag{2.52}$$

$$\begin{aligned} \boldsymbol{\Phi}'_r &= \boldsymbol{\Phi}_r e^{j\theta_r} = L_r \boldsymbol{i}'_r + L_m \boldsymbol{i}_s \\ &= L_r \boldsymbol{i}_r e^{j\theta_r} + L_m \boldsymbol{i}_s = \Phi_{rd} + j\Phi_{rq}, \end{aligned} \tag{2.53}$$

and also the space vectors of the stator voltages, currents and flux linkages are given in the rotating reference frame fixed to the rotor as

$$\boldsymbol{u}'_s = \boldsymbol{u}_s e^{-j\theta_r} = u_{sd} + j u_{sq} \tag{2.54}$$

$$\boldsymbol{i}'_s = \boldsymbol{i}_s e^{-j\theta_r} = i_{sd} + j i_{sq} \tag{2.55}$$

$$\boldsymbol{\Phi}'_s = \boldsymbol{\Phi}_s e^{-j\theta_r} = \Phi_{sd} + j\Phi_{sq}. \tag{2.56}$$

Eqs. (2.43) and (2.44) with the flux linkage equations, (2.47), (2.50) and (2.53) are also valid under saturated conditions.

If the flux-linkage space vectors defined by (2.47) and (2.53) are substituted into (2.43) and (2.44), then the space vector voltage equations become as follows:

$$\boldsymbol{u}_s = R_s \boldsymbol{i}_s + \frac{d L_s \boldsymbol{i}_s}{dt} + \frac{d L_m \boldsymbol{i}'_r}{dt} \tag{2.57}$$

$$\boldsymbol{u}'_r = R_r \boldsymbol{i}'_r + \frac{d L_r \boldsymbol{i}'_r}{dt} + \frac{d L_m \boldsymbol{i}_s}{dt} - j\omega_r (L_r \boldsymbol{i}'_r + L_m \boldsymbol{i}_s) \tag{2.58}$$

These equations can also be rewritten by the matrix form:

$$\begin{bmatrix} \boldsymbol{u}_s \\ \boldsymbol{u}'_r \end{bmatrix} = \begin{bmatrix} R_s & 0 \\ 0 & R_r \end{bmatrix} \begin{bmatrix} \boldsymbol{i}_s \\ \boldsymbol{i}'_r \end{bmatrix} + \frac{d}{dt} \begin{bmatrix} L_s & L_m \\ L_m & L_r \end{bmatrix} \begin{bmatrix} \boldsymbol{i}_s \\ \boldsymbol{i}'_r \end{bmatrix} - j\omega_r \begin{bmatrix} 0 & 0 \\ L_m & L_r \end{bmatrix} \begin{bmatrix} \boldsymbol{i}_s \\ \boldsymbol{i}'_r \end{bmatrix} \tag{2.59}$$

If these space vectors are resolve into their real- and imaginary- axis component in accordance with (2.45), (2.46), (2.51) and (2.52), then (2.59) becomes as follows:

$$\begin{bmatrix} u_{s\alpha} \\ u_{s\beta} \\ u_{rd} \\ u_{rq} \end{bmatrix} = \begin{bmatrix} R_s + pL_s & 0 & pL_m & 0 \\ 0 & R_s + pL_s & 0 & pL_m \\ pL_m & \omega_r L_m & R_r + pL_r & \omega_r L_r \\ -\omega_r L_m & pL_m & -\omega_r L_r & R_r + pL_r \end{bmatrix} \begin{bmatrix} i_{s\alpha} \\ i_{s\beta} \\ i_{rd} \\ i_{rq} \end{bmatrix} \tag{2.60}$$

This form is so-called the quadrature-phase commutator model. The ability to obtain various models of a machine, in various reference frames, without using matrix transformations, is an advantage of the application of space vectors over the application of the conventional generalized matrix theory of electrical machines.

Furthermore, from (2.51) and (2.52), $\boldsymbol{u}_r = \boldsymbol{u}'_r e^{-j\theta_r}$ and $\boldsymbol{i}_r = \boldsymbol{i}'_r e^{-j\theta_r}$, and the rotor quantities can be expressed in the reference frame fixed to rotor and (2.59) becomes

$$\begin{bmatrix} \boldsymbol{u}_s \\ \boldsymbol{u}_r \end{bmatrix} = \begin{bmatrix} R_s & 0 \\ 0 & R_r \end{bmatrix} \begin{bmatrix} \boldsymbol{i}_s \\ \boldsymbol{i}_r \end{bmatrix} + \frac{d}{dt} \begin{bmatrix} L_s & L_m e^{j\theta_r} \\ L_m e^{-j\theta_r} & L_r \end{bmatrix} \begin{bmatrix} \boldsymbol{i}_s \\ \boldsymbol{i}_r \end{bmatrix}. \tag{2.61}$$

If all the space vector quantities are expressed in terms of their real- and imaginary-axis components, from (2.45), (2.46), (2.48) and (2.49), (2.61) yields

$$\begin{bmatrix} u_{s\alpha} \\ u_{s\beta} \\ u_{r\alpha} \\ u_{r\beta} \end{bmatrix} = \begin{bmatrix} R_s + pL_s & 0 & pL_m \cos\theta_r & -pL_m \sin\theta_r \\ 0 & R_s + pL_s & pL_m \sin\theta_r & pL_m \cos\theta_r \\ pL_m \cos\theta_r & pL_m \sin\theta_r & R_r + pL_r & 0 \\ -pL_m \sin\theta_r & pL_m \cos\theta_r & 0 & R_r + pL_r \end{bmatrix} \begin{bmatrix} i_{s\alpha} \\ i_{s\beta} \\ i_{r\alpha} \\ i_{r\beta} \end{bmatrix}. \tag{2.62}$$

This form is so-called the quadrature-phase slip-ring model. For slip-ring induction machines with short-circuited rotor windings, or induction machines with squirrel cage rotor, $\boldsymbol{u}_r = 0$.

2.7 Electromagnetic torque in the reference frame fixed to the rotor flux-linkage space vector

This section discusses the expression of electromagnetic torque in the reference frame fixed to the rotor flux-linkage space vector, which is important if the rotor flux estimation

for the field oriented control is used. The expression of the electromagnetic torque is similar to the expression for the electromagnetic torque produced by a separately excited dc machine. The analogy serves as a basis for various forms of the field oriented control, where the torque control of the ac machine is similar to the torque control of the separately excited dc machine.

If the rotating reference frame is used, where the quadrature-axis component of the rotor flux-linkage space vector is zero, the electromagnetic torque will be produced by the interaction of the rotor flux-linkage in the direct and the quadrature-axis component of the stator currents in the reference frame.

The rotor flux-linkage space vector in the stationary reference frame (α-β) can be expressed as

$$\boldsymbol{\Phi}_r' = \boldsymbol{\Phi}_r e^{j\theta_r} = \Phi_{r\alpha} + j\Phi_{r\beta} = |\boldsymbol{\Phi}_r| e^{j\alpha_\mu} \tag{2.63}$$

where $|\boldsymbol{\Phi}_r|$ and α_μ are the magnitude and phase angle of the rotor flux-linkage space vector in the stationary reference frame. Fig. 2.4 shows the relationship between the stator current components in the stationary reference frame and the reference frame fixed to $\boldsymbol{\Phi}_r$.

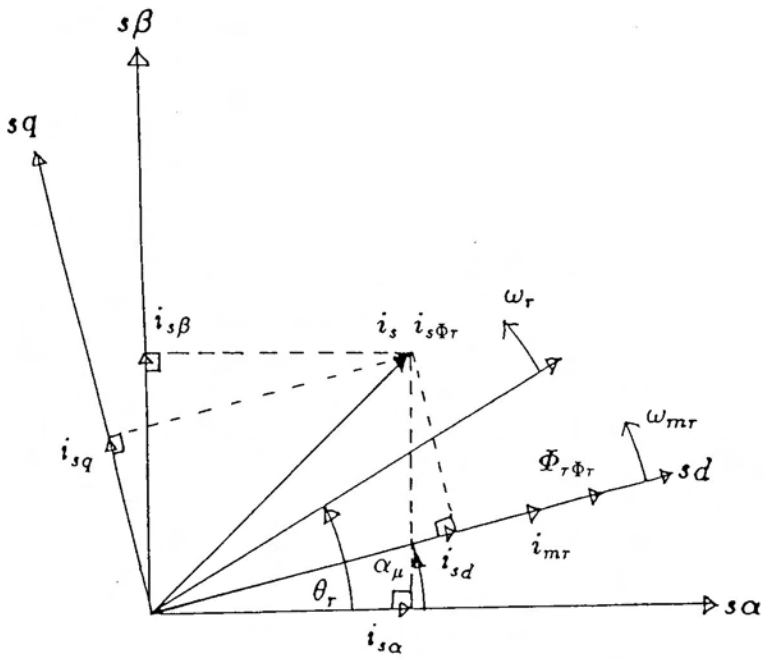

Fig. 2.4. Stator current and rotor flux-linkage space vectors in the stationary reference frame and in the reference frame fixed to the rotor flux-linkage space vector.

The d-q reference frame shown in Fig. 2.4 rotates at the angular velocity of the rotor flux-linkage space vector,

$$\omega_{mr} = \frac{d\alpha_\mu}{dt}. \tag{2.64}$$

The stator current space vector in the reference frame fixed to $\boldsymbol{\Phi}_r$ is

$$\boldsymbol{i}_{s\Phi r} = \boldsymbol{i}_s e^{-j\alpha_\mu} = i_{sd} + j i_{sq} \tag{2.65}$$

where $\boldsymbol{i}_s$ is the space vector of the stator currents in the stationary reference frame.

The rotor flux-linkage space vector in the reference frame fixed to $\boldsymbol{\Phi}_r$ has only a direct-axis component,

$$\begin{aligned} \boldsymbol{\Phi}_{r\Phi r} &= \boldsymbol{\Phi}_r e^{-j(\alpha_\mu - \theta_r)} = \boldsymbol{\Phi}_r e^{j\theta_r} e^{-j\alpha_\mu} \\ &= \boldsymbol{\Phi}'_r e^{-j\alpha_\mu} \\ &= |\boldsymbol{\Phi}_r| e^{j\alpha_\mu} e^{-j\alpha_\mu} \\ &= |\boldsymbol{\Phi}_r| = \Phi_{rd}, \end{aligned} \tag{2.66}$$

and $\Phi_{rq} = 0$.

The electromagnetic torque is expressed as follows:

$$T_e = \frac{3}{2} P \frac{L_m}{L_r} \boldsymbol{\Phi}_{r\Phi r} \times \boldsymbol{i}_{s\Phi r} \tag{2.67}$$

where $\times$ denotes an outer product. Thus, by substituting (2.65) and (2.66) into (2.67),

$$\begin{aligned} T_e &= \frac{3}{2} P \frac{L_m}{L_r} (\Phi_{rd} i_{sq} - \Phi_{rq} i_{sd}) \\ &= \frac{3}{2} P \frac{L_m}{L_r} \Phi_{rd} i_{sq} \end{aligned} \tag{2.68}$$

where P is the number of pole-pairs, $\Phi_{rd} = |\boldsymbol{\Phi}_r|$, and i_{sq} is the quadrature-axis stator current in the reference frame.

The relationship between the stator current components ($i_{s\alpha}$, $i_{s\beta}$) in the stationary reference frame and the stator current components (i_{sd}, i_{sq}) in the reference frame fixed to $\boldsymbol{\Phi}_r$ can be obtained by considering (2.65) as

$$\begin{bmatrix} i_{sd} \\ i_{sq} \end{bmatrix} = \begin{bmatrix} \cos\alpha_\mu & \sin\alpha_\mu \\ -\sin\alpha_\mu & \cos\alpha_\mu \end{bmatrix} \begin{bmatrix} i_{s\alpha} \\ i_{s\beta} \end{bmatrix}. \tag{2.69}$$

The rotor flux-linkage space vector is also expressed with the terms of the stator and rotor currents:

$$\boldsymbol{\Phi}_{r\Phi r} = \Phi_{rd} = |\boldsymbol{\Phi}_r| = L_r \boldsymbol{i}_{r\Phi r} + L_m \boldsymbol{i}_{s\Phi r} \tag{2.70}$$

where the rotor current space vector in the reference frame fixed to $\boldsymbol{\Phi}_r$ is obtained,

$$\begin{aligned} \boldsymbol{i}_{r\Phi r} &= i_{rd} + j i_{rq} \\ &= \boldsymbol{i}_r e^{-j(\alpha_\mu - \theta_r)} = \boldsymbol{i}_r e^{j\theta_r} e^{-j\alpha_\mu} \\ &= \boldsymbol{i}'_r e^{-j\alpha_\mu} \\ &= (i_{r\alpha} + j i_{r\beta}) e^{-j\alpha_\mu} \end{aligned} \tag{2.71}$$

where $\boldsymbol{i}'_r$ is the rotor current space vector in the stationary reference frame and $\boldsymbol{i}_r$ is the rotor current space vector in the rotating reference frame fixed to the rotor.

From (2.70), the so-called rotor magnetizing current in the reference frame is defined in terms of the stator and rotor current space vectors given by (2.65) and (2.71) as follows:

$$\begin{aligned} \boldsymbol{i}_{mr} &= \frac{\boldsymbol{\Phi}_{r\Phi r}}{L_m} \\ &= \frac{L_r}{L_m} \boldsymbol{i}_{r\Phi r} + \boldsymbol{i}_{s\Phi r} \\ &= \boldsymbol{i}_{s\Phi r} + (1 + \sigma_r) \boldsymbol{i}_{r\Phi r} \end{aligned} \tag{2.72}$$

where $\sigma_r = L_{rl}/L_m$ is the rotor leakage factor (L_{rl} and L_r are the rotor leakage inductance and self-inductance respectively). In Fig. 2.4 the rotor magnetizing current space vector is also indicated. The space vector $\boldsymbol{i}_{mr}$ has a component only along the real-axis of the reference frame as follows:

$$\begin{aligned} \boldsymbol{i}_{mr} &= i_{mrd} + j i_{mrq} \\ &= i_{mrd} = |\boldsymbol{i}_{mr}| \\ &= \frac{|\boldsymbol{\Phi}_r|}{L_m} \\ &= \boldsymbol{i}_{s\Phi r} + (1 + \sigma_r) \boldsymbol{i}_{r\Phi r} \end{aligned} \tag{2.73}$$

Thus, if $\Phi_{rd} = |\boldsymbol{\Phi}_r|$, and $\sigma_r = L_{rl}/L_m$, substitution of (2.73) into (2.68) yields :

$$T_e = \frac{3}{2} P \frac{L_m^2}{L_r} |\boldsymbol{i}_{mr}| i_{sq} = \frac{3}{2} P \frac{L_m}{1 + \sigma_r} |\boldsymbol{i}_{mr}| i_{sq} \tag{2.74}$$

This is a very important feature because the electromagnetic torque can be controlled by $|\boldsymbol{i}_{mr}|$ and i_{sq} independently. When the machine parameters are constant, the expression for the torque is similar to that of the separately excited dc machine. It will be shown that i_{sd} is equal to $|\boldsymbol{i}_{mr}|$ under the steady state condition. Thus when i_{sd} is kept constant, the torque is proportional to i_{sq}.

Torque control schemes of induction machines based on (2.74) have found the most widespread applications so far. This type of control is often referred to as field oriented control.

Chapter 3

Principle of field oriented control

3.1 Introduction

In this chapter, the principle of the field oriented control are described for induction machines. The preceding section showed the electromagnetic torque in the reference frames fixed to the rotor flux-linkage space vector ($\boldsymbol{\Phi}_r$); the expression for the electromagnetic torque of the induction machine is similar to the expression for the torque of the separately excited dc machine. Thus the torque control of the induction machine can be performed by the decoupled control of (i_{sd}) and (i_{sq}) of the stator currents, which is similar to controlling the field and armature currents in the separately excited dc machine. However, it should be noted that in the squirrel-cage induction machine it is not possible to monitor the rotor currents directly. The field oriented control requires the information of the magnitude and phase angle of $\boldsymbol{\Phi}_r$, and then i_{sd} and i_{sq} are obtained.

In the field oriented control there are two methods to obtain the magnitude and phase angle of $\boldsymbol{\Phi}_r$, which are direct and indirect methods. In the direct method, these quantities are directly measured (by Hall-effect sensors, search coils, or tapped stator windings of the machine) or they are calculated from a so-called flux estimation model. In the indirect method, the magnitude and phase angle of $\boldsymbol{\Phi}_r$ are obtained by utilizing the measured stator currents and the rotor angular velocity. The phase angle of $\boldsymbol{\Phi}_r$ is obtained as the sum of the measured rotor phase angle and the computed reference value of the slip angle which are calculated from the reference values of i_{sd} and i_{sq}.

Field oriented control can be applied to an induction machine supplied by a voltage source inverter, by a current source inverter, or by a cycloconverter, although this dissertation discusses a current source inverter. The field oriented controlled induction machine can achieve four-quadrant operation with high dynamic response.

In the following sections, the principle of the field oriented control of induction machines is discussed, where the flux estimation models are shown.

3.2 Stator voltage equation in the field oriented reference frame

In this section the stator voltage equations are derived in the reference frame fixed to $\boldsymbol{\Phi}_r$ based on Fig. 2.4, and the reference frame is called "the field oriented reference frame" in the following.

The stator voltage equation in the stator windings is

$$\boldsymbol{u}_s = R_s \boldsymbol{i}_s + \frac{d\boldsymbol{\Phi}_s}{dt}. \tag{3.1}$$

From Chapter 2,

$$\begin{aligned} \boldsymbol{i}_{s\Phi r} &= i_{sd} + j i_{sq} = \boldsymbol{i}_s e^{-j\alpha_\mu} \\ \boldsymbol{u}_{s\Phi r} &= u_{sd} + j u_{sq} = \boldsymbol{u}_s e^{-j\alpha_\mu} \\ \boldsymbol{\Phi}_{s\Phi r} &= \boldsymbol{\Phi}_s e^{-j\alpha_\mu} = L_s \boldsymbol{i}_{s\Phi r} + L_m \boldsymbol{i}_{r\Phi r} \end{aligned} \tag{3.2}$$

By substitution of (3.2) into (3.1), and considering that the differential equation of the stator flux linkage space vector is expressed as

$$\frac{d\boldsymbol{\Phi}_s}{dt} = e^{j\alpha_\mu} \frac{d\boldsymbol{\Phi}_{s\Phi r}}{dt} + e^{j\alpha_\mu} (j\omega_{mr}) \boldsymbol{\Phi}_{s\Phi r} \ ,$$

we have

$$\begin{aligned} \boldsymbol{u}_{s\Phi r} &= R_s \boldsymbol{i}_{s\Phi r} + \frac{d\boldsymbol{\Phi}_{s\Phi r}}{dt} + j\omega_{mr} \boldsymbol{\Phi}_{s\Phi r} \\ &= R_s \boldsymbol{i}_{s\Phi r} + L_s \frac{d\boldsymbol{i}_{s\Phi r}}{dt} + L_m \frac{d\boldsymbol{i}_{r\Phi r}}{dt} + j\omega_{mr} L_s \boldsymbol{i}_{s\Phi r} + j\omega_{mr} L_m \boldsymbol{i}_{r\Phi r} \end{aligned} \tag{3.3}$$

where it is assumed that L_m is constant and the leakage inductances are also constant.

Since from (2.72),

$$\boldsymbol{i}_{r\Phi r} = \frac{|\boldsymbol{i}_{mr}| - \boldsymbol{i}_{s\Phi r}}{1+\sigma_r} \ , \tag{3.4}$$

substitution of (3.4) into (3.3) yields the following differential equation:

$$\sigma T_s \frac{d\boldsymbol{i}_{s\Phi r}}{dt} + \boldsymbol{i}_{s\Phi r} = \frac{\boldsymbol{u}_{s\Phi r}}{R_s} - j\omega_{mr}\sigma T_s \boldsymbol{i}_{s\Phi r} - (T_s - \sigma T_s)(j\omega_{mr}|\boldsymbol{i}_{mr}| + \frac{d|\boldsymbol{i}_{mr}|}{dt}) \tag{3.5}$$

where σT_s is the stator transient time constant of the machine,

σ is the total leakage factor (i.e., $\sigma = 1 - \frac{1}{(1+\sigma_r)(1+\sigma_s)}$),

σL_s is the stator transient inductance (i.e., $\sigma L_s = L_s - L_m^2/L_r$),

and T_s is the stator time constant (i.e., $T_s = L_s/R_s$).

By resolving (3.5) into its real(d) and imaginary(q) components, the following two-axis differential equations are obtained for stator currents:

$$\begin{aligned} \sigma T_s \frac{di_{sd}}{dt} + i_{sd} &= \frac{u_{sd}}{R_s} + \omega_{mr}\sigma T_s i_{sq} - (1-\sigma)T_s \frac{d|\boldsymbol{i}_{mr}|}{dt} \\ \sigma T_s \frac{di_{sq}}{dt} + i_{sq} &= \frac{u_{sq}}{R_s} - \omega_{mr}\sigma T_s i_{sd} - (1-\sigma)T_s \omega_{mr}|\boldsymbol{i}_{mr}| \end{aligned} \tag{3.6}$$

or

$$\begin{aligned} \sigma L_s \frac{di_{sd}}{dt} + R_s i_{sd} &= u_{sd} + \omega_{mr}\sigma L_s i_{sq} - (1-\sigma)L_s \frac{d|\boldsymbol{i}_{mr}|}{dt} \\ \sigma L_s \frac{di_{sq}}{dt} + R_s i_{sq} &= u_{sq} - \omega_{mr}\sigma L_s i_{sd} - (1-\sigma)L_s \omega_{mr}|\boldsymbol{i}_{mr}| \end{aligned} \tag{3.7}$$

Eq. (3.6) is a first order lag system whose gain is equal to the inverse of the stator resistance. For the purpose of the field oriented control, the direct-axis stator current (i_{sd}) and the quadrature-axis stator current (i_{sq}) must be independently controlled.

However, since the voltage equations in (3.6) are coupled, by the terms ($\omega_{mr}\sigma T_s i_{sq}$) and ($\omega_{mr}\sigma T_s i_{sd}$). The stator currents ($i_{sd}$, i_{sq}) can be independently controlled if the decoupled control is implemented. This decoupled control is only possible to implement in the voltage controlled type inverter drive system, but still has difficulty due to machine parameter (σL_s) variations.

In the current controlled type inverter drive system like the current source inverter drive system, the complete decoupled control cannot be considered.

3.3 Rotor voltage equation for the rotor flux estimation model in the field oriented reference frame

The rotor voltage equations expressed in the field oriented reference frame can be used to obtain the magnitude and phase angle of the rotor flux space vector or they can be used to obtain the magnitude of the rotor magnetizing current $\boldsymbol{i}_{mr}$ and its angular velocity ω_{mr}. This flux model is derived in this section.

The rotor voltage equation is expressed as follows:

$$\boldsymbol{u}_r = R_r \boldsymbol{i}_r + \frac{d\boldsymbol{\Phi}_r}{dt} \tag{3.8}$$

where $\boldsymbol{u}_r = 0$.

The rotor current, voltage, and flux-linkage space vector equations in the field oriented reference frame are expressed as follows:

$$\begin{aligned} \boldsymbol{i}_{r\Phi r} &= i_{rd} + j i_{rq} = \boldsymbol{i}_r e^{-j(\alpha_\mu - \theta_r)} \\ \boldsymbol{u}_{r\Phi r} &= u_{rd} + j u_{rq} = \boldsymbol{u}_s e^{-j(\alpha_\mu - \theta_r)} \\ \boldsymbol{\Phi}_{r\Phi r} &= \boldsymbol{\Phi}_r e^{-j(\alpha_\mu - \theta_r)} \end{aligned} \tag{3.9}$$

By substitution of (3.9) into (3.8), since the differential equation of $\boldsymbol{\Phi}_r$ is expressed as

$$\frac{d\boldsymbol{\Phi}_r}{dt} = e^{j(\alpha_\mu - \theta_r)} \frac{d\boldsymbol{\Phi}_{r\Phi r}}{dt} + e^{j(\alpha_\mu - \theta_r)} j(\omega_{mr} - \omega_r) \boldsymbol{\Phi}_{s\Phi r},$$

the rotor voltage equation in the field oriented reference frame are expressed as follows:

$$\boldsymbol{u}_{r\Phi r} = R_r \boldsymbol{i}_{r\Phi r} + \frac{d\boldsymbol{\Phi}_{r\Phi r}}{dt} + j(\omega_{mr} - \omega_r) \boldsymbol{\Phi}_{r\Phi r} = 0 \tag{3.10}$$

In (3.11) $\boldsymbol{\Phi}_{r\Phi r}$ is the rotor flux-linkage space vector in the field oriented reference frame where $\boldsymbol{i}_{mr} = |\boldsymbol{i}_{mr}|$. Thus, from (2.72),

$$\boldsymbol{\Phi}_{r\Phi r} = L_m |\boldsymbol{i}_{mr}| \tag{3.11}$$

which gives a linear relationship if the magnetizing inductance L_m is assumed to be constant. Substitution of (3.12) into (3.11) yields the following rotor voltage differential equation:

$$0 = R_r \boldsymbol{i}_{r\Phi r} + L_m \frac{d|\boldsymbol{i}_{mr}|}{dt} + j(\omega_{mr} - \omega_r) L_m |\boldsymbol{i}_{mr}| \tag{3.12}$$

By substitution of (3.4) into (3.12) and dividing by R_r, (3.12) becomes

$$0 = \frac{|\boldsymbol{i}_{mr}| - \boldsymbol{i}_{s\Phi r}}{1+\sigma_r} + \frac{L_m}{R_r}\frac{d|\boldsymbol{i}_{mr}|}{dt} + j(\omega_{mr} - \omega_r)\frac{L_m}{R_r}|\boldsymbol{i}_{mr}|.$$

Since $L_m = L_r/(1+\sigma_r)$, the above equation is rearranged as follows:

$$T_r\frac{d|\boldsymbol{i}_{mr}|}{dt} + |\boldsymbol{i}_{mr}| = \boldsymbol{i}_{s\Phi r} - j(\omega_{mr} - \omega_r)T_r|\boldsymbol{i}_{mr}| \tag{3.13}$$

where T_r is the rotor time constant (i.e., $T_r = L_r/R_r$). By resolving into the real- and imaginary-axis components, the following extremely simple equations are obtained:

$$T_r\frac{d|\boldsymbol{i}_{mr}|}{dt} + |\boldsymbol{i}_{mr}| = i_{sd} \tag{3.14}$$

$$\omega_{mr} = \omega_r + \frac{i_{sq}}{T_r|\boldsymbol{i}_{mr}|} \tag{3.15}$$

where $i_{sq}/(T_r|\boldsymbol{i}_{mr}|)$ shows the slip angular velocity, ω_{sl}.

The angular velocity of the rotor flux is equal to the sum of the rotor angular velocity and the slip angular velocity of the rotor flux. If $|\boldsymbol{i}_{mr}|$ is constant, it follows from (3.14) that $|\boldsymbol{i}_{mr}| = i_{sd}$. The magnitude of the rotor flux-linkage space vector can be kept at a desired level by controlling the direct-axis stator current (i_{sd}), and then the electromagnetic torque is determined by the quadrature-axis stator current (i_{sq}).

Fig. 3.1 shows the flux models of the induction machine in the field oriented reference frame, based on (3.14) and (3.15). The implementation shown in Fig. 3.1(a) utilizes the measured values of the stator currents (i_{sU}, i_{sV}, i_{sW}), the measured value of the rotor velocity (ω_r) and the rotor time constant (T_r). The three stator currents are transformed into their two-axis components by the application of the three-phase to two-phase transformation. In the absence of zero-sequence currents, it is sufficient to monitor only two stator currents. The direct- and quadrature-axis stator currents ($i_{s\alpha}$, $i_{s\beta}$), which are formulated in the stationary reference frame fixed to the stator, are then transformed into the two-axis stator current components in the field oriented reference frame (i_{sd}, i_{sq}), utilizing the following relation:

$$i_{sd} + ji_{sq} = \boldsymbol{i}_s e^{-j\alpha_\mu} = (i_{s\alpha} + ji_{s\beta})e^{-j\alpha_\mu}$$

The current component (i_{sd}) serves as an input to a first order lag system with gain 1 and time constant (T_r), the output of which is the magnitude of $\boldsymbol{i}_{mr}$.

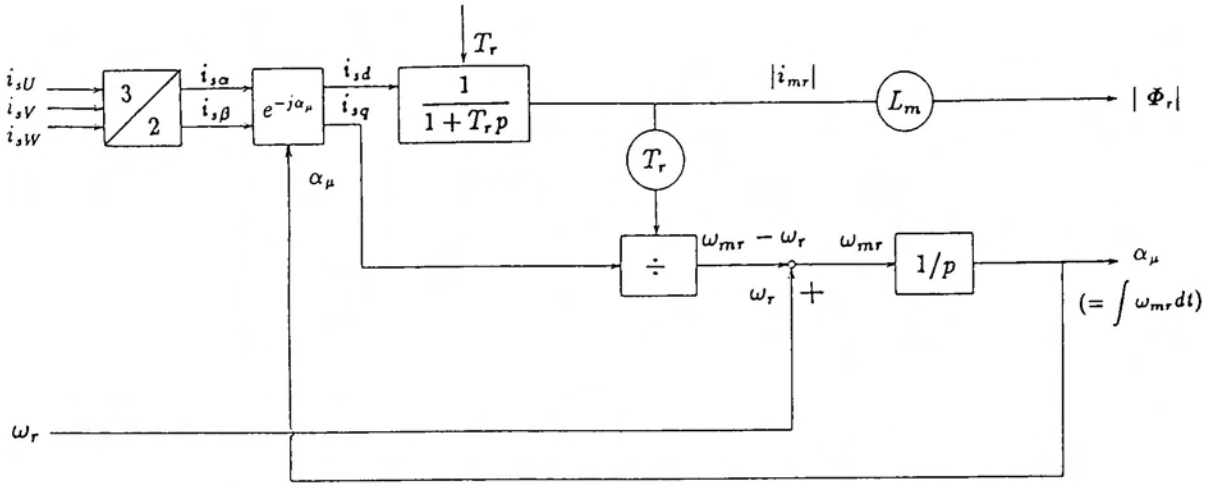

(a)

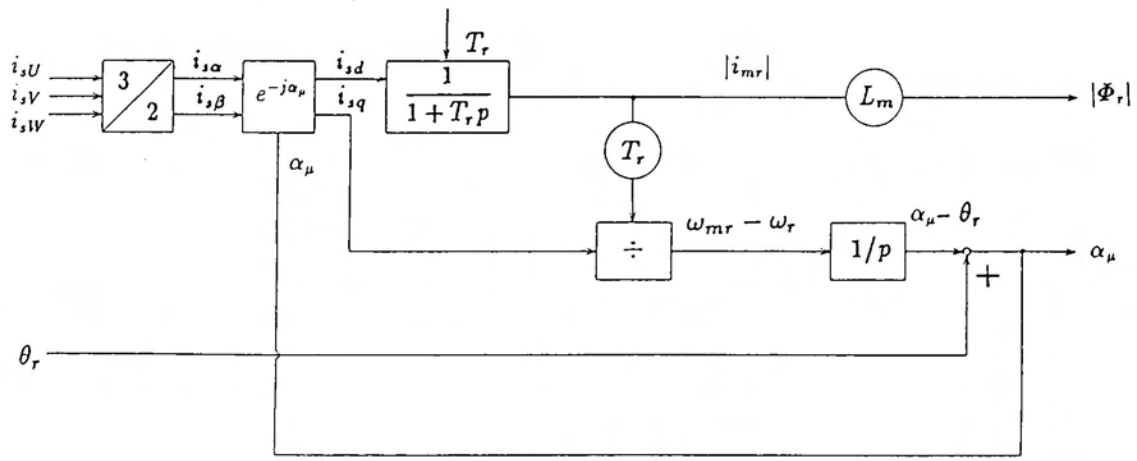

(b)

Fig. 3.1. Flux models in the field oriented reference frame. (a). Flux model with inputs i_{sU}, i_{sV}, i_{sW}, and ω_r. (b). Flux model with inputs i_{sU}, i_{sV}, i_{sW}, and θ_r.

One of the output of the system, $\boldsymbol{\Phi}_r$, is obtained by multiplying $|\boldsymbol{i}_{mr}|$ by L_m. The quadrature-axis stator current (i_{sq}) is divided by ($T_r|\boldsymbol{i}_{mr}|$), thus yielding the slip angular velocity of the rotor flux, and when the rotor angular velocity is added to this, ω_{mr} is obtained. The integration of ω_{mr} yields the angle (α_μ), which defines the phase angle of $\boldsymbol{\Phi}_r$ with respect to the real axis of the stationary reference frame. This angle is fed back to the transformation block $e^{-j\alpha_\mu}$.

However, it is possible to have another flux model where the measured values of the rotor angle (θ_r) are utilized instead of using the measured values of the rotor angular velocity (ω_r). This is shown in Fig. 3.1(b). It can be seen that the outputs of this flux-model are again $|\boldsymbol{i}_{mr}|$, α_μ and $|\boldsymbol{\Phi}_r|$, but the term of ω_r disappears. Accuracy of these flux models have a strong dependency on T_r. If T_r is inaccurate, then it could lead to an unwanted coupling between the d and q axes, and therefore to a deteriorated dynamic performance of the drive with unwanted instabilities. This problem may be avoided by the application of on-line parameter adaptation which will be discussed in the latter chapter.

3.4 Rotor voltage equation for the rotor flux estimation models in the stationary reference frame

There are several methods to estimate the magnitude and phase angle of the rotor flux space vector by utilizing certain machine parameters and various measured quantities, such as the actual stator currents, the rotor angular velocity and the stator voltages. Here three methods are discussed and the equations are formulated in the stationary reference frame fixed to the stator.

3.4.1 Flux model utilizing the measured rotor speed and stator current

In the case of using the stationary reference frame, $\boldsymbol{i}_s$ do not have to be transformed into $\boldsymbol{i}_{s\Phi_r}$ in the field oriented reference frame as Fig. 3.1. For the purpose, the rotor voltage space-vector equation is used, but in order to have an equation which directly contains the

stator currents expressed in the stationary reference frame fixed to the stator, the rotor voltage equation formulated in the stationary reference frame must be used. It should be noted that the effects of magnetic saturation are neglected.

The rotor voltage equation (3.8) is

$$0 = R_r \boldsymbol{i}_r + \frac{d\boldsymbol{\Phi}_r}{dt}.$$

The rotor current, voltage, flux-linkage space vector equations in the stationary reference frame are expressed as follows:

$$\begin{aligned} \boldsymbol{i}'_r &= i_{r\alpha} + j i_{r\beta} = \boldsymbol{i}_r e^{j\theta_r} \\ \boldsymbol{u}'_r &= u_{r\alpha} + j u_{r\beta} = \boldsymbol{u}_r e^{j\theta_r} = 0 \\ \boldsymbol{\Phi}'_r &= \boldsymbol{\Phi}_r e^{j\theta_r} \end{aligned} \tag{3.16}$$

By substitution of (3.17) into (3.9), since the differential equation of $\boldsymbol{\Phi}_r$ is expressed as

$$\frac{d\boldsymbol{\Phi}_r}{dt} = e^{-j\theta_r}\frac{d\boldsymbol{\Phi}'_r}{dt} + e^{-j\theta_r} j(-\omega_r)\boldsymbol{\Phi}'_r,$$

the rotor voltage equation in the stationary reference frame are expressed as follows:

$$0 = R_r \boldsymbol{i}'_r + \frac{d\boldsymbol{\Phi}'_r}{dt} - j\omega_r \boldsymbol{\Phi}'_r \tag{3.17}$$

Similarly to the definition used in (2.72), $\boldsymbol{i}_{mr}$ is obtained by dividing the rotor flux-linkage space vector expressed in the stationary reference frame by L_m:

$$\boldsymbol{i}_{mr} = \frac{\boldsymbol{\Phi}'_r}{L_m} = \frac{L_r}{L_m}\boldsymbol{i}'_r + \boldsymbol{i}_s = \boldsymbol{i}_s + (1+\sigma_r)\boldsymbol{i}'_r \tag{3.18}$$

where $\boldsymbol{i}_{mr} = i_{mr\alpha} + j i_{mr\beta}$.

From (3.18),

$$\boldsymbol{i}'_r = \frac{\boldsymbol{i}_{mr} - \boldsymbol{i}_s}{1+\sigma_r}.$$

By eliminating $\boldsymbol{i}'_r$ and $\boldsymbol{\Phi}'_r$ from (3.17) with this equation and (3.18), the following equation is obtained:

$$0 = R_r \frac{\boldsymbol{i}_{mr} - \boldsymbol{i}_s}{1+\sigma_r} + \frac{d}{dt} L_m \boldsymbol{i}_{mr} - j\omega_r L_m \boldsymbol{i}_{mr} \tag{3.19}$$

Since $L_m = L_r/(1+\sigma_r)$ and $T_r = L_r/R_r$, by dividing (3.19) by R_r and $1/(1+\sigma_r)$, the following equation is obtained:

$$T_r \frac{d\boldsymbol{i}_{mr}}{dt} = \boldsymbol{i}_s - \boldsymbol{i}_{mr} + j\omega_r T_r \boldsymbol{i}_{mr} \tag{3.20}$$

Therefore the resolution of (3.20) into the real- and imaginary-axis component gives the following two differential equations:

$$\begin{aligned} T_r \frac{di_{mr\alpha}}{dt} &= i_{s\alpha} - i_{mr\alpha} - j\omega_r T_r i_{mr\beta} \\ T_r \frac{di_{mr\beta}}{dt} &= i_{s\beta} - i_{mr\beta} + j\omega_r T_r i_{mr\alpha} \end{aligned} \tag{3.21}$$

An implementation of (3.21) is shown in Fig. 3.2, where the three-phase stator currents are transformed into $(i_{s\alpha}, i_{s\beta})$ by the application of the three-phase to two-phase transformation. In accordance with (3.21), the signals $(i_{s\alpha} - i_{mr\alpha} - j\omega_r T_r i_{mr\beta})$ and $(i_{s\beta} - i_{mr\beta} + j\omega_r T_r i_{mr\alpha})$ are obtained. They are divided by the rotor time constant (T_r) and are integrated to yield the direct- and quadrature-axis rotor magnetizing current components $(i_{mr\alpha}, i_{mr\beta})$. A rectangular to polar converter is used to obtain the magnitude $(|\boldsymbol{i}_{mr}|)$ and the phase angle (α_μ) of $\boldsymbol{\Phi}_r$. If required, $|\boldsymbol{i}_{mr}|$ can be multiplied by the magnetizing inductance (L_m) to yield the magnitude of the rotor flux- linkage space vector. This scheme is also dependent on the rotor time constant of the machine and can be used over the entire speed range, including standstill. When this model is used, the phase angle (α_μ) at the output of the model has to be differentiated to obtain ω_{mr}.

When compared with the flux model of Fig. 3.1, the flux model of Fig. 3.2 yields less accurate values of the magnitude and phase angle of $\boldsymbol{\Phi}_r$. This reason is described as follows: By considering (3.21), in the steady state where $p = d/dt = j\omega_i$, the rotor magnetizing current can be expressed in terms of the stator current vector as

$$\boldsymbol{I}_{mr} = \frac{\boldsymbol{I}_s}{1 + j(\omega_i - \omega_r)T_r} \,. \tag{3.22}$$

where $\boldsymbol{I}_{mr}$ and $\boldsymbol{I}_s$ denote the complex phasors for sinusoidal variables of the rotor magnetizing and the stator current respectively. At high speed condition and small slip (i.e., the difference of $(\omega_i - \omega_r) = s\omega_i$ (s is slip) becomes small), a small error in the measured value of the rotor speed will results in its large error in the rotor magnetizing current and this is especially

pronounced in its phase angle. The other source of errors is T_r which is also temperature dependent, although it follows from (3.22) that the rotor magnetizing current (or rotor flux) only at no load ($s = 0$) is not influenced by T_r. This is a physically expected result, since at no load condition there are no currents in the rotor. In the next section, it is shown that the flux model by a linear combination of the stator and rotor voltage equations are not so sensitive to the rotor speed. Thus an implementation based on these equations requires less accurate rotor speed monitoring.

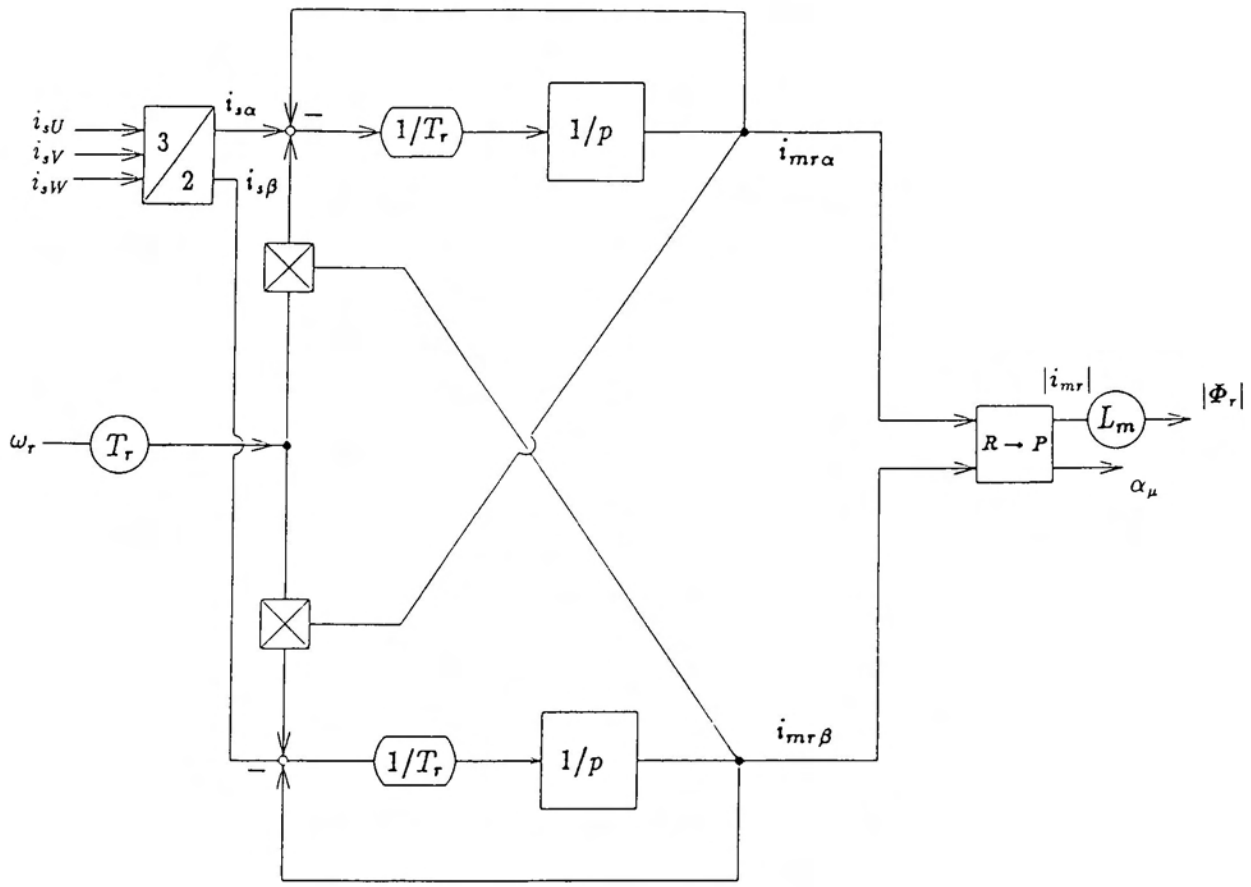

Fig. 3.2. Flux models in the stationary reference frame with inputs i_{sU}, i_{sV}, i_{sW}, and ω_r.

3.4.2 Flux model utilizing the measured rotor speed, stator voltage and current

The stator voltage and flux linkage equations in the stationary reference frame are expressed as follows:

$$\begin{aligned} \boldsymbol{u}_s &= R_s \boldsymbol{i}_s + \frac{d\boldsymbol{\Phi}_s}{dt} \\ \boldsymbol{\Phi}_s &= L_s \boldsymbol{i}_s + L_m \boldsymbol{i}'_r \\ \boldsymbol{u}_s &= R_s \boldsymbol{i}_s + L_s \frac{d\boldsymbol{i}_s}{dt} + L_m \frac{d\boldsymbol{i}'_r}{dt} \end{aligned} \tag{3.23}$$

where the effects of magnetic saturation are neglected.

From (3.18) and (3.23),

$$\begin{aligned} \boldsymbol{i}'_r &= \frac{\boldsymbol{i}_{mr} - \boldsymbol{i}_s}{1 + \sigma_r} \\ L_m \frac{d}{dt} \boldsymbol{i}'_r &= \frac{L_s}{(1+\sigma_s)(1+\sigma_r)} \frac{d}{dt}(\boldsymbol{i}_{mr} - \boldsymbol{i}_s) = (1-\sigma) L_s \frac{d}{dt}(\boldsymbol{i}_{mr} - \boldsymbol{i}_s) \end{aligned}$$

where σ is the resultant leakage constant and is defined as

$$\begin{aligned} \sigma &= 1 - \frac{1}{(1+\sigma_s)(1+\sigma_r)} \\ &= 1 - \frac{L_m^2}{L_s L_r}. \end{aligned}$$

Thus the following space-vector voltage equation is obtained:

$$\boldsymbol{u}_s = R_s \boldsymbol{i}_s + \sigma L_s \frac{d\boldsymbol{i}_s}{dt} + (1-\sigma) L_s \frac{d\boldsymbol{i}_{mr}}{dt} \tag{3.24}$$

Furthermore (3.24) becomes

$$(1-\sigma) T_s \frac{d\boldsymbol{i}_{mr}}{dt} = \frac{\boldsymbol{u}_s}{R_s} - \boldsymbol{i}_s - \sigma T_s \frac{d\boldsymbol{i}_s}{dt} \tag{3.25}$$

where T_s is the stator time constant, σT_s is the stator transient time constant.

If (3.25) is added to (3.20), the following equation is obtained:

$$\frac{d\boldsymbol{i}_{mr}}{dt} [T_r + T_s(1-\sigma)] = \frac{\boldsymbol{u}_s}{R_s} + (j\omega_r T_r - 1)\boldsymbol{i}_{mr} - \sigma T_s \frac{d\boldsymbol{i}_s}{dt} \tag{3.26}$$

It is possible to use (3.26) directly to obtain $\boldsymbol{i}_{mr}$, if $\boldsymbol{u}_s$ and $\boldsymbol{i}_s$ are measured.

From (3.26), its real- and imaginary-axis forms are expressed as follows:

$$\begin{aligned}
\frac{di_{mr\alpha}}{dt}\left[T_r + T_s(1-\sigma)\right] + i_{mr\alpha} &= \frac{u_{s\alpha}}{R_s} - \omega_r T_r i_{mr\beta} - \sigma T_s \frac{di_{s\alpha}}{dt} \\
\frac{di_{mr\beta}}{dt}\left[T_r + T_s(1-\sigma)\right] + i_{mr\beta} &= \frac{u_{s\beta}}{R_s} + \omega_r T_r i_{mr\alpha} - \sigma T_s \frac{di_{s\beta}}{dt}
\end{aligned} \tag{3.27}$$

An implementation of (3.28) is shown in Fig. 3.3 where the input quantities are the measured values of the rotor speed (ω_r), and the three-phase stator voltages and currents. These are then transformed into the two-axis components of the stator currents ($i_{s\alpha}, i_{s\beta}$) and stator voltages ($u_{s\alpha}, u_{s\beta}$) by the application of the three-phase to two-phase transformation. The rotor magnetizing current ($i_{mr\alpha}, i_{mr\beta}$) are converted into the magnitude and phase angle by a rectangular-to-polar converter.

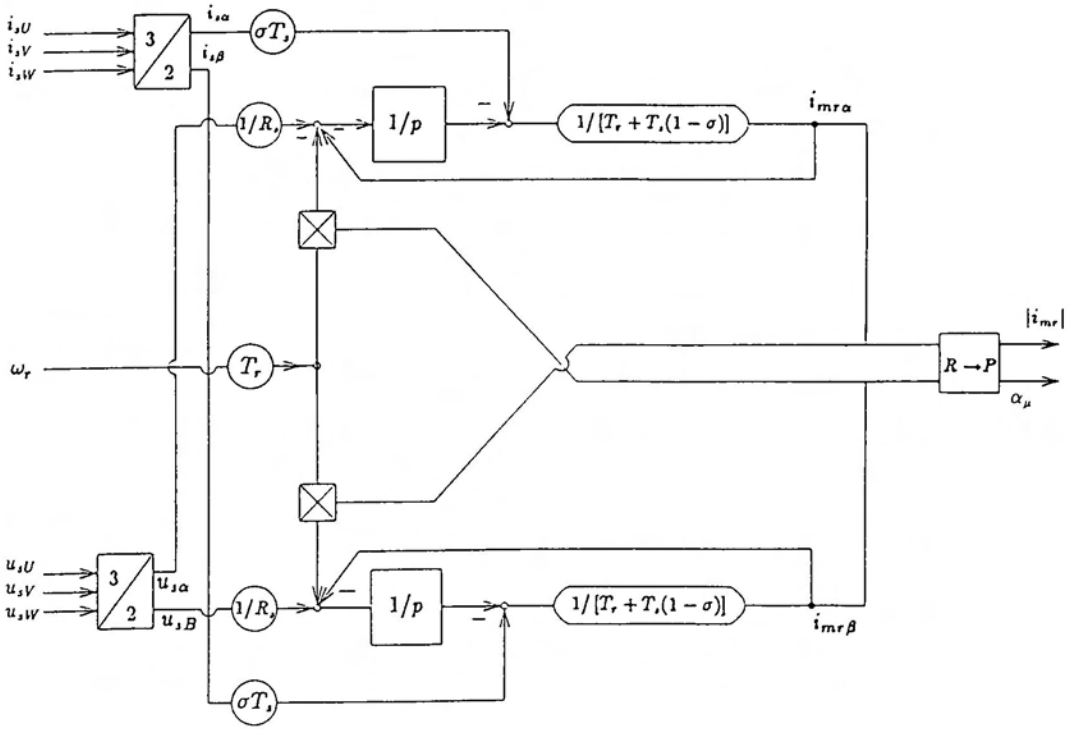

Fig. 3.3. Flux models in the stationary reference frame with inputs u_{sU}, u_{sV}, u_{sW}, i_{sU}, i_{sV}, i_{sW} and ω_r.

The used machine parameters are R_s, σ, T_s, and T_r. If the off-line parameter identification is used, these values can be obtained by the application of conventional tests. By considering (3.26) in the steady state where $p = d/dt = j\omega_i$, the rotor magnetizing current can be expressed in terms of the stator current vector as follows:

$$\boldsymbol{I}_{mr} = \frac{\boldsymbol{u}_s/R_s - j\omega_i\sigma T_s \boldsymbol{I}_s}{1 + j\left[(\omega_i - \omega_r)T_r + \omega_i T_s(1-\sigma)\right]} \tag{3.28}$$

At high speed region and small slip, $(\omega_i - \omega_r)$ becomes small, a small error in the measured value of the rotor speed will not influence $\boldsymbol{I}_{mr}$ as much as in (3.22). Because, at high values of the rotor speed, the term $(\omega_i T_s(1-\sigma))$ will dominate in the imaginary part of the denominator of (3.28) and is independent of the measured rotor speed. At low speed region, however, the influence of the parameter changes due to the stator temperature must be considered. This reason is described as follows: Both the numerator and denominator of (3.28) are multiplied by R_s/L_s, thus (3.28) becomes

$$\boldsymbol{I}_{mr} = \frac{\boldsymbol{u}_s/L_s - j\omega_i\sigma \boldsymbol{I}_s}{R_s/L_s + j\left[(\omega_i - \omega_r)R_s T_r/L_s + \omega_i(1-\sigma)\right]} \,. \tag{3.29}$$

When $\omega_i = \omega_r$ (no-load), the denominator becomes $(R_s/L_s + j\omega_i(1-\sigma))$ where the only parameter influenced by the stator temperature change is R_s. A large error occurs in $\boldsymbol{I}_{mr}$ at low speed region or at stand still, since R_s dominates in the denominator.

3.4.3 Flux model utilizing the measured stator voltage and current

It is possible to construct a flux model which does not use the measured rotor speed, but only the measured values of the stator voltages and stator currents for the determination of the magnitude and phase angle of $\boldsymbol{i}_{mr}$. For this purpose (3.25) can be used.

In the stationary reference frame, the resolution of (3.25) into its real- and imaginary-axis components yields the following equations:

$$\begin{aligned}
(1-\sigma)T_s\frac{di_{mr\alpha}}{dt} &= \frac{u_{s\alpha}}{R_s} - i_{s\alpha} - \sigma T_s\frac{di_{s\alpha}}{dt} \\
(1-\sigma)T_s\frac{di_{mr\beta}}{dt} &= \frac{u_{s\beta}}{R_s} - i_{s\beta} - \sigma T_s\frac{di_{s\beta}}{dt}
\end{aligned} \tag{3.30}$$

An implementation of (3.30) is shown in Fig. 3.4 where the input quantities are the measured values of the three-phase stator voltages and currents respectively (u_{sU}, u_{sV}, u_{sW}, i_{sU}, i_{sV}, and i_{sW}) and the required parameters are R_s, σ and L_s. It follows that by integrating (3.30), $i_{mr\alpha}$ and $i_{mr\beta}$ are obtained.

By considering (3.25) in the steady state, where $\alpha_\mu = d/dt = j\omega_i$, the rotor magnetizing current can be expressed in terms of the stator current vector as follows:

$$\begin{aligned} \boldsymbol{I}_{mr} &= \frac{\boldsymbol{u}_s/R_s - (1 + j\sigma T_s\omega_i)\boldsymbol{I}_s}{(1-\sigma)j\omega_i T_s} \\ &= \frac{\boldsymbol{u}_s - (R_s + j\sigma L_s\omega_i)\boldsymbol{I}_s}{(1-\sigma)j\omega_i L_s} \end{aligned} \tag{3.31}$$

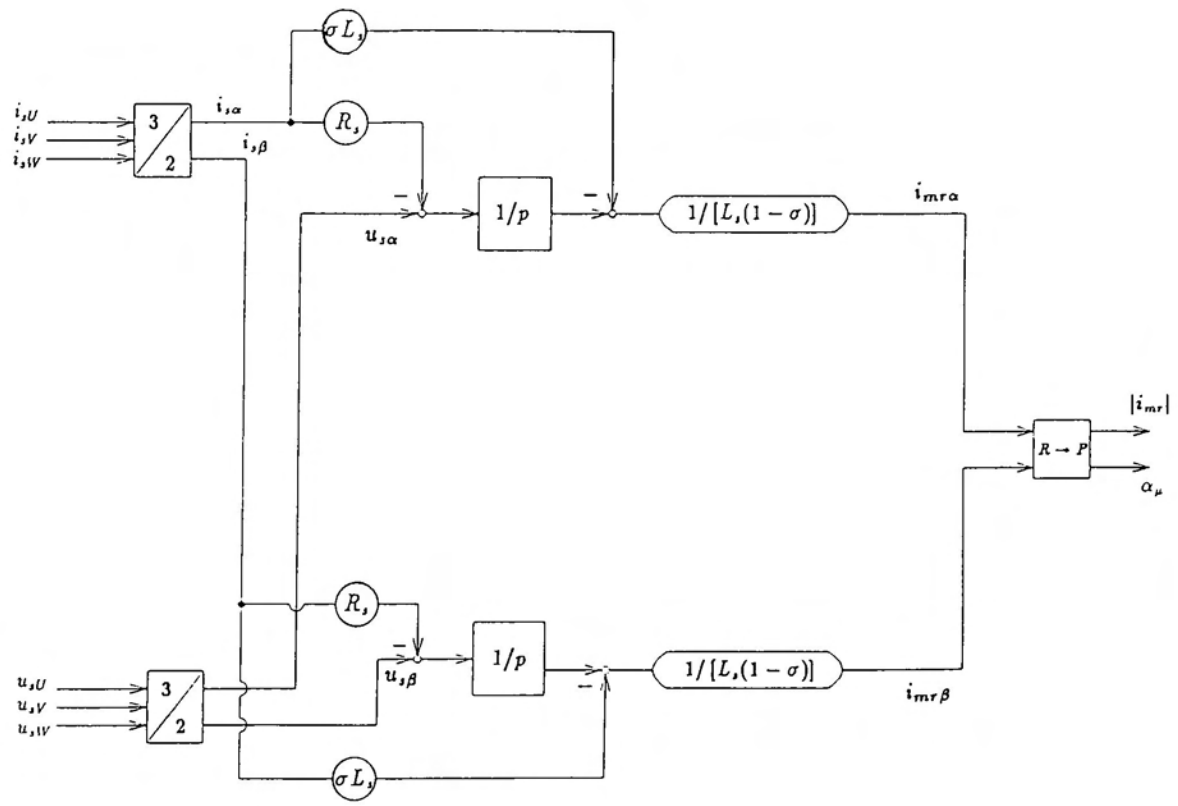

Fig. 3.4. Flux models in the stationary reference frame with inputs u_{sU}, u_{sV}, u_{sW}, i_{sU}, i_{sV}, and i_{sW}.

At low stator frequencies, the stator ohmic drops would dominate and accurate ohmic voltage drop compensation has to be performed prior to the integration. Due to the temperature dependency of the stator resistance, this is difficult to perform, and with such an implementation a lower frequency limit for useful operation is approximately 3Hz with a 50Hz supply. It should be noted that at low frequencies it is not possible to perform drift-free analogue integration.

3.5 Comparison of flux estimation models

The several flux estimation models for the field oriented control are shown in the preceding chapter. Here some issues about these models with a practical point are discussed briefly.

As compared with all of the flux estimation models, at high speed region such as field-weakening, i.e. above a rated speed, the models of Fig. 3.1 and Fig. 3.2 are inferior to those of Fig. 3.3 and Fig. 3.4. The main flux saturation would influence the model of Fig. 3.1 and Fig. 3.2 more than those of Fig. 3.3 and Fig. 3.4 and the error of slip frequency calculation must be significant during this region and also rapid acceleration.

On the other hand, at low speed region or stand still, the models of Fig. 3.3 and Fig. 3.4 are inferior to those of Fig. 3.1 and Fig. 3.2. Because they are including the stator resistance (R_s), the existence of R_s would be significant and the drift of the open loop integration would occur.

The model of Fig. 3.3 requires input values more than the others, so it seems to be reliable, while this flux model is complicated and needs accurate machine parameters more than the others, and furthermore accurate voltage measurements on a PWM inverter are difficult because the voltages are highly distorted requiring a high sampling frequency.

Consequently, the model of Fig. 3.1 (Flux models in the field oriented reference frame) is useful. Although T_r and L_m should be accurate at that time, it is not fatal problem. Thus, the flux model of Fig. 3.1 can be used over the entire speed range.

Those machine parameters identification and compensation will be discussed in the latter chapter.

Chapter 4

Vector approximation method

4.1 Introduction

The principle of field oriented control are shown in the preceding chapter. By the field oriented control, the magnetizing and torque component of the stator current are decoupled and the transient response characteristics are similar to those of a separately excited dc machine and the system will adapt to any load disturbances and reference value variations as fast as a dc machine. The field oriented control of various types of ac machines with rapid developments in the power electronics can be available as servo-drives to reliability and energy saving. For ac drives there is much greater variety than for dc ones, due to the different types of inverters which can be combined with various types of ac machines.

In recent years, voltage source inverters (VSI) are more popular than current source inverters (CSI) for ac drives, perhaps because the VSI has faster current response and can be applied to a PWM system in the high frequency region more easily due to the low impedance. This is why field oriented control is often applied to control VSI drive ac motor drive systems [1]. The CSI, however, still has better features, such as capability of four-quadrant operation without any extra power circuit for regeneration, ruggedness and reliability, and no shoot-through fault. Moreover, high precision of current control with the CSI is possible. Thus, the CSI seems to be appropriate for large capacity drive systems such as steel mills, elevator motors, and so on. However, the CSI drive ac motor has problems in the low frequency region, where torque pulsation and harmonic heating occur because of a rectangular current

wave with 120° conduction. In order to cope with these problems, the PWM−type CSI drive induction motor system has been proposed as well as VSI drive in [3][4] and the design of the PWM signal is considered to decrease the higher harmonic components of current waveforms. The pattern of the PWM signal is memorized in a memory ROM in advance and is read out by the designed timing.

On the other hand, the vector approximation method was proposed [2] with the different concept. This method would not only decrease torque ripple but also control the instantaneous torque of an induction motor driven by the CSI, that is, not only in steady state but also in transient state, the desirable current is computed as follows. The magnitude of the desirable current is adjusted by the control of the dc link current for each instant, while, the phase angle of the desirable stator current is determined by utilizing the rotor flux angle, which is computed by the rotor flux estimation shown in the preceding chapter. Since the inverter is a current source type, the desirable stator current cannot realized exactly but can be approximated by two of six realizable current vectors, which are adjacent to the desirable one, where the current vectors composed based on sense of time average. This approximation is done for every sampling period of a control loop; thus, the torque is to be controlled almost instantaneously.

The following sections are concerned with the vector approximation method of CSI drive induction motor, where the method are verified with the simulation and the experiments.

4.2 Basic theory

In this section, the basic theory for the vector approximation is reviewed. The space vector voltage equations of a symmetrical induction machine from (2.57) and (2.58) are given as follows:

$$\begin{bmatrix} \boldsymbol{u}_s \\ \mathbf{o} \end{bmatrix} = \begin{bmatrix} R_s + L_s p & L_m p \\ L_m(p - j\omega_r) & R_r + L_r(p - j\omega_r) \end{bmatrix} \begin{bmatrix} \boldsymbol{i}_s \\ \boldsymbol{i}'_r \end{bmatrix} \tag{4.1}$$

From (3.18), the rotor magnetizing current space vector is expressed as

$$\boldsymbol{i}_{mr} = \boldsymbol{i}_s + \frac{L_r}{L_m}\boldsymbol{i}'_r \tag{4.2}$$

where $\boldsymbol{u}_s$, $\boldsymbol{i}_s$, $\boldsymbol{i}'_r$, and $\boldsymbol{i}_{mr}$ are the complex numbers of stator voltage, current, rotor current and rotor magnetizing current respectively in the stationary reference frame fixed to the stator, that is, α-β axes in Fig. 4.1. The equivalent circuit is shown in Fig. 4.2. R_s and R_r are the stator and rotor resistance, L_s and L_r are the stator and rotor self inductance, L_m is the magnetizing inductance, ω_r is the rotor angular velocity, ω_{mr} is the angular velocity of $\boldsymbol{i}_{mr}$, and p is the differential operator.

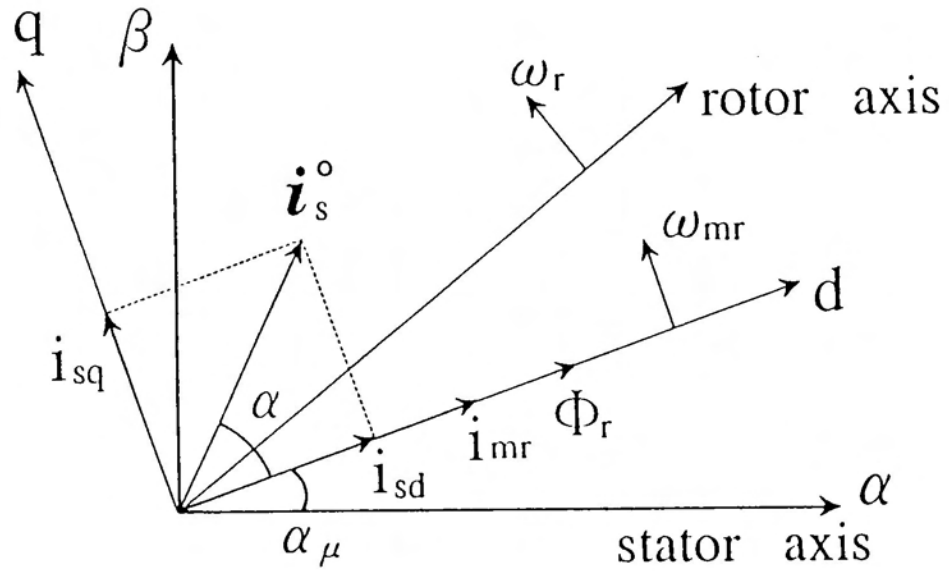

Fig. 4.1. Relation of current vectors.

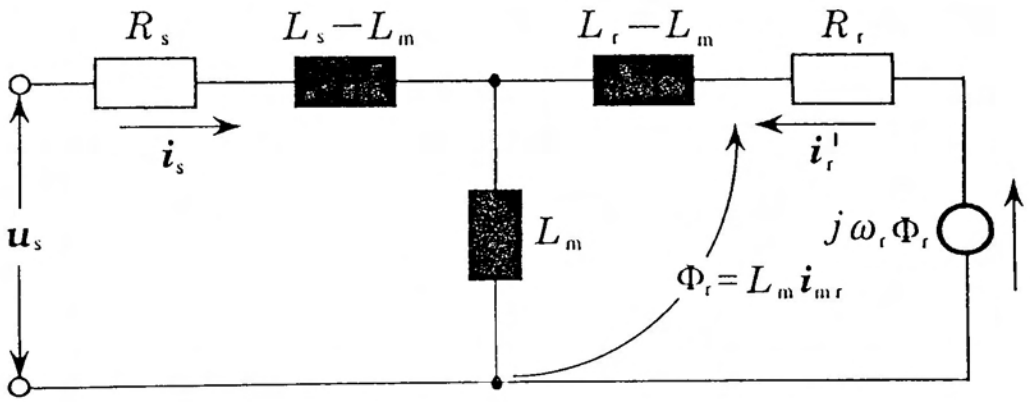

Fig. 4.2. Equivalent circuit in the stationary reference frame.

By eliminating $\boldsymbol{i}_r'$ from (4.1) and (4.2), the same equation as (3.20) is obtained.

$$p\boldsymbol{i}_{mr} = (-\gamma + j\omega_r)\boldsymbol{i}_{mr} + \gamma \boldsymbol{i}_s \tag{4.3}$$

where γ is the inverse of thr rotor time constant,

$$\gamma = R_r/L_r = 1/T_r \ . \tag{4.4}$$

Since it is difficult to detect $\boldsymbol{i}_{mr}$, a magnetizing current estimation is used.

$$p\hat{\boldsymbol{i}}_{mr} = (-\gamma + j\omega_r)\hat{\boldsymbol{i}}_{mr} + \gamma \boldsymbol{i}_s \tag{4.5}$$

Subtracting (4.3) from (4.5), we have

$$p\boldsymbol{e} = (-\gamma + j\omega_r)\boldsymbol{e} \tag{4.6}$$

where

$$\boldsymbol{e} = \boldsymbol{i}_{mr} - \hat{\boldsymbol{i}}_{mr} \ . \tag{4.7}$$

This indicates that the error $\boldsymbol{e}$ asymptotically decreases by $e^{-\gamma t}$. The instantaneous torque in (2.74) is expressed again by

$$T_e = k_t \Im(\boldsymbol{i}_s \boldsymbol{i}_{mr}^*) = k_t |\boldsymbol{i}_s||\boldsymbol{i}_{mr}| \sin\alpha \tag{4.8}$$

where

$$k_t = \frac{3}{2} P \frac{L_m^2}{L_r} \ . \tag{4.9}$$

P is the number of the pole-pairs of thc induction motor, $\Im$ means an imaginary part of a complex number, $(^*)$ means the conjugate of a complex number, and α is the angle between $\boldsymbol{i}_s$ and $\boldsymbol{i}_{mr}$.

4.3 Principle of the vector approximation

The vector approximation method approximates the desirable stator current vector $\boldsymbol{i}_s^\circ$ in the sense of time average by the realizable six current vectors. The phase angle of $\boldsymbol{i}_s^\circ$ is determined with regard to the phase angle of the rotor magnetizing current $\boldsymbol{i}_{mr}$ and the

magnitude of the required torque as follows: where Δt is the calculating time in one cycle of a microprocessor program. The space vector of the rotor magnetizing current is

$$\boldsymbol{i}_{mr} = i_{mr} e^{j\alpha_\mu} \tag{4.10}$$

where the symbol $\boldsymbol{i}_{mr}$ is used instead of $\hat{\boldsymbol{i}}_{mr}$ because of (4.7), i_{mr} is the magnitude and α_μ is the phase angle of $\boldsymbol{i}_{mr}$ with respect to the α-axis in the stationary reference frame. The transformation from the stationary reference frame (α-β) to the rotational reference frame (d-q) for (4.3) gives the following equations:

$$\frac{d}{dt} i_{mr} = \gamma \left(i_{sd} - i_{mr} \right) \tag{4.11}$$

$$\omega_{mr} = \omega_r + \omega_{sl} \tag{4.12}$$

where

$$\omega_{sl} = \gamma \frac{i_{sq}}{i_{mr}} , \tag{4.13}$$

ω_{sl} is slip angular velocity, i_{sd} and i_{sq} are the direct- and the quadrature-axis component of the stator current in the rotational reference frame respectively. It is noted that (4.11) and (4.12) show the same result of (3.14) and (3.15) which are the flux estimation model in the rotor flux oriented reference frame [see Fig. 3.1]. For a digital control system, (4.11) and (4.12) are expressed as follows, assuming that ω_r does not change during a sampling period Δt:

$$i_{mr}(k+1) = i_{mr}(k) e^{-\gamma \Delta t} + i_{sd}(k)(1 - e^{-\gamma \Delta t}) \tag{4.14}$$

$$\omega_{mr}(k) = \omega_r(k) + \omega_{sl}(k) \tag{4.15}$$

where k means $k\Delta t$. Then the phase angle of $\boldsymbol{i}_{mr}$ is obtained as follows:

$$\alpha_\mu(k+1) = \alpha_\mu(k) + \omega_{mr}(k) \Delta t \tag{4.16}$$

Consider, as the controlled variables, both the torque and the magnitude of $\boldsymbol{i}_{mr}$. That is, $|\boldsymbol{i}_s| \sin\alpha$ denoted by i_{sq} is determined by the required torque, and $|\boldsymbol{i}_s| \cos\alpha$ denoted by i_{sd} is determined with regard to i_{mr}. In Fig. 4.1, i_{sd} and i_{sq} are shown as the decomposed vectors of $\boldsymbol{i}_s^o$. Thus, the desired stator current vector $\boldsymbol{i}_s^o$ is given as follows:

$$|\boldsymbol{i}_s^o| \equiv i_s = \sqrt{i_{sd}^2 + i_{sq}^2} \tag{4.17}$$

$$\alpha = \tan^{-1} \frac{i_{sq}}{i_{sd}} \tag{4.18}$$

On the other hand, Fig. 4.3 shows $\boldsymbol{i}_{mr}$, $\boldsymbol{i}_s^o$, and six stator current vectors which can be realized by the CSI drives, so that in this case $\boldsymbol{i}_s^o$ is approximated by $\boldsymbol{i}_{s1}$ and $\boldsymbol{i}_{s2}$ which are applied during the interval Δt_1 and Δt_2 respectively.

Fig. 4.4 shows the sector I in Fig. 4.3. Thus, $\boldsymbol{i}_s^o$ is expressed by the view point of the composition of vectors as follows:

$$\boldsymbol{i}_s^o = \{\frac{\Delta t_1}{\Delta t}\frac{\boldsymbol{i}_{s1}}{|\boldsymbol{i}_{s1}|} + \frac{\Delta t_2}{\Delta t}\frac{\boldsymbol{i}_{s2}}{|\boldsymbol{i}_{s2}|}\}\, i_s \tag{4.19}$$

where $\boldsymbol{i}_s^o$ can be assumed to be constant during one switching cycle Δt because of sufficiently high switching frequency. The content of the parentheses of (4.19) gives the angle α_1 and i_s is the magnitude of $\boldsymbol{i}_s^o$, and Δt_1 and Δt_2 are geometrically calculated as follows [2]:

$$\Delta t_1 = \frac{\sin(\pi/3 - \alpha_1)}{\sin(\pi/3 + \alpha_1)}\Delta t \tag{4.20}$$

$$\Delta t_2 = \Delta t - \Delta t_1 \tag{4.21}$$

For the other sectors the same rules are applied. The phase angle α_p in Fig. 4.3 is obtained as $\alpha_p = \alpha_\mu + \alpha$. If the sector 0 is determined as the first switching state of inverter, by checking the values of $\alpha_p + \pi/6$, the next switching state and α_1 can be obtained.

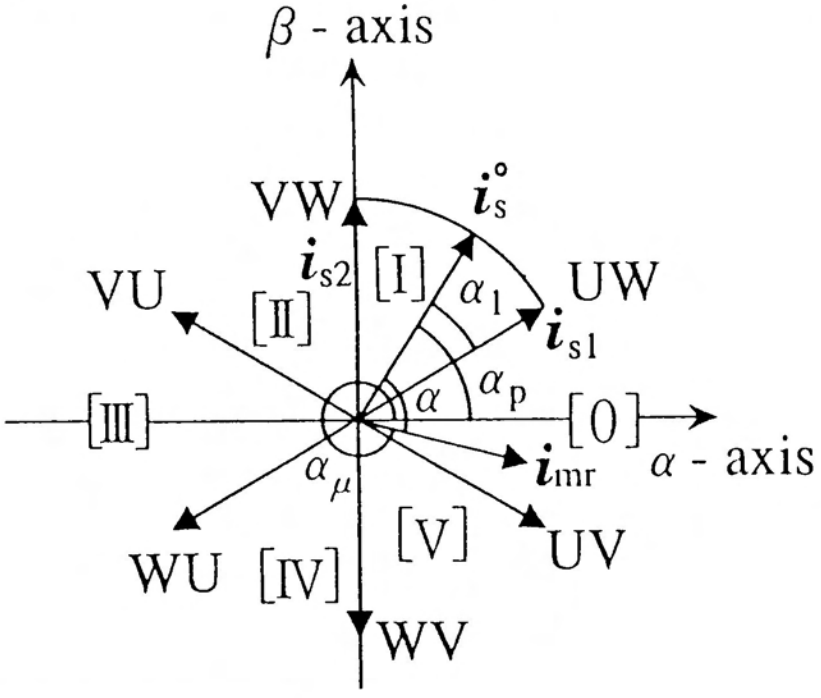

Fig. 4.3. Six realizable current vectors and i_s^o.

Then the switching intervals Δt_1 and Δt_2 are calculated with α_1 from (4.20) and (4.21). Since it is impossible to apply $\boldsymbol{i}_{s1}$ and $\boldsymbol{i}_{s2}$ at the same moment, the composition of vectors is done by time average sense.

The dc link current kept constant as

$$I_{DC} = \frac{\sqrt{3}}{2}\, i_s \,, \tag{4.22}$$

however, is not sufficient to make the composition of the vectors $\boldsymbol{i}_{s1}$ and $\boldsymbol{i}_{s2}$ agree with $\boldsymbol{i}_s^o$. Fig. 4.4 indicates the composed vector on the line between the tips of vectors $\boldsymbol{i}_{s1}$ and $\boldsymbol{i}_{s2}$ does not reach $\boldsymbol{i}_s^o$.

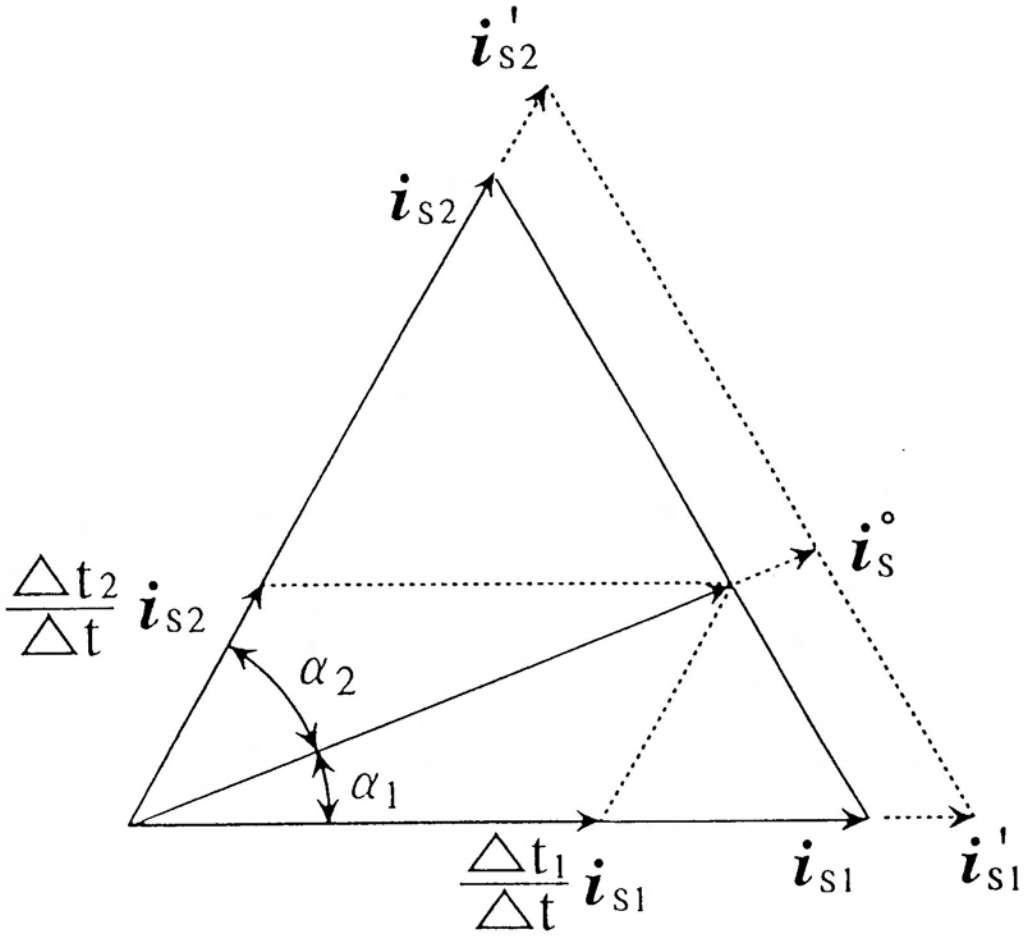

Fig. 4.4. Principle of the vector approximation.

Thus, the dc link current should be controlled so as to

$$I_{DC} = i_s \cos(\pi/6 - \alpha_1) \ . \tag{4.23}$$

In this case, the tip of the composed vector is on the line between the tips of the vectors $\boldsymbol{i}'_{s1}$ and $\boldsymbol{i}'_{s2}$ in Fig. 4.4. Consequently, $\boldsymbol{i}^o_s$ is realizable with the dc link current control.

Then the average torque during Δt is given as follows:

$$\bar{T}_e = \frac{k'_t}{\Delta t} \Im \{ \int_0^{\Delta t_1} \frac{\boldsymbol{i}_{s1}}{|\boldsymbol{i}_{s1}|} \boldsymbol{i}^*_{mr} dt + \int_{\Delta t_1}^{\Delta t} \frac{\boldsymbol{i}_{s2}}{|\boldsymbol{i}_{s2}|} \boldsymbol{i}^*_{mr} dt \} \tag{4.24}$$

where

$$k'_t = k_t \ i_s \ . \tag{4.25}$$

Since Δt is assumed to be sufficiently short, the rotor magnetizing current vector $\boldsymbol{i}_{mr}$ is also considered to be constant for Δt. Thus, (4.24) becomes

$$\bar{T}_e = k'_t \Im \{ (\frac{\Delta t_1}{\Delta t} \frac{\boldsymbol{i}_{s1}}{|\boldsymbol{i}_{s1}|} + \frac{\Delta t_2}{\Delta t} \frac{\boldsymbol{i}_{s2}}{|\boldsymbol{i}_{s2}|}) \boldsymbol{i}^*_{mr} \} = k_t \Im \{ \boldsymbol{i}^o_s \boldsymbol{i}^*_{mr} \} \ . \tag{4.26}$$

From (4.26), the required torque is realized in the sense of the time average. As mentioned above, the main purpose of vector approximation is to control the instantaneous torque arbitrarily. This can be achieved by controlling the stator current arbitrarily. If required, the tip of the current vector can be controlled to have the locus of a circle. In this case, the phase currents are sinusoidal. This fact is confirmed by the simulations and the experiments in Section 4.5.

4.4 System configuration

The experimental system is shown in Fig. 4.5. The capacitors parallel with the induction motor act as smoothing filter of pulsating phase current. The dc generator is coupled with the induction motor as a load which does not appear in Fig. 4.5. The nominal ratings of the main pieces of equipment in the experimental system are listed in Table 4.1. The photos of the experimental system are shown in Figs. 4.6, 4.7, and 4.8 which are the induction motor coupled with the dc generator, the CSI system, and the PC (NEC-PC9801DA) with AD and DA converter, and DSP (NEC-μPD77230). The PC is used for the change of the speed reference value and the control gains. The control algorithm as shown in Fig. 4.9 is executed by using DSP. The computational time is about 0.55 ms for one cycle.

Table 4.1
NOMINAL RATINGS OF EQUIPMENTS

	Induction motor	dc generator
Output	7.5 kw	7.5 kw
No. of poles	4	6
Voltage	200 V ac	220 V dc
Current	27.2 A ac	34.1 A dc
Speed	1740 rpm	1200 rpm
L_r	0.04647 H	
R_r	0.335 Ω	
L_m	0.04557 H	
dc Reactor		
L_d	0.1432 H R_d	0.0495 Ω
Capacitor		
80 μF		

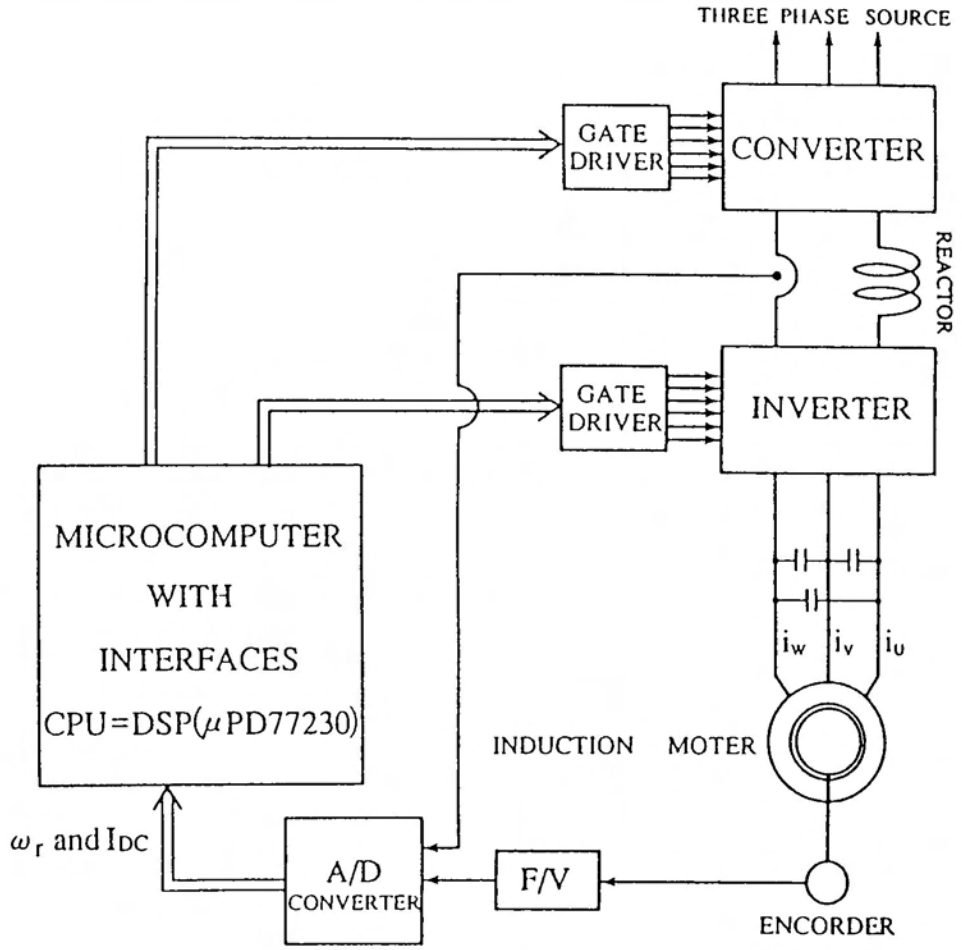

Fig. 4.5. Configuration of the experimental system.

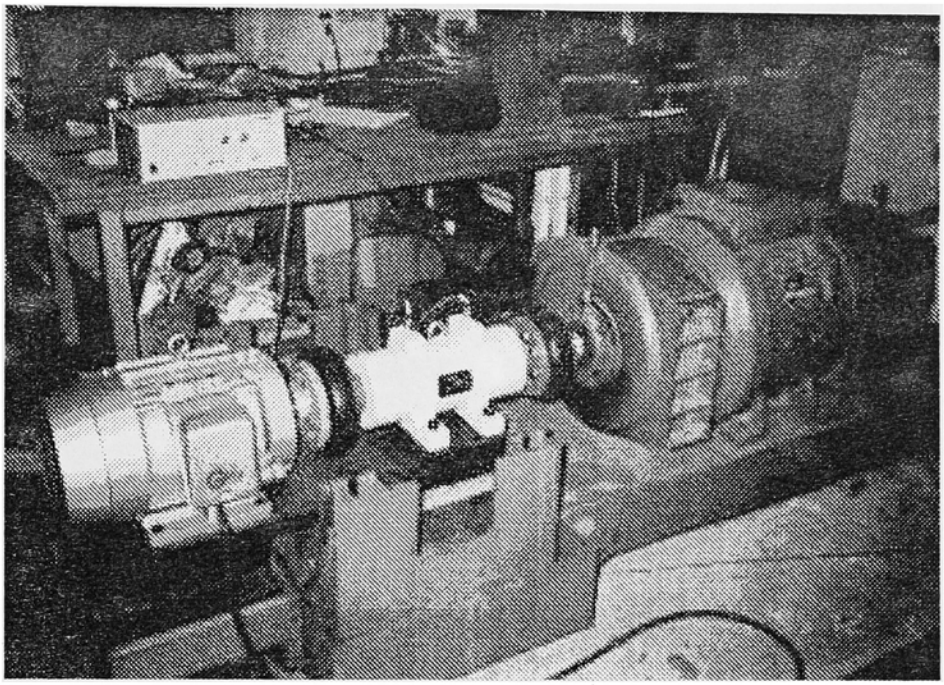

Fig. 4.6. Induction motor coupled with the dc generator.

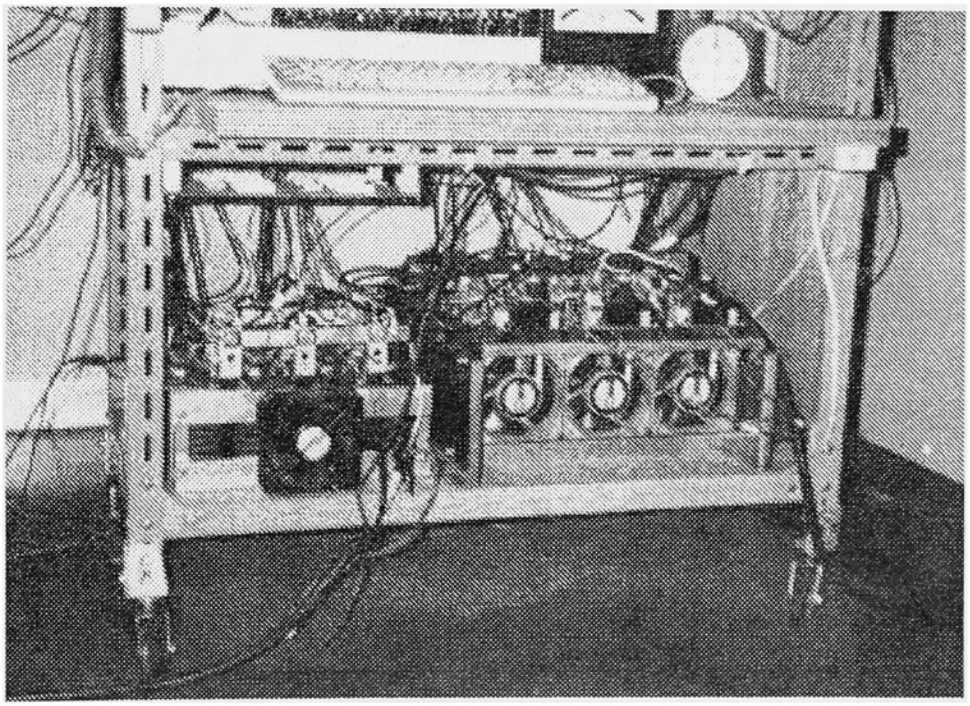

Fig. 4.7. CSI system.

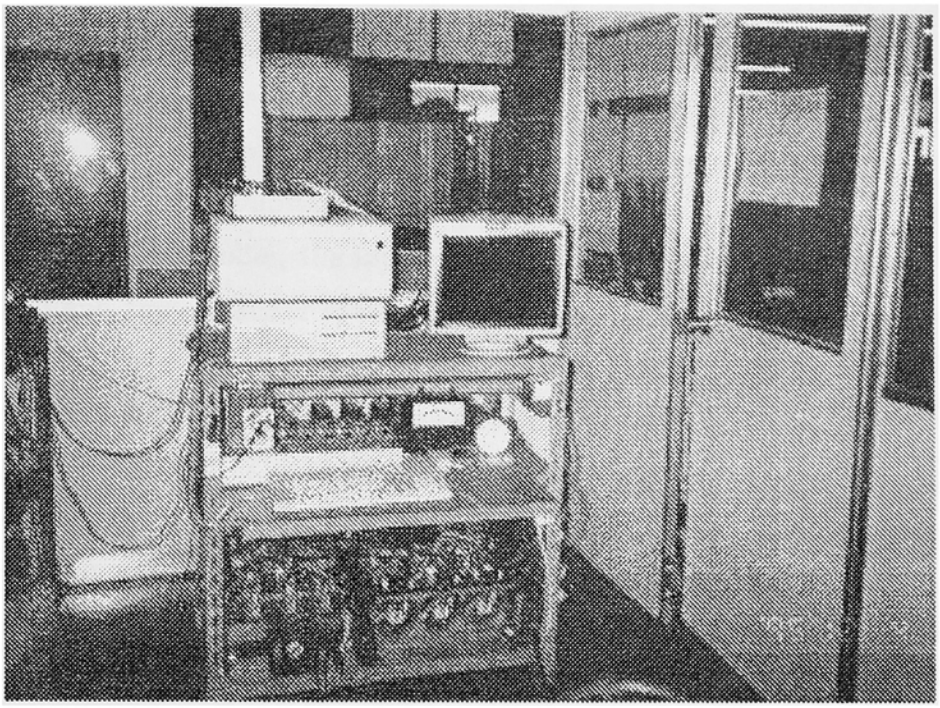

Fig. 4.8. PC (NEC-PC9801DA) with AD and DA converter, and DSP (NEC-μPD77230).

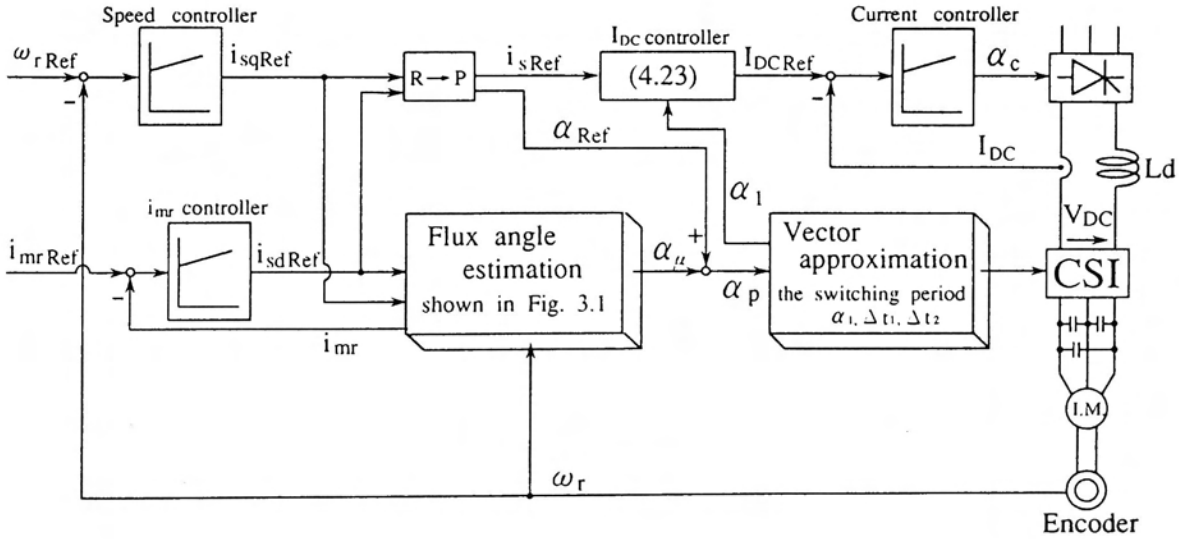

Fig. 4.9. Control algorithm of the vector approximation.

In Fig. 4.9, i_{sdRef} and i_{sqRef} are the reference values of i_{sd} and i_{sq}. The value of i_{sdRef} is obtained as the output of the magnetizing current controller (i.e., the flux controller) the input of which is the error signal between the reference value of the rotor magnetizing current (i_{mrRef}) and the estimated value (i_{mr}), and the value of i_{sqRef} is obtained as the output of the speed controller, the input of which is the error signal between the reference speed (ω_{rRef}) and the measured speed (ω_r). Then i_{sdRef} and i_{sqRef} are converted into the polar coordinates by a rectangular-to-polar converter (R→P), and thus the outputs of the (R→P) are the magnitude of the reference stator current (i_{sRef}) together with the phase angle α_{Ref} as shown in (4.17) and (4.18), moreover, i_{sdRef} and i_{sqRef} are inputs to the flux estimation shown in (4.14), (4.15), and (4.16). The outputs of the flux estimation are the rotor magnetizing current i_{mr} and the phase angle α_μ. The reference dc link current (I_{DCRef}) is determined by the dc link current controller shown in (4.23) with i_{sRef} and α_1 which is found in the vector approximation unit. Fig. 4.10 shows the flowchart diagram of the vector approximation.

In the converter, the maintain the required dc link current specified by I_{DCRef}, there is a current control loop where I_{DCRef} is compared with the measured dc link current I_{DC} and the obtained error signal between I_{DCRef} and I_{DC} serves as input to the current controller. The output of the current controller is used to control the firing angle of the converter. For the controllers of the rotor magnetizing current, the speed, and the current controller, the PI or PID control law is used as follows:

The magnetizing current control law:

$$i_{sdRef} = K_{mp}(i_{mrRef} - i_{mr}(k)) + K_{mi}\Delta t \sum (i_{mrRef} - i_{mr}(k)) \tag{4.27}$$

The speed control law:

$$i_{sqRef} = K_{wp}(\omega_{rRef} - \omega_r(k)) + K_{wi}\Delta t \sum (\omega_{rRef} - \omega_r(k)) \tag{4.28}$$

The current control law:

$$\begin{aligned} \frac{E_d}{E_{dmax}} &= K_{ip}(I_{DCRef} - I_{DC}(k)) + K_{ii}\Delta t \sum (I_{DCRef} - I_{DC}(k)) \\ &+ K_{id}\frac{(I_{DC}(k-1) - I_{DC}(k))}{\Delta t} \end{aligned} \tag{4.29}$$

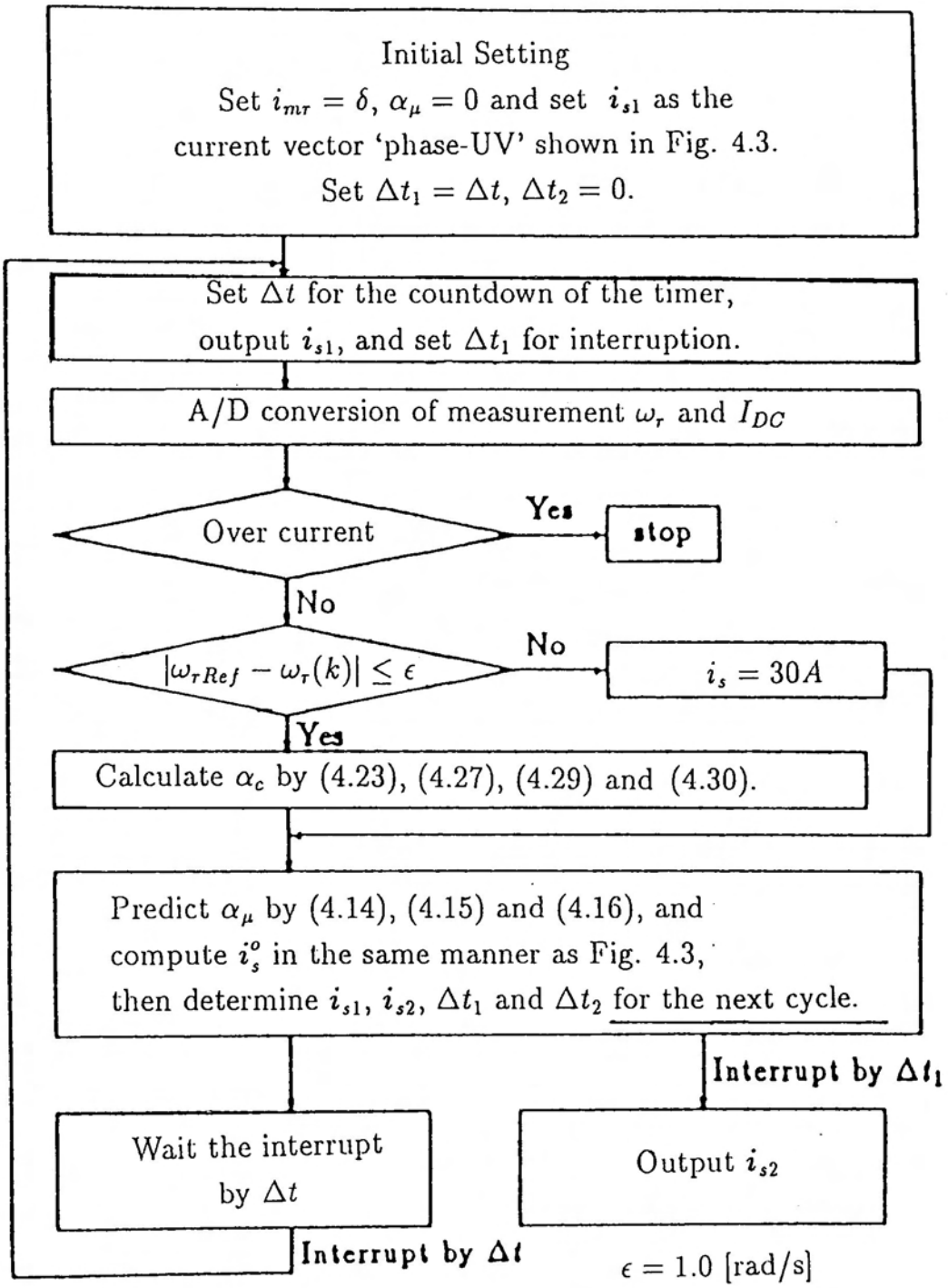

Fig. 4.10. Flowchart diagram of the vector approximation.

where K_{mp}, K_{mi}, K_{wp}, K_{wi}, K_{ip}, K_{ii}, and K_{id} are the control gains, and E_d denotes the output voltage of the converter and E_{dmax} denotes the maximum value of the output voltage of the converter. The firing angle of the converter (α_c) is obtained as follows:

$$\alpha_c = \cos^{-1} \frac{E_d}{E_{dmax}} \tag{4.30}$$

Because the average quantitiy E_d are calculated over the firing period of a phase voltage as follows:

$$\begin{aligned} E_d &= \frac{3}{\pi} \int_{\frac{\pi}{3}+\alpha_c}^{\frac{2\pi}{3}+\alpha_c} \sqrt{2} E_{rms} \sin\theta_f d\theta_f \\ &= \frac{3\sqrt{2}}{\pi} E_{rms} [-\cos\theta]_{\frac{\pi}{3}+\alpha_c}^{\frac{2\pi}{3}+\alpha_c} \\ &= \frac{3\sqrt{2}}{\pi} E_{rms} \cos\alpha_c \\ &\equiv E_{dmax} \cos\alpha_c \end{aligned} \tag{4.31}$$

where E_{rms} and θ_f is the root mean square value and the phase angle of the line-to-line voltage respectively.

4.5 Verification of the vector approximation

4.5.1 Simulation results

Fig. 4.11(a) and (b) shows computer simulation results of the steady state locus of the tip of the stator current vector ((a)) and the corresponding phase current ((b)) by the vector approximation method with the dc link current kept constant (the left) and with the instantaneous control of the dc link current (the right). It should be noted that the smoothing filter is assumed for both cases. The dark parts in Fig. 4.11(a) mean the limiting area of the vector approximation method to avoid such conditions that Δt_1 or Δt_2 is less than the turn-off time of the GTO's (see (4.20)(4.21)). The minimum of Δt_1 or Δt_2 is set to the greater value than the turn-off time of the GTO's, which is 50 μsec in the experiments. This effect appears as the jumps of the waveform in Fig. 4.11(b).

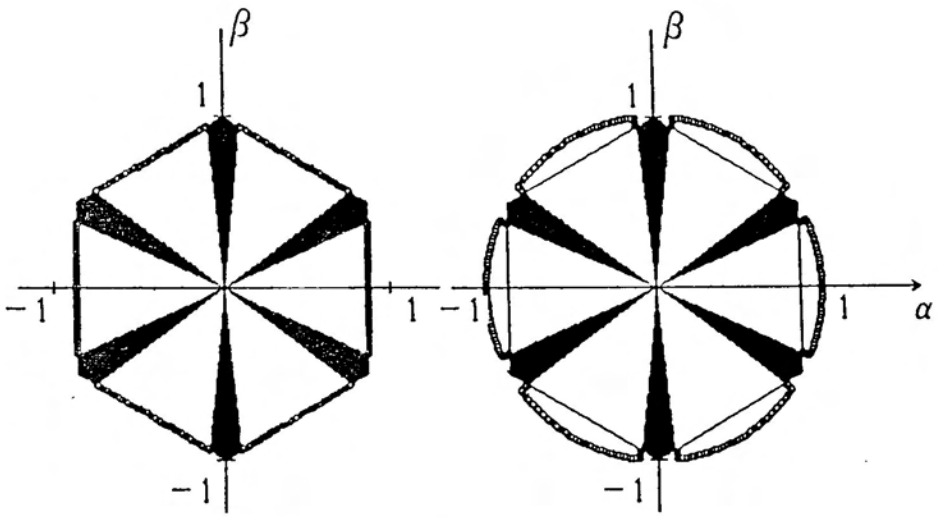

(a)

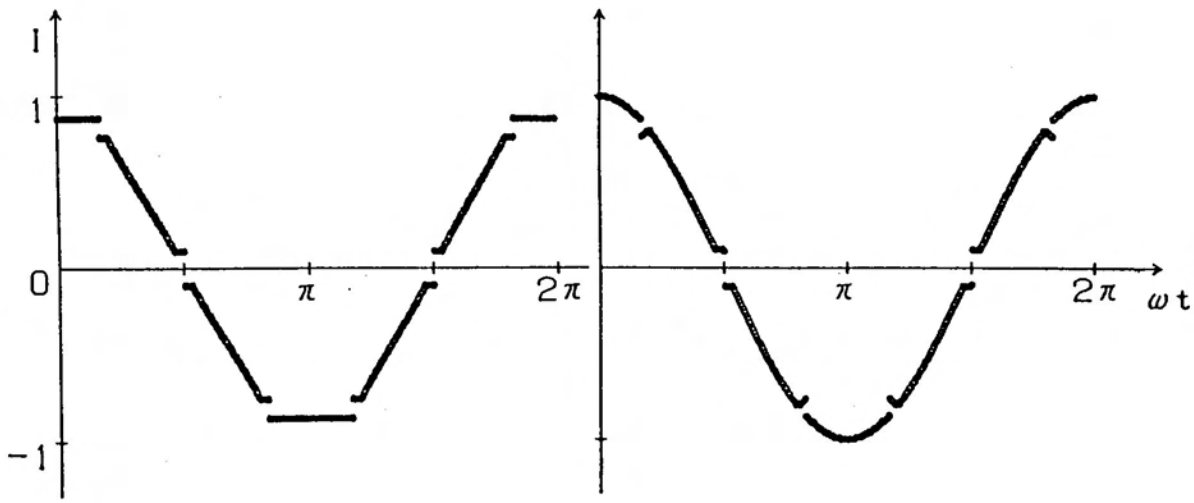

(b)

Fig. 4.11. Simulation results by vector approximation with the constant dc link current and with the dc link current control. (a) Locus of the tip of the stator current vector. (b) Corresponding stator phase current.

In the experiment, this vector approximation is executed in about 1.8 kHz, whereas dc link current control by the converter is done in 360 Hz. This shows that dc link current control can be controlled once in every five execution of the vector approximation and then for effective approximation of the desirable stator current vector the operating frequency seems to be lower than 10 Hz. Therefore, the vector approximation method seems to be suitable for medium and large-size drives with low speed where dc link current control becomes much effective.

4.5.2 Experimental results

Fig. 4.12 and Fig. 4.13 show the experimental results of the phase current by the vector approximation method with the dc link current kept constant and with the instantaneous control of the dc link current respectively. The capacitor as a smoothing filter is determined experimentally to be 80 μF, since the increase of the size of capacitors does not affect the current waveform. As mentioned above, the experiments are done at low speed condition. The results in Fig. 4.12 and Fig. 4.13 almost coincide with the simulation results, which show the validity of our assumptions with respect to vector approximation. Moreover, the phase current waveform is improved by the vector approximation with the instantaneous control of the dc link current.

In the extended PWM method [20] using the auxiliary two GTO's in the inverter, the zero vector is used for shaping of sinusoidal current waveform in addition to six realizable stator vectors in Fig. 4.2. The constant dc link current control with the zero vector method is sufficient to do shaping in steady state, while the purpose of the vector approximation is to control i_s^o not only in steady state but also in transient state as mentioned before. Thus the vector approximation method is independent on the PWM method with the zero vector method. In the established PWM method, the modulation index m is defined as the rate of the amplitued of modulating wave against the amplitude of carrier wave, and can be determined in the range between 0 and 1. In this case, the rms output current I_s of the inverter is given by

$$I_s \cong \frac{m \cdot I_{DC}}{\sqrt{2}}. \tag{4.32}$$

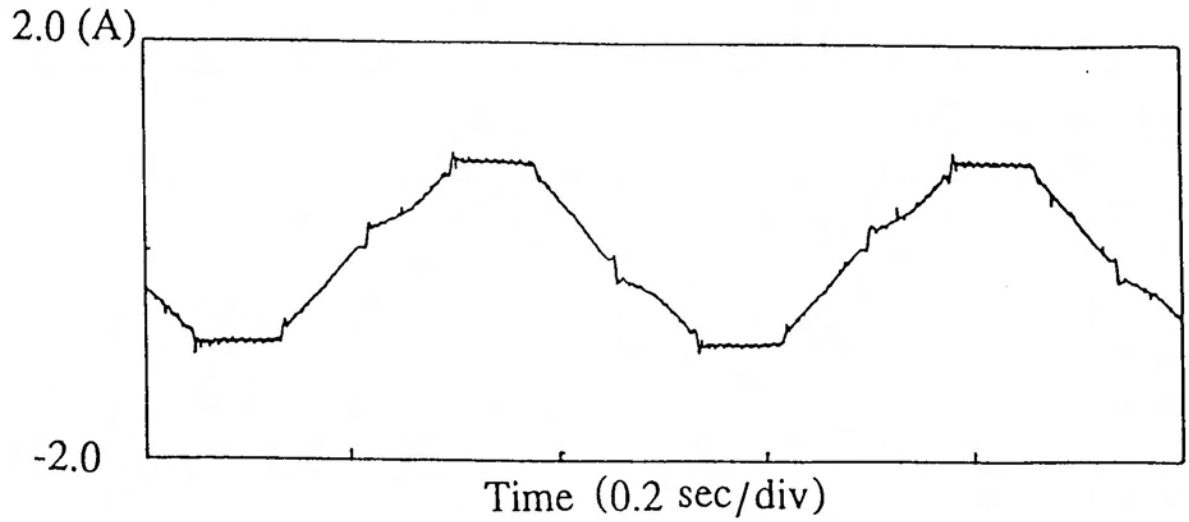

Fig. 4.12. Experimental waveform of the phase current by vector approximation with the constant dc link current.

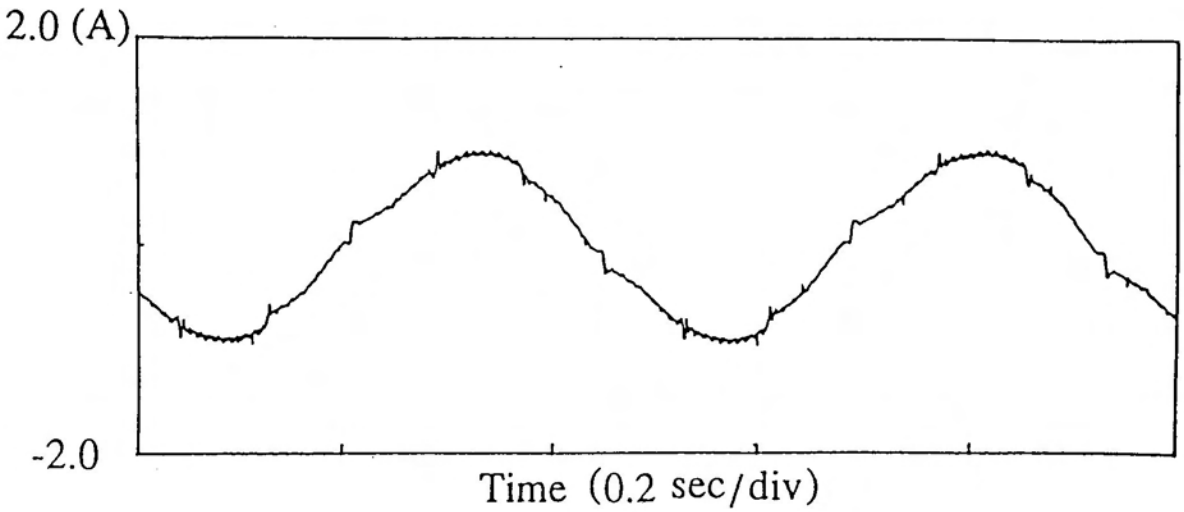

Fig. 4.13. Experimental waveform of the phase current by vector approximation with the dc link current control.

This leads to the maximum modulation index in the case of vector approximation method theoretically:

$$m = \frac{2}{\sqrt{3}} \tag{4.33}$$

This means that the vector approximation method can produce the output current of inverter about 15 % more than the established PWM method. This is also one of advantages of the vector approximation method.

Figs. 4.14, 4.15, and 4.16 show the responses of the starting, the acceleration, and the deceleration, where the speed reference is changed from 0 to 120 rpm, from 120 to 240 rpm, and from 240 to 120 rpm in each test of the responses. The values of the control gains are as follows:

(at the transient state)

$$K_{mp} = 9.0 \ , \ K_{mi} = 3.0 \cdot 10^{-2}$$
$$i_{sRef} \text{ is limited to 30 A.}$$
$$K_{ip} = 1.75 \cdot 10^{-2}, \ K_{ii} = 1.5 \cdot 10^{-4}, \ K_{id} = 1.2 \cdot 10^{-2}$$

(at the steady state)

$$K_{mp} = 7.0, \ K_{mi} = 2.2 \cdot 10^{-2}$$
$$K_{wp} = 3.5, \ K_{wi} = 1.3 \cdot 10^{-4}$$
$$K_{ip} = 2.5 \cdot 10^{-2}, \ K_{ii} = 1.2 \cdot 10^{-4}, \ K_{id} = 1.8 \cdot 10^{-5}$$

These values are determined empirically. The results indicate that the speed control of the CSI drive induction motor by the vector approximation is possible, and the instantaneous torque control by controlling the current is also achieved even at the transient state.

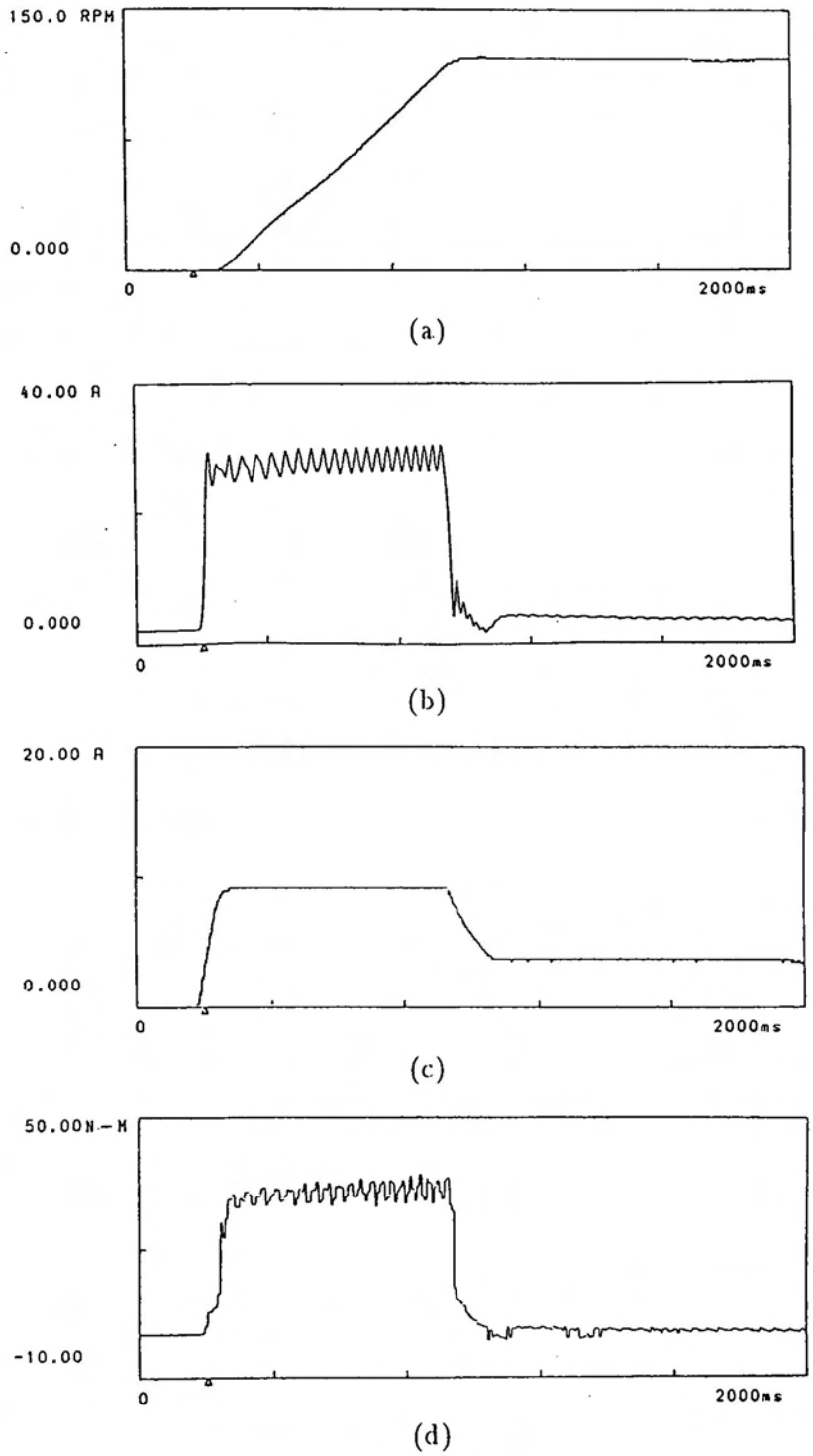

Fig. 4.14. Step response (in the starting) of (a) speed, (b) dc link current, (c) rotor magnetizing current, and (d) torque.

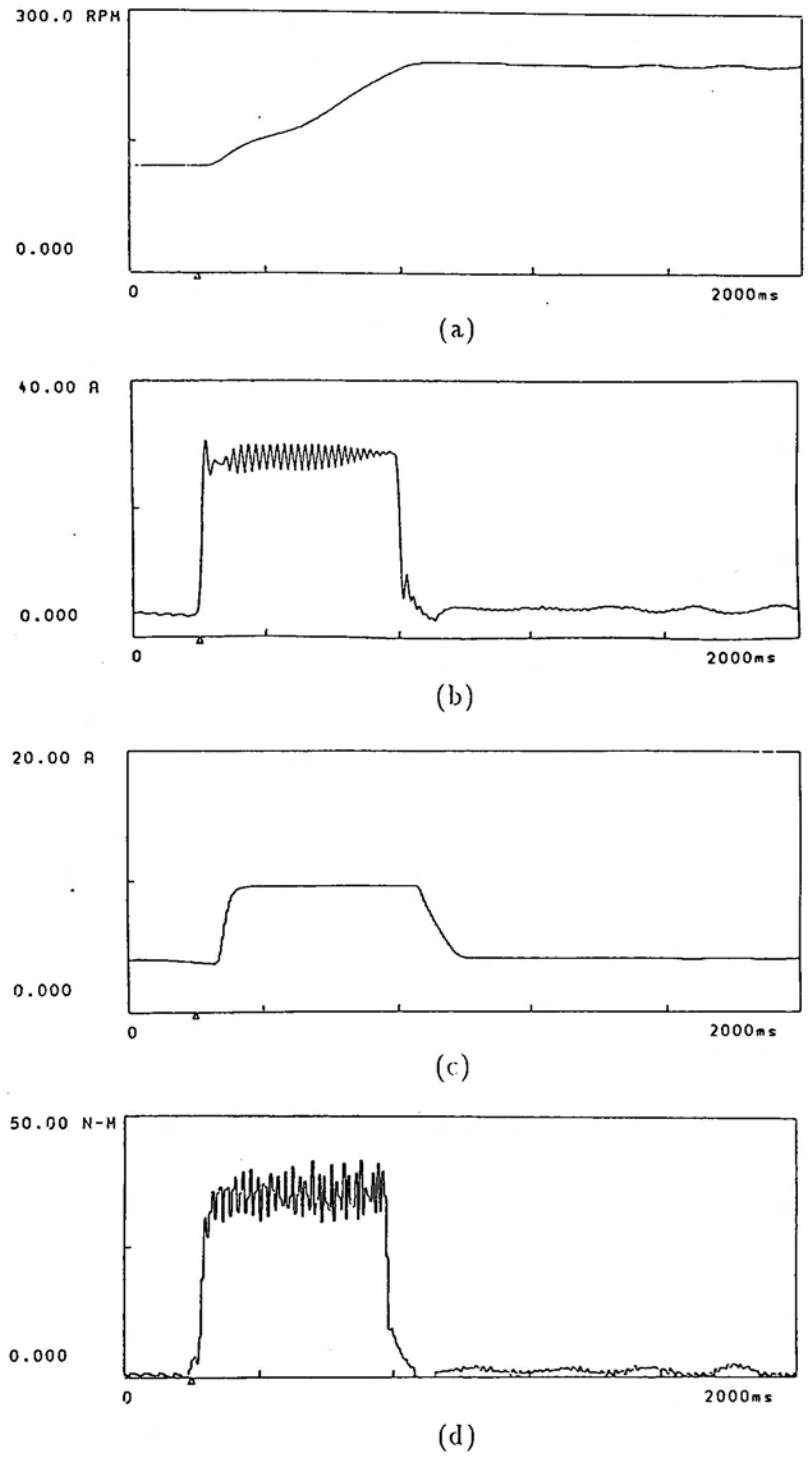

Fig. 4.15. Step response (in the acceleration) of (a) speed, (b) dc link current, (c) rotor magnetizing current, and (d) torque.

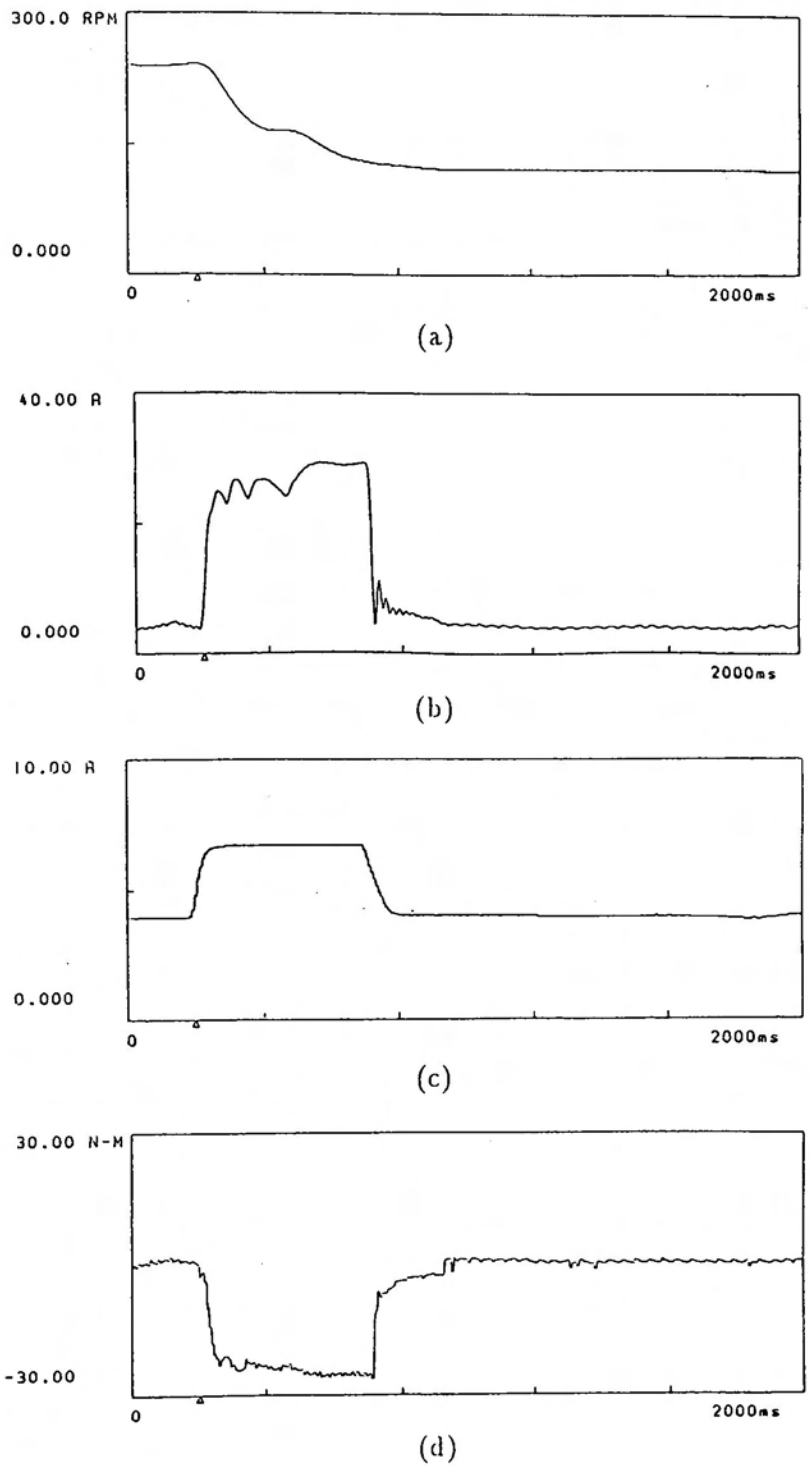

Fig. 4.16. Step response (in the deceleration) of (a) speed, (b) dc link current, (c) rotor magnetizing current, and (d) torque.

4.6 Conclusion

In the CSI drive induction motor system, the control theory and the vector approximation method of the stator current have been shown, and the application of this theory and the method for the speed control have been examined experimentally. Theoretically, the direct torque control is possible by this method. The torque ripple could be decreased, which has been proved by the sinusoidal phase current waveform. For the precise control of torque, however, it is important to know the precise value of rotor parameters in γ of (4.4) since the value of γ affects not only the magnetizing current estimation error but also the estimation of the torque magnitude directly. In the next chapter, these problems are discussed.

Chapter 5

Parameter adaptation and torque control

5.1 Introduction

As mentioned in the preceding section, for the precise torque control by the vector approximation, it is important to know the precise values of the rotor parameters since the value of the rotor parameters affect not only the magnetizing current estimation error but also the estimation of the torque magnitude directly.

In the vector approximation, the phase angle of the desirable stator current is determined by utilizing the rotor flux angle, which is computed by the on-line simulation (i.e., (4.14) and (4.15)) of the mathematical equation of the induction motor. If the rotor flux angle is estimated correctly, the magnetizing and torque component of the stator current can be decoupled precisely and so controlled independently by the field oriented control [5]. However, the field oriented control is influenced by the rotor parameter variation, that is, the rotor resistance varies with temperature and the inductance is a function of main flux saturation. To solve these problems, many identification or adaptation schemes have already been proposed [6]~[13]. An off-line automated identification scheme [6] and an adaptation scheme with using the reactive power transferred to the rotor [7] have been evaluated as effective methods. With different approaches, model reference adaptive systems (MRAS) [8], [9] have been presented. The adaptive system estimates the error between the outputs of

the motor and the reference model, and tunes the adaptive gains or parameters to decrease the error to zero. As a result, the degradation of torque control by the rotor resistance variation is observed in [8] and [9]. On the other hand, the selection of flux level with regard to magnetic saturation effects was discussed in [10]. Saturated dynamic models of induction motors with the field oriented control have been proposed in [11]~[13].

This chapter shows a parameter adaptation system containing a magnetic saturation model and a MRAS, which is a method to solve both resistance and inductance variation problems as follows: The vector approximation system shown in the preceding chapter newly includes a magnetic saturation model which is obtained by a novel off-line identification method, and on-line compensation of magnetizing inductance becomes possible. This system also includes MRAS using the model reference error of torque to compensate rotor resistance variation. Consequently, this method makes it possible to asymptotically track the actual torque and estimate accurate rotor resistance without the influence of inductance variation, which occurs at the field weakening or the optimal efficiency control. The effectiveness of the parameter adaptation system is verified by the simulation and the experiments.

5.2 Rotor parameter identification

This section shows an identification method for the values of k_t and γ off-line. The value of k_t is the torque coefficient and the value of γ is the inverse rotor time constant. The changes of k_t and γ cause errors in the torque and in the phase angle of $\boldsymbol{i}_s^o$. In order to control the torque precisely, it is necessary to know the characteristics of the parameter variation. The identification algorithm and the experimental results are shown in this section.

5.2.1 Definition of the torque coefficient and the rotor time constant

Assume a sinusoidal phase current at the steady state condition. Since $i_{mr} = i_{sd}$ from (4.11) at the steady state, (4.17) is replaced with

$$i_s = \sqrt{i_{mr}^2 + i_{sq}^2} \tag{5.1}$$

and the electrical magnetic torque T_e is from (4.8)

$$T_e = k_t i_{mr} i_{sq} \ . \tag{5.2}$$

Parameter k_t and γ are expressed as

$$k_t = \frac{3}{2} P \frac{L_m^2}{L_r} = \frac{3}{2} P \frac{L_m^2}{l_r + L_m}, \qquad \gamma = \frac{R_r}{L_r} = \frac{R_r}{l_r + L_m} \tag{5.3}$$

where l_r is the rotor leakage inductance.

5.2.2 Identification of the inertia and the viscous friction

The identification of k_t and γ requires the value of the torque, and then the torque measurement is required. The torque can be measured by measuring the motor speed; in this case, the inertia and the viscous friction must be known in advance. Therefore the identification of the inertia and the viscous friction should be done by the experimental test which is called the run-down test. The run-down test is described in the following. The rotor angular velocity is related to the torque as

$$\frac{J}{P} \frac{d\omega_r}{dt} + \frac{f_v}{P} \omega_r = T_e - T_L. \tag{5.4}$$

where J is the moment of inertia, f_v is the viscous friction, P is the number of the pole-pairs, and T_L is the load torque. When the dc generator is used as a load, the load torque is expressed as

$$T_L = k_v \omega_r + T_0 \tag{5.5}$$

where

$$k_v = \frac{K_m^2}{R_a + R_L} \ , \tag{5.6}$$

T_0 is Coulomb torque, K_m comes from the dc generator load, R_a is the armature resistance, and R_L is the resistance connected with the output of the dc generator. By substitution of (5.5) into (5.4), (5.4) becomes

$$J \frac{d\omega_r}{dt} + (f_v + P k_v) \omega_r = P(T_e - T_0) \ . \tag{5.7}$$

Considering the power system switched off where $T_e = 0$, (5.7) becomes

$$J \frac{d\omega_r}{dt} + (f_v + P k_v) \omega_r = -P T_0 \ . \tag{5.8}$$

By solving (5.8), the rotor angular velocity is obtained as follows:

$$\omega_r(t) = \omega_r(0)e^{-\frac{t}{\tau}} - \frac{PT_0}{f_v + Pk_v}(1 - e^{-\frac{t}{\tau}}) \tag{5.9}$$

where

$$\tau = \frac{J}{f_v + Pk_v}. \tag{5.10}$$

For the run-down test, the drive is accelerated to some initial speed $\omega_r(0)$, where the drive power is switched off so that the plant is decelerating due to the load torque with the speed measured as a function of time, $\omega_r(t)$. In the response of the deceleration, τ is determined by the time where the speed is 36% of the initial speed $\omega_r(0)$. The two kinds of the load should be prepared by changing the value of R_L. Assume the measured time constant τ_1 and τ_2 which are determined in the test when R_L is set to R_{L1} and R_{L2} respectively. From the obtained data, (5.6), and (5.10), the inertia and the viscous friction are obtained as follows:

$$f_v = \frac{PK_m^2(\tau_1(R_a + R_{L2}) - \tau_2(R_a + R_{L1}))}{(R_a + R_{L1})(R_a + R_{L2})(\tau_2 - \tau_1)} \tag{5.11}$$

$$J = \frac{PK_m^2\tau_1\tau_2(R_{L2} - R_{L1})}{(R_a + R_{L1})(R_a + R_{L2})(\tau_2 - \tau_1)} \tag{5.12}$$

where K_m is determined by the induced voltage V_a (i.e., EMF) and the rotor angular velocity ω_r as follows:

$$K_m = \frac{PV_a}{\omega_r} \tag{5.13}$$

In the test, V_a should also be measured.

5.2.3 Identification of the torque coefficient and the rotor time constant

The proposed identification method uses the experimental system shown in Fig. 5.1, which is the vector approximation system for identification. Let i_s and α_{Ref} be the reference input to the system shown in Fig. 5.1. Then the reference value of i_{mr} is written as

$$i_{mrRef} = i_s \cos\alpha_{Ref} . \tag{5.14}$$

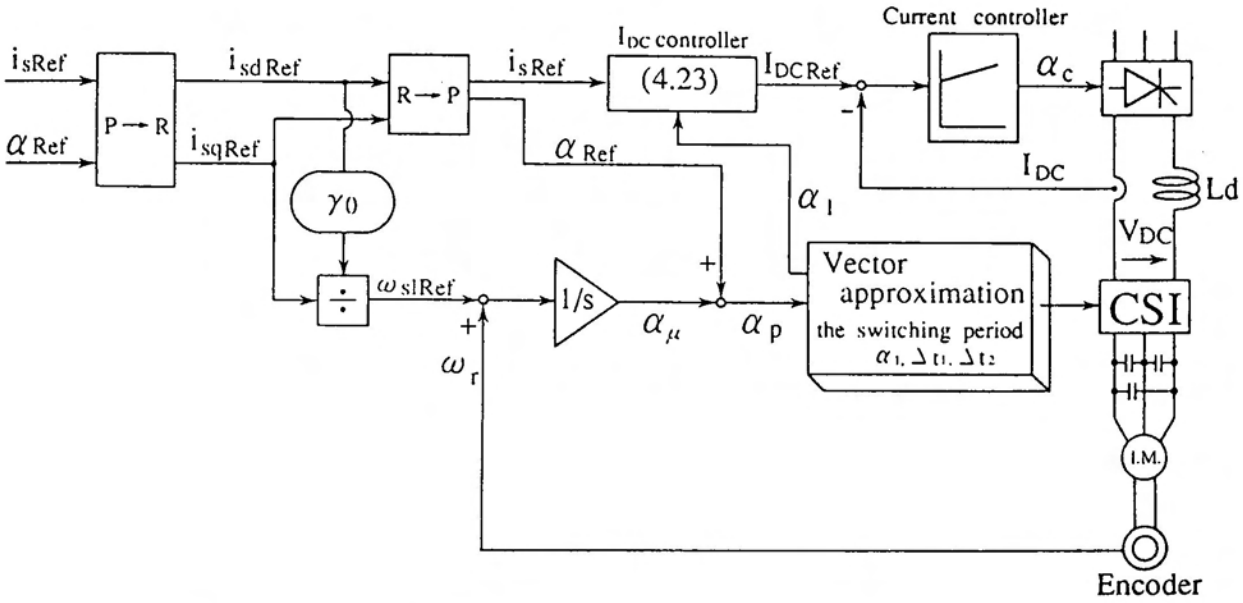

Fig. 5.1. Control system of the identification.

The real α does not coincide with α_{Ref}, if the value of γ is not correctly set. Then i_{mr} does not coincide with the reference value. In the magnetic unsaturation region, however, if for constant i_s the maximum torque $T_{e(max)}$ is obtained for some α, then from (5.1) and (5.2), i_{mr} is equal to i_{sq}, so that the actual α should be 45° against α_{Ref}. Thus, torque coefficient k_t is identified as follows:

$$k_t = \frac{2}{i_s^2} T_{e(max)} \tag{5.15}$$

In order to measure the torque, the following relation is used at no-load and low speed condition:

$$T_e = J\frac{d\omega_r}{dt} + T_0 \tag{5.16}$$

where J is the moment of inertia obtained in the preceding section, and T_0 is Coulomb torque. The Coulomb torque can be computed by experimental measurements with the two kinds of constant stator current i_s and i_s' when $J\frac{d\omega_r}{dt}$ and $J\frac{d\omega_r'}{dt}$ are measured. In fact, if k_t is constant, T_0 is given from (5.15) and (5.16) as

$$T_0 = \frac{i_s^2 J\frac{d\omega_r'}{dt} - i_s'^2 J\frac{d\omega_r}{dt}}{i_s'^2 - i_s^2} . \tag{5.17}$$

Thus, k_t can be identified. The identification of γ is done by the following theory. Assume α_{Ref} gives maximum torque under the condition of constant i_s, such α_{Ref} would be confirmed experimentally by changing α_{Ref} and measuring the torque. As mentioned above, the actual α should be 45° so that $i_{mr} = i_{sq}$. Thus, γ is identified with the nominal value, γ_0 and α_{Ref} as follows:

$$\gamma = \omega_{sl}\frac{i_{mr}}{i_{sq}} = (\gamma_0\frac{i_s \sin\alpha_{Ref}}{i_s \cos\alpha_{Ref}})\frac{i_{mr}}{i_{sq}} = \gamma_0 \tan\alpha_{Ref} \tag{5.18}$$

Thus, the term $(\tan\alpha_{Ref})$ in (5.18) represents the deviation rate of actual γ from the nominal value.

In the magnetic saturation region, however, α at the maximum torque may become larger than 45°. In order to identify k_t in the magnetic saturation region, the following algorithm is needed.

i) For each i_s, $T_{e(max)}$ is obtained experimentally.

ii) Assume initially that $\alpha = 45°$ for $T_{e(max)}$, and so $i_{mr} = i_s \cos 45°$. Then the relation

$$k_t = f(i_{mr}) \tag{5.19}$$

is obtained using

$$T_e = k_t\, i_{mr} i_{sq} = k_t\, \frac{i_s^2}{2} \sin 2\alpha \tag{5.20}$$

but since α is not necessarily 45°, we can make a relation between T_e and α using (5.19) and (5.20), for example Fig. 5.2.

iii) From Fig. 5.2, for each i_s we have α which gives $T_{e(max)}$ and T_e when $\alpha = 45°$, and again k_t's when $\alpha = 45°$ are obtained with the torque deviation ratio from $T_{e(max)}$. Then we have another relation of such a type as (5.19).

iv) Repeat ii), iii) until the graph of $k_t = f(i_{mr})$ does not change.

Fig. 5.3 shows the result by using the above algorithm, that is, starting from the initial graph (the upper dots), the algorithm converges to the final graph (the solid curve) by 5 times iteration. If the rotor leakage inductance l_r is assumed to be constant, the magnetizing inductance L_m is obtained by (5.3). This relation is shown in Fig. 5.4.

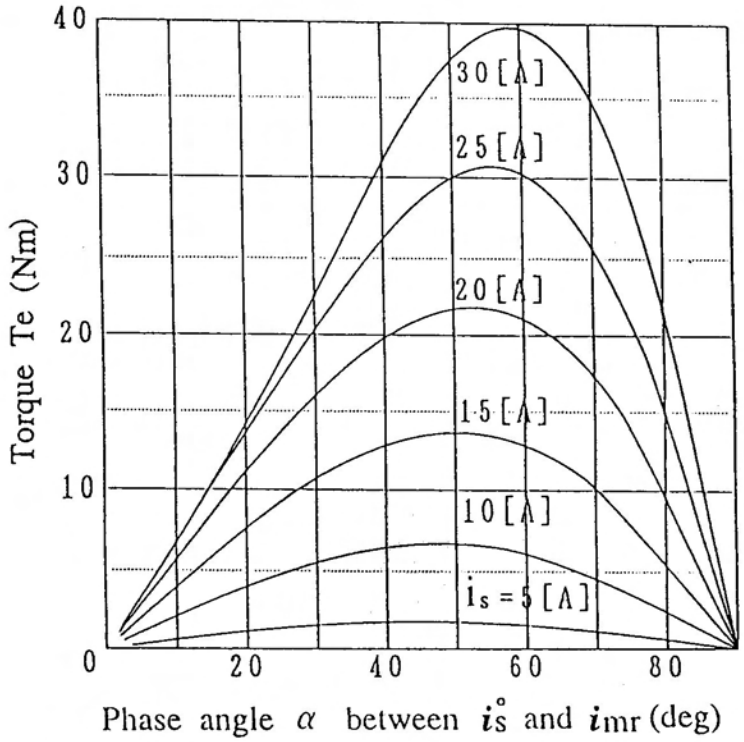

Fig. 5.2. Relation between T_e and α.

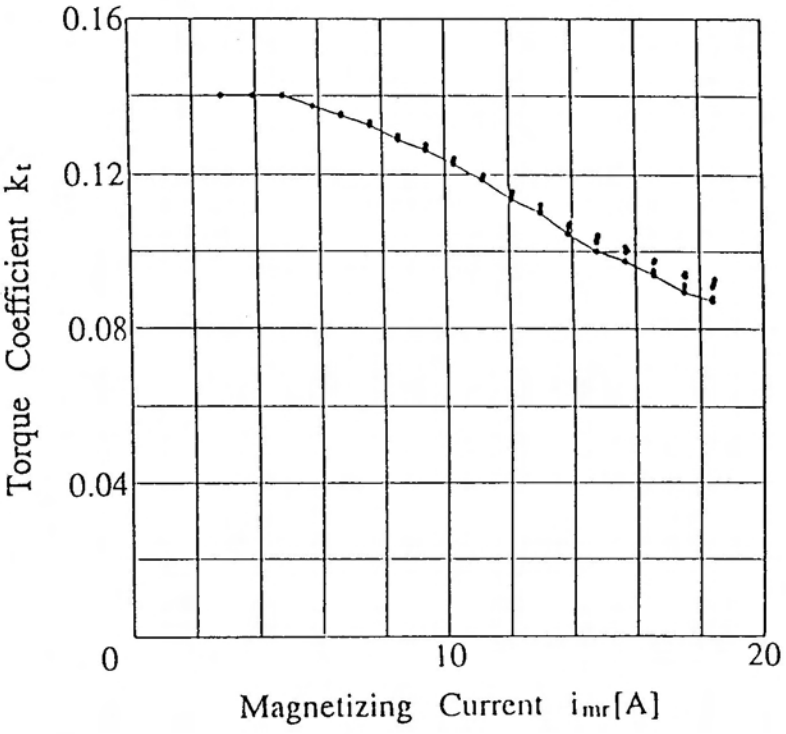

Fig. 5.3. Experimental identification results of k_t.

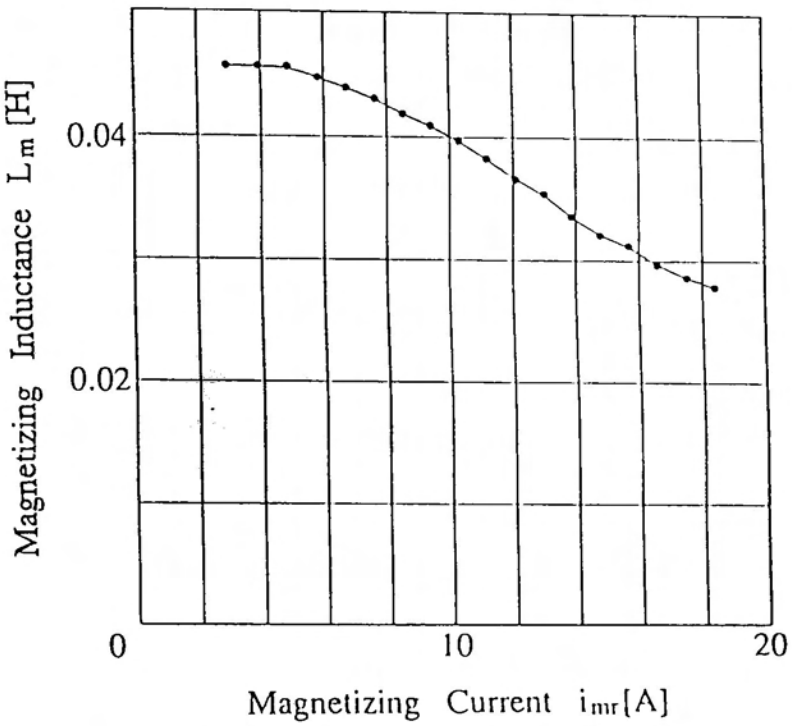

Fig. 5.4. Experimental identification results of L_m.

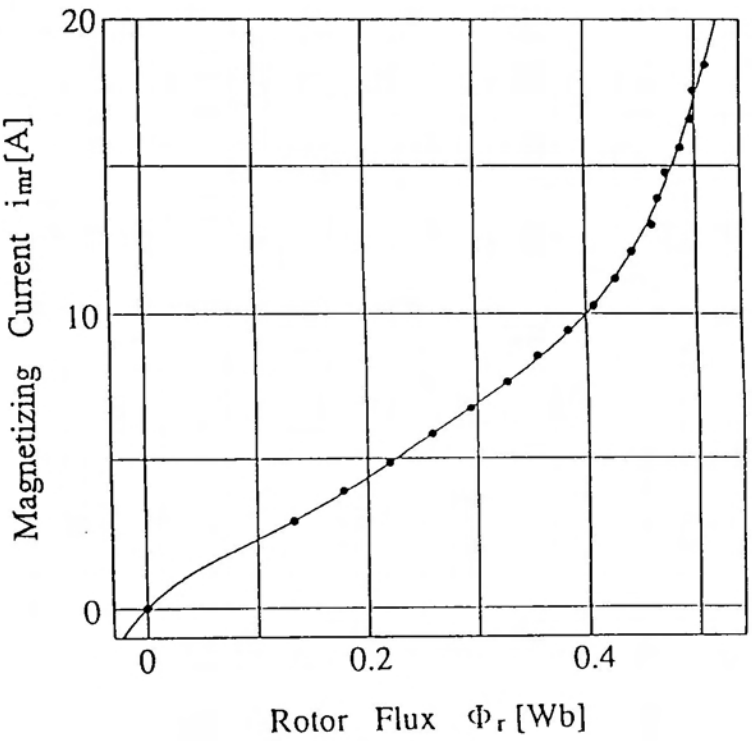

Fig. 5.5. Inverse magnetizing curve obtained by the identification results.

From Fig. 5.4, an inverse magnetizing curve is obtained as shown in Fig. 5.5. The relation shown in Fig. 5.5 is used to identify the rotor resistance. In the experimental system, a look-up table is used to produce the relation of Fig. 5.5.

5.3 Rotor parameter adaptation

This section shows a novel method of the rotor parameter adaptation containing a magnetic saturation model and a MRAS. The rotor parameter γ changes by temperature and magnetic saturation. For precise torque control by the parameter adaptation, both variation effects have to be considered. Therefore, the MRAS is designed so as to make the error of the torque magnitude zero and estimate the precise rotor resistance at the constant flux. The saturation model obtained in the preceding section compensates inductance variation for flux change. As a result, the proposed parameter adaptation works at any constant flux level.

5.3.1 Design of the adaptation law

Compensation of the rotor resistance variation which depends on the temperature is considered here. In order to do an on-line adaptation, the MRAS approach utilizing the model reference error of torque is applied, which assures stability. Now, notice equations (4.3) and (4.5) which are the actual and the mathematical models respectively. Since (4.3) and (4.5) are nonlinear, they are linearized by Taylor expansion around an operating point after each variable is expressed by the d-q components in the rotational reference frame.

$$p\begin{bmatrix}\Delta i_{mrd}\\ \Delta i_{mrq}\end{bmatrix} = \begin{bmatrix}-\gamma_0 & \omega_{sl0}\\ -\omega_{sl0} & -\gamma_0\end{bmatrix}\begin{bmatrix}\Delta i_{mrd}\\ \Delta i_{mrq}\end{bmatrix} + \begin{bmatrix}0\\ 1\end{bmatrix}\frac{i_{sq0}}{L_r}\Delta R_r \tag{5.21}$$

$$p\begin{bmatrix}\Delta \hat{i}_{mrd}\\ 0\end{bmatrix} = \begin{bmatrix}-\hat{\gamma}_0 & \omega_{sl0}\\ -\omega_{sl0} & -\hat{\gamma}_0\end{bmatrix}\begin{bmatrix}\Delta \hat{i}_{mrd}\\ 0\end{bmatrix} + \begin{bmatrix}0\\ 1\end{bmatrix}\frac{i_{sq0}}{L_r}\Delta \hat{R}_r \tag{5.22}$$

where $(_0)$ denotes the operating points, $(\hat{\ })$ denotes estimated values, and L_r is assumed not to change, since it is not necessary to consider the saturation effect in the small range around the operating point. Subtracting (5.22) from (5.21), the state error equation can be

obtained as follows [15]:

$$p\begin{bmatrix}\Delta i_{mrd}-\Delta\hat{i}_{mrd}\\ \Delta i_{mrq}\end{bmatrix}=\begin{bmatrix}-\hat{\gamma}_0 & \omega_{sl0}\\ -\omega_{sl0} & -\hat{\gamma}_0\end{bmatrix}\begin{bmatrix}\Delta i_{mrd}-\Delta\hat{i}_{mrd}\\ \Delta i_{mrq}\end{bmatrix}+\begin{bmatrix}0\\1\end{bmatrix}\frac{i_{sq0}}{L_r}(\Delta R_r-\Delta\hat{R}_r) \tag{5.23}$$

where estimated rotor parameter is assumed to converge to the actual value at the operating points, that is, $\hat{\gamma}_0=\gamma_0$.

In the same way, the linearized torque equation around an operating point are expressed from (4.8) as follows:

$$\begin{aligned}\Delta T_e = {} & k_t\left[(i_{sq0}+\Delta i_{sq0})(i_{mrd0}+\Delta i_{mrd})\right.\\ & \left.-(i_{sd0}+\Delta i_{sd0})(i_{mrq0}+\Delta i_{mrq})\right] \qquad (5.24)\\ \Delta\hat{T}_e = {} & k_t(i_{sq0}+\Delta i_{sq0})(\hat{i}_{mrd0}+\Delta\hat{i}_{mrd}) \qquad (5.25)\end{aligned}$$

Subtracting (5.25) from (5.24), the torque error between the actual and the mathematical models are

$$\Delta T_e-\Delta\hat{T}_e=k_t\left[i_{sq0}(\Delta i_{mrd}-\Delta\hat{i}_{mrd})-i_{sd0}\Delta i_{mrq}\right] \tag{5.26}$$

where $i_{mrq0}=0$, $\Delta i_{sq}\Delta i_{mrd}$, $\Delta i_{sq}\Delta\hat{i}_{mrd}$ and $\Delta i_{sd}\Delta\hat{i}_{mrq}$ are omitted due to negligible small values. From (5.23) and (5.26), the transfer function from the rotor resistance estimation error $(\Delta R_r-\Delta\hat{R}_r)$ to the output $(\Delta T_e-\Delta\hat{T}_e)$ is obtained as follows:

$$\begin{aligned}\mathbf{G}(s) &= \frac{\Delta T_e-\Delta\hat{T}_e}{\Delta R_r-\Delta\hat{R}_r}\\ &= K_t\frac{i_{sd0}i_{sq0}\left[s+\hat{\gamma}_0\{1-(i_{sq0}/i_{sd0})^2\}\right]}{s^2+2\hat{\gamma}_0 s+\hat{\gamma}_0^2\{1+(i_{sq0}/i_{sd0})^2\}} \qquad (5.27)\end{aligned}$$

where

$$K_t=-k_t/L_r\ . \tag{5.28}$$

Thus, the adaptation law for $\Delta\hat{R}_r$ must be determined so that $(\Delta T_e-\Delta\hat{T}_e)$ converges to zero. This means $\Delta\hat{R}_r$ converges to ΔR_r. In many cases, the adaptation law is chosen according to Popov's hyperstability theorem [16][17]; however, in our case the adaptation law can be linear as follows:

$$\Delta\hat{R}_r=(K_P+K_I/s)(\Delta T_e-\Delta\hat{T}_e)V_{sign} \tag{5.29}$$

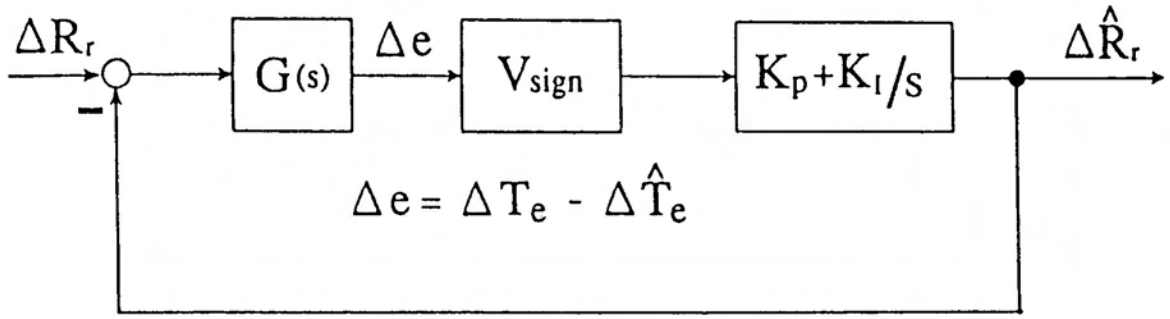

Fig. 5.6. Rotor resistance adaptation block diagram.

where K_P and K_I are the adaptive gains. From (5.27) and (5.29), the transfer function from ΔR_r to $\Delta \hat{R}_r$ is

$$\frac{\Delta \hat{R}_r}{\Delta R_r} = \frac{K_t V_{sign} i_{sd0} i_{sq0} [s + \hat{\gamma}_0 \{1 - (i_{sq0}/i_{sd0})^2\}] (sK_P + K_I)}{s^3 + as^2 + bs + c} \tag{5.30}$$

where

$$\begin{aligned} a &= 2\hat{\gamma}_0 + K_t V_{sign} i_{sd0} i_{sq0} K_P \\ b &= K_t V_{sign} i_{sd0} i_{sq0} K_I + K_t V_{sign} i_{sd0} i_{sq0} \hat{\gamma}_0 \{1 - (i_{sq0}/i_{sd0})^2\} K_P \\ &\quad + \hat{\gamma}_0^2 \{1 + (i_{sq0}/i_{sd0})^2\} \\ c &= K_t V_{sign} i_{sd0} i_{sq0} \hat{\gamma}_0 \{1 - (i_{sq0}/i_{sd0})^2\} K_I \ . \end{aligned} \tag{5.31}$$

Fig. 5.6 shows the block diagram of the adaptation.

For the stability of the system, a, b, and c should be positive and $ab - c > 0$ by the Routh-Hurwitz condition. V_{sign}, K_P and K_I are thus determined. That is, V_{sign} is the sign function as follows:

$$V_{sign} = \begin{cases} \text{i)} & \text{if} \quad i_{sq0} \geq 0 \text{ and } |i_{sq0}| \geq i_{sd0} \quad \text{then} \quad 1 \\ \text{ii)} & \text{if} \quad i_{sq0} \geq 0 \text{ and } |i_{sq0}| < i_{sd0} \quad \text{then} \quad -1 \\ \text{iii)} & \text{if} \quad i_{sq0} < 0 \text{ and } |i_{sq0}| \geq i_{sd0} \quad \text{then} \quad -1 \\ \text{iv)} & \text{if} \quad i_{sq0} < 0 \text{ and } |i_{sq0}| < i_{sd0} \quad \text{then} \quad 1 \end{cases} \tag{5.32}$$

In the case i) and iii) of (5.32), K_P and K_I are determined as

$$0 \ < \ K_P < \frac{2\hat{\gamma}_0}{i_{sd0} |K_t i_{sq0}|}$$

$$0 < K_I < \frac{2\hat{\gamma}_0 - i_{sd0}|K_t i_{sq0}|K_P}{i_{sd0}|K_t i_{sq0}|} \times \frac{\hat{\gamma}_0^2\{1+(i_{sq0}/i_{sd0})^2\} - \hat{\gamma}_0 i_{sd0}|K_t i_{sq0}|K_P\{1-(i_{sq0}/i_{sd0})^2\}}{2\hat{\gamma}_0 - i_{sd0}|K_t i_{sq0}|K_P - \hat{\gamma}_0\{1-(i_{sq0}/i_{sd0})^2\}} \tag{5.33}$$

while in the case ii) and iv) of (5.32), K_P and K_I can be determined as

$$K_P > 0, \quad K_I > 0 \, . \tag{5.34}$$

5.3.2 Adaptation with the saturation model

In the adaptation mentioned above, the inductance variation has not been considered yet. The inductance variation depends on i_{mr}, and i_{mr} depends on i_{sd}. Assume i_{sd} changes stepwise, then i_{mr} can be considered to be the piecewise constant compared with the resistance variation which depends on temperature. From (4.3), the d-axis equation can be rewritten as

$$p\left(\frac{L_r}{R_r} i_{mr}\right) + i_{mr} = i_{sd} \tag{5.35}$$

where L_r and R_r denote actual values. Let L_{r0} and R_{r0} denote the nominal value of L_r and R_r respectively, then we have from (5.35),

$$\frac{1}{\gamma_0} p\left(\frac{L_r}{L_{r0}} i_{mr}\right) = \frac{R_r}{R_{r0}}\left(i_{sd} - i_{mr}\right) \, . \tag{5.36}$$

In order to take the saturation into consideration, (5.36) is used instead of (4.11) as follows. The rotor leakage inductance l_r is so small compared with L_r and L_m that the following relation can be assumed:

$$\frac{L_m}{L_{m0}} = \frac{L_r}{L_{r0}} \tag{5.37}$$

where L_{m0} denotes the nominal value of L_m. Thus, the modified rotor flux angle estimation for α_μ can be obtained with the adaptation and the saturation model by (4.15), (4.16), (5.29) and (5.36). These are shown in Fig. 5.7, where the estimated rotor resistance is used.

This method has a drawback only in the following case. When the flux level changes, and the inductance changes, the adaptation may not work correctly because the inductance value is assumed to be the constant in (5.29) and (5.36). However, once the flux level is steady at any operating point, the correct inductance value is informed to the adaptation system indirectly from the saturation model.

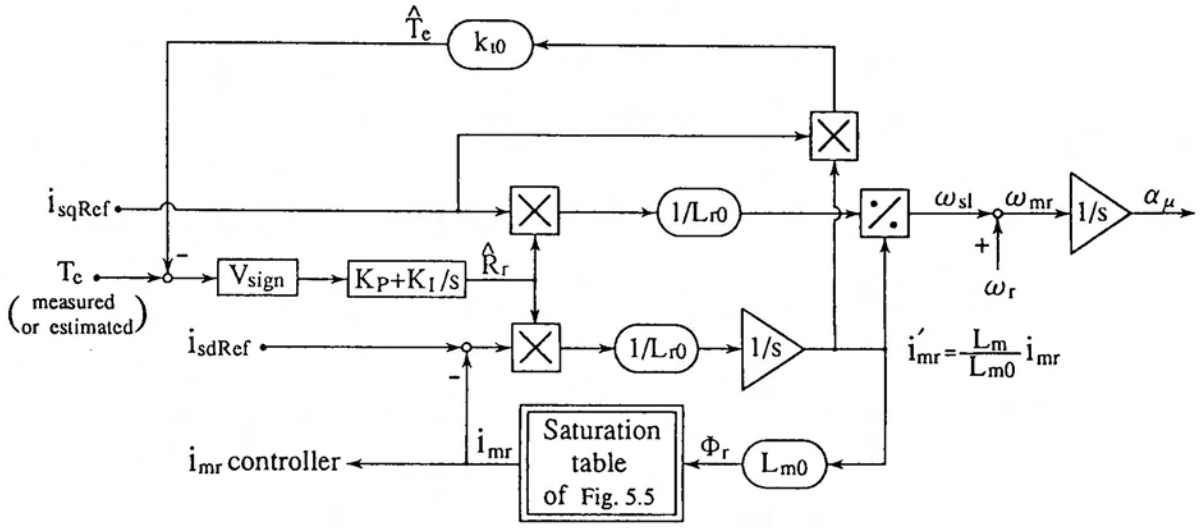

Fig. 5.7. Flux angle estimation with the adaptation and the saturation model.

This adaptation system can estimate rotor resistance correctly at each constant level of flux. In (5.29), the torque of the mathematical model is calculated with $i'_{mr}(=\frac{L_m}{L_{m0}}i_{mr})$ as shown in Fig. 5.7.

$$\hat{T}_e = k_{t0} i'_{mr} i_{sq} \tag{5.38}$$

where k_{t0} is the nominal value of the torque coefficient. It can be seen that i'_{mr} compensates the inductance variation. On the other hand, the actual torque can be obtained by the measurement by a torque detector [15] or the estimation with dc link power [18]. For the torque estimation at the steady state, the feature of CSI may be useful. That is assuming no power loss in the inverter, the power into and out of the inverter is identical [19]. In this case, torque is expressed as follows:

$$T_e = 3[(2/3)V_{DC}I_{DC} - R_s|\boldsymbol{i}_s|^2]/\omega_i \tag{5.39}$$

where V_{DC} is the inverter input voltage, R_s is the stator resistance and ω_i is the stator synchronous angular velocity. The measuring dc link power seems to be much simpler than measuring the inverter output. $|\boldsymbol{i}_s|$ and ω_i can be obtained with each reference value. However, since some power losses which are regarded due to the switching losses and smoothing filters are certain to exist, the power efficiency of the inverter should be measured beforehand.

5.4 System configuration

The control algorithm of the proposed system in the preceding section is shown in Fig. 5.8. The difference from Fig. 4.9 is the flux angle estimation block which includes the magnetic saturation model shown in Fig. 5.5 and the MRAS using the model reference error of torque to compensate rotor resistance variation. The proposed method is verified by the simulation and the experiments in the next section. The experimental system is shown in Section 4.4. The control algorithm as shown in Fig. 5.8 is executed by using DSP (NEC-μPD77230). The computational time is about 0.55 ms for one cycle.

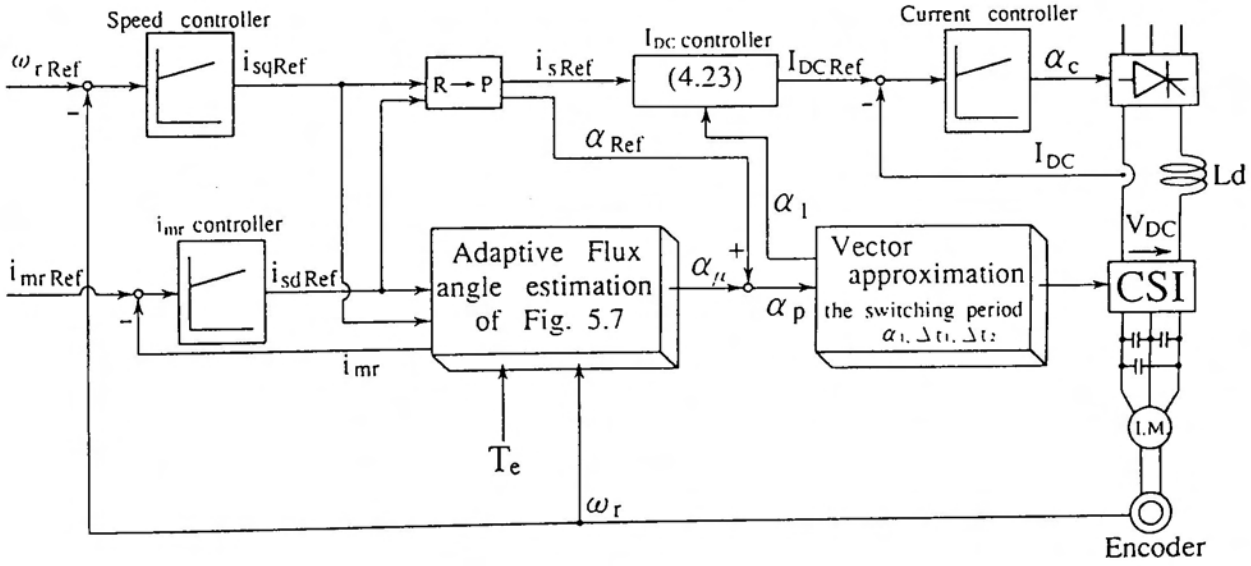

Fig. 5.8. Control algorithm of the vector approximation with the parameter adaptation.

5.5 Verification of the parameter adaptation

5.5.1 Simulation results

Fig. 5.9 evaluates the rotor parameter variation effects on the vector approximation system by the computer simulation, where the rotor speed is 120 rpm at the steady state, the reference magnetizing current i_{mr} is 10 A, the load torque is 6.0 Nm (about 20 % of the rated torque) and the machine nominal parameters are set to the ratings of the experimental system as shown in Table 4.1. If the rotor resistance of the machine model is increased with step-change 50% more than the nominal value, while the rotor resistance set in the control part is still the nominal value, then the stator current in Fig. 5.9(a) changes from the solid line to the dashed line. The solid line shows the stator current in the case that the machine model's rotor resistance does not change from the nominal value. It can be seen how the phase and amplitude deviate from the ideal behavior. Fig. 5.9(b) shows the error of α between the actual and the reference. Since α is the angle between $\boldsymbol{i}_s$ and $\boldsymbol{i}_{mr}$, torque must be also influenced. It can be understood apparently from (4.8). Fig. 5.9(c) shows the reference torque by the dashed line and the actual one by the solid line.

Next the parameter adaptation proposed in Section 5.3 is tested under the introduced condition in Fig. 5.9. Fig. 5.10(a) shows the estimated rotor resistance by MRAS and the actual rotor resistance in the machine model, where both of them are indicated with the dashed and solid line respectively. The estimated rotor resistance converges to the actual one within 0.8 seconds. This convergence time is seems to be sufficiently fast because the real rotor resistance varys slowly due to the slow variation of temperature. In Fig. 5.10(b), the stator current is shown by the dashed line, where it should be noticed that the amplitude is compensated for the same time as the rotor resistance convergence. Fig. 5.10(c) shows the error of α between the actual and the reference, and Fig. 5.10(d) shows the reference torque and the actual one as well as Figs. 5.9(b) and (c). The error of α and the deviation of the reference torque from the actual one are also corrected with the rotor resistance convergence.

These simulation results evaluate the parameter variation effects to the system and the necessity of the parameter compensation, and then the rotor resistance adaptation also shows the capability of precise torque control.

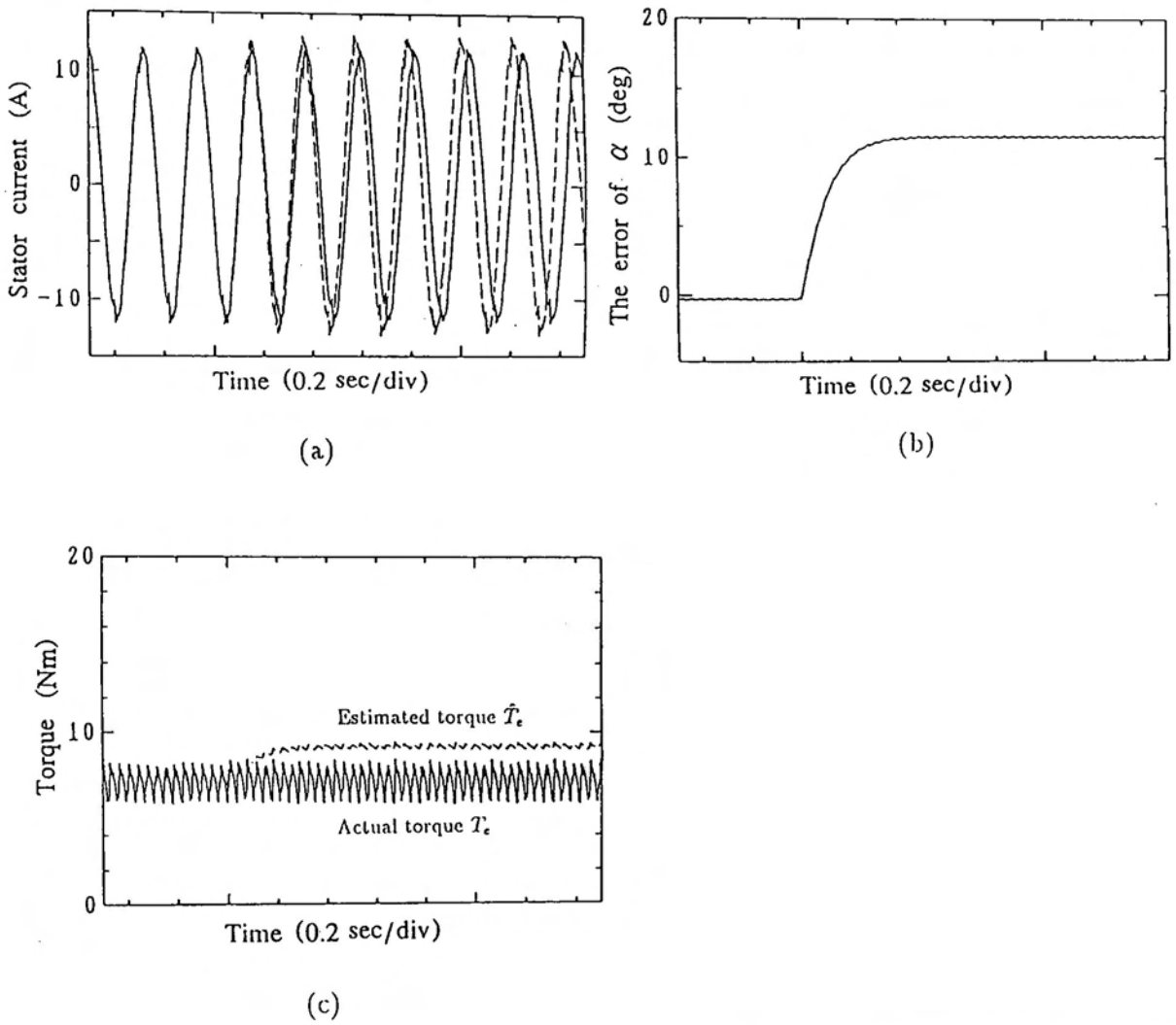

Fig. 5.9. Evaluation of rotor parameter variation effects. (a) Stator current waveform. (b) Error of α between the actual and reference. (c) Reference and actual torque.

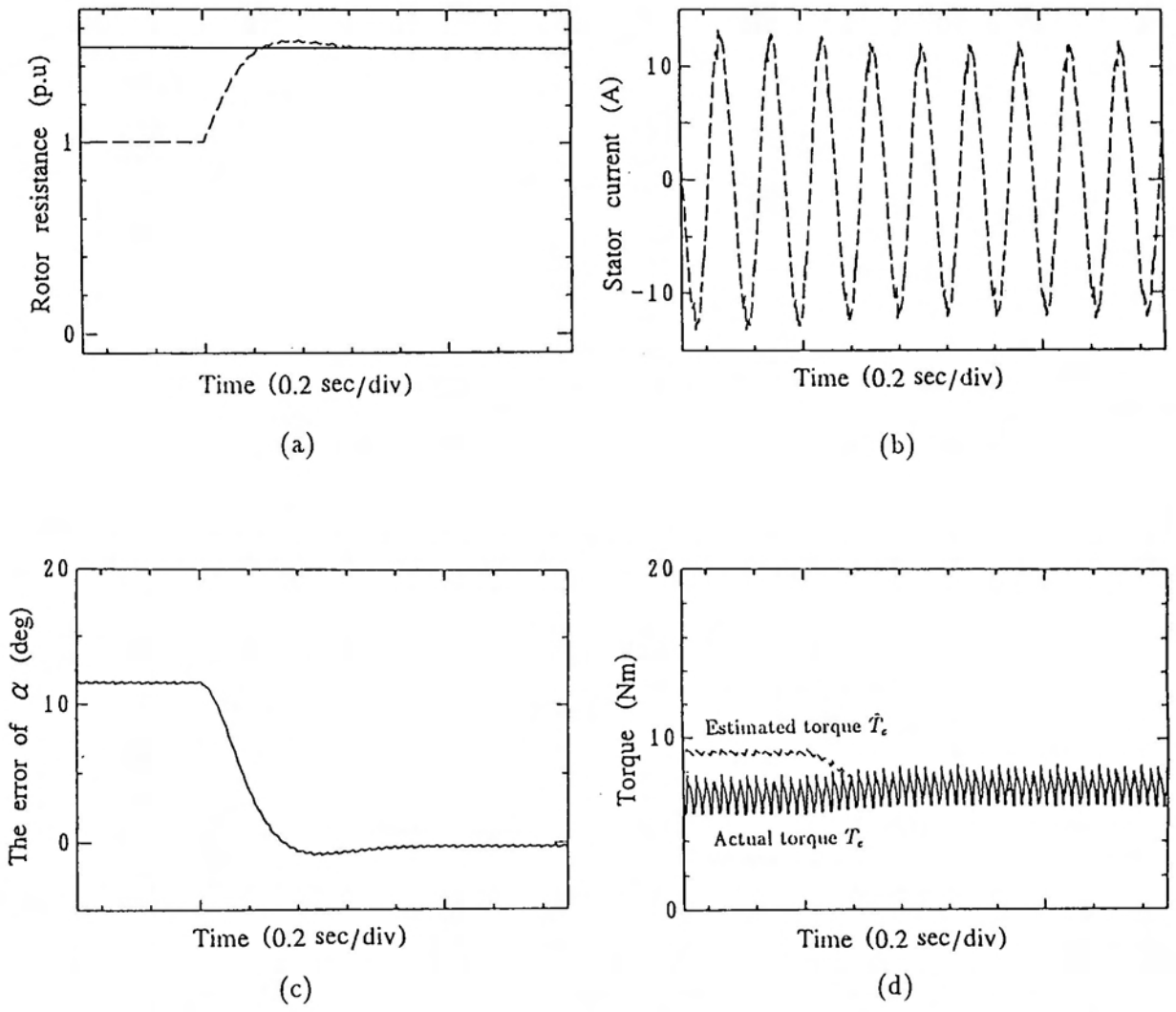

Fig. 5.10. Evaluation of the parameter adaptation. (a) Estimated rotor resistance by MRAS. (b) Stator current waveform. (c) Error of α between the actual and reference. (d) Reference and actual torque.

5.5.2 Experimental results

The parameter adaptation proposed in Section 5.3 is tested on condition that the rotor speed is 120 rpm at the steady state, the reference magnetizing current i_{mr} is 10 A, and the load torque is 6.0 Nm (about 20% of the rated torque) which was measured by a torque detector. This load condition is suitable to test the switching algorithm (5.32). The nominal ratings of machine parameters in Table 4.1 are used. Fig. 5.11 shows the estimated torque responses and the estimated rotor resistance. The estimated torque converges to the actual value 6.0 Nm, and then the estimated rotor resistance converges to 69% of the initial value 0.335 Ω, which would mean that the initial rotor resistance has been set to 1.45 times more than the actual value. According to (5.27), when the estimated torque coincided with the actual value, because the estimated rotor resistance also would coincide with the actual value.

In order to confirm our theory more certainly, another condition is tested, where the reference magnetizing current is 10 A initially, and after the operation reaches the steady state the reference magnetizing current is changed from 10 A to 6 A stepwise. The initial condition of the rotor resistance is the same as in Fig. 5.11, and the change of the rotor resistance can be negligible since the experiment is done for the short term so that the temperature of the machine cannot change. Since the control system has a magnetic saturation model to compensate inductance variation due to the change of flux level, the rotor resistance is expected to estimate the same value as shown in Fig. 5.11. Fig. 5.12 shows the expected result, that is, the estimated rotor resistance converges to the same value of Fig. 5.11, and the estimated torque also coincides with 6.0 Nm. This result shows the capability of the proposed system for the rotor resistance estimation at the different flux levels. In the experiment, the adaptive gains are selected as $K_P = 0.16 \cdot 10^{-4}$, $K_I = 0.771 \cdot 10^{-4}$ which are relatively small to avoid oscillations in the estimated rotor resistance.

Finally, the speed and dc link current responses in the case where the updated rotor resistance value is used in the control system are compared with those in the case where an incorrect rotor resistance value is used in the control system. Fig. 5.13 shows the responses in the latter case, and Fig. 5.14 shows the responses in the former case.

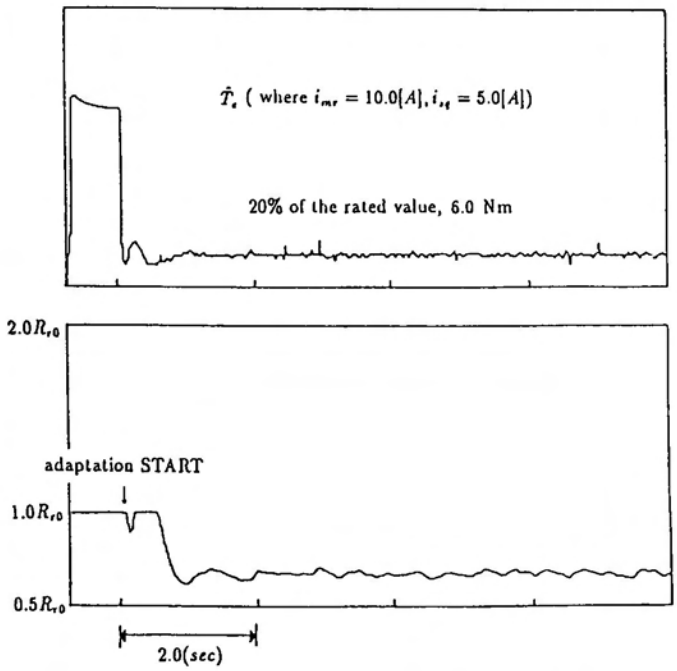

Fig. 5.11. Estimated torque responses and estimated rotor resistance (i_{mr} = 10 A).

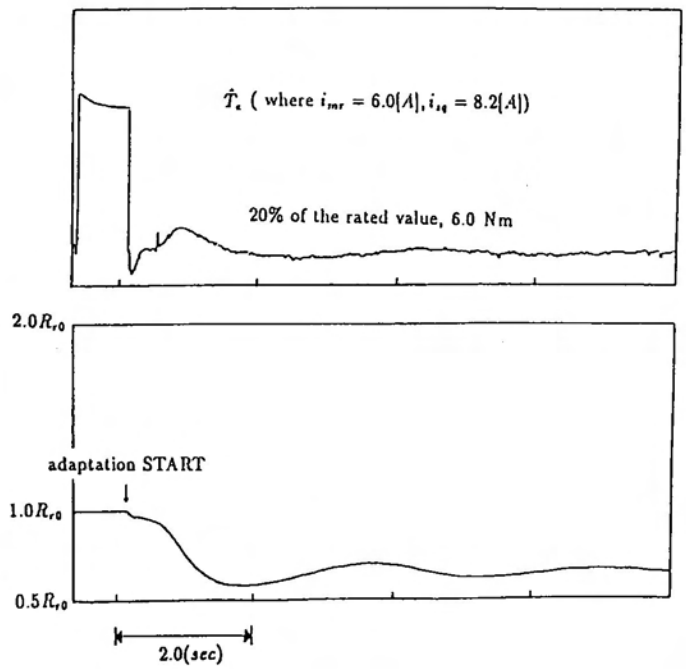

Fig. 5.12. Estimated torque responses and estimated rotor resistance (i_{mr} = 6 A).

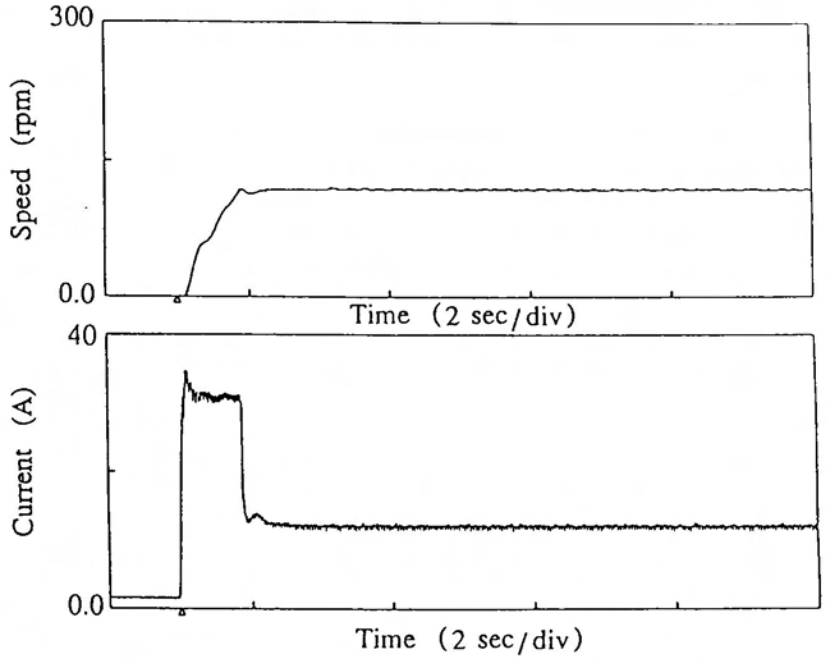

Fig. 5.13. Rotor speed and dc link current responses with incorrect parameters.

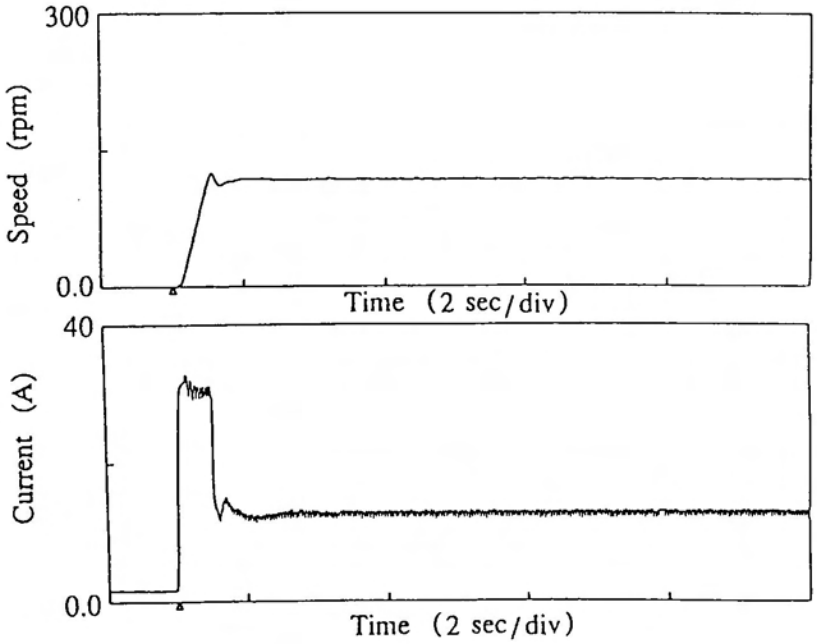

Fig. 5.14. Rotor speed and dc link current responses with correct parameters.

From these results, it can be noticed clearly that the acceleration property is improved in the former case. This reason is understood as follows: Even though the estimated torque is set to the rated value during the transient state, the actual torque in the case of Fig. 5.13 cannot reach the rated value, but the actual torque in the case of Fig. 5.14 can coincide with the estimated torque.

5.6 Conclusion

This chapter has shown the vector approximation method with the parameter adaptation for CSI-fed induction motors. The parameter adaptation with the saturation model can estimate the rotor resistance correctly at each different flux level, and the estimated torque coincides with the actual value which shows the capability of precise torque control. As mentioned in Section 3.2, where the stator voltage equation in the field oriented reference frame is shown, the complete decoupled control of i_{sd} and i_{sq} of the stator currents like the separately excited dc machine is said to be difficult by the field oriented control in the CSI drive system; because the voltage equations of the induction machine are coupled as shown in (3.6) and (3.7).

The direct torque control with the proposed method, however, can force to realize the precise torque control, which is effective as well as the decoupled control. The proposed method in this chapter is not so complicated to implement, and is adequate for the precise torque control of medium and large-size drives with low speed.

Chapter 6

Applications of robust control

6.1 Introduction

In Chapter 4 and Chapter 5, the vector approximation, the parameter adaptation, and the torque control are discussed. The remainder topic to be discussed is the robust control for the CSI drive induction motor.

Conventional linear control methods such as PI control have been widely used in industry electrical drives and also used in the preceding chapter [see (4.27), (4.28), and (4.29)], however, dynamic performance of the control system is often limited due to the conflict between overshoot and long setting time of the system response. There are inadequate rejections against external disturbance as well as the sensitivity in performance to the system parameter variation and nonlinearity. Thus, robust stable drive systems are required for any applications.

This chapter concerns with the applications of robust control, an H_∞ control and a simplified adaptive control. In order to design the robust speed control system, first, the nonlinear dynamical model of the rotor angular velocity and the dc link current is linearized by exact linearization. Then the linearized system is applied to design the H_∞ and the simplified adaptive controller, respectively. The robustness of these systems compared with the PI control system based on the conventional control theory are verified by the simulation and the experiments.

6.2 Modelling of the CSI drive induction motor

This section shows a modelling method of the CSI drive induction motor. The basic equation of a symmetrical induction motors shown in (4.1) and (4.2) are reviewed:

$$\begin{bmatrix} \boldsymbol{u}_s \\ \mathbf{o} \end{bmatrix} = \begin{bmatrix} R_s + L_s p & L_m p \\ L_m(p - j\omega_r) & R_r + L_r(p - j\omega_r) \end{bmatrix} \begin{bmatrix} \boldsymbol{i}_s \\ \boldsymbol{i}'_r \end{bmatrix} \tag{6.1}$$

$$\boldsymbol{i}_{mr} = \boldsymbol{i}_s + \frac{L_r}{L_m}\boldsymbol{i}'_r \tag{6.2}$$

where $\boldsymbol{u}_s$, $\boldsymbol{i}_s$, $\boldsymbol{i}'_r$, and $\boldsymbol{i}_{mr}$ are the complex numbers of stator voltage, current, rotor current and rotor magnetizing current, respectively, in the stationary reference frame fixed to the stator, that is, α-β axes in Fig. 4.1. R_s and R_r are the stator and the rotor resistance, L_s and L_r are the stator and the rotor self-inductance, L_m is the magnetizing inductance, ω_r is the rotor angular velocity, and p is the differential operator. The rotor magnetizing current in the reference frame is defined as $\boldsymbol{i}_{mr} = i_{mr\alpha} + ji_{mr\beta}$.

From (6.1) and (6.2), the following equations are obtained:

$$u_{s\alpha} = (R_s + \sigma L_s p)i_{s\alpha} + \frac{L_m^2}{L_r} p i_{mr\alpha} \tag{6.3}$$

$$p\boldsymbol{i}_{mr} = (-\frac{R_r}{L_r} + j\omega_r)\boldsymbol{i}_{mr} + \frac{R_r}{L_r}\boldsymbol{i}_s \tag{6.4}$$

where $\sigma = 1 - L_m^2/(L_s L_r)$. From (6.4), the phase angle of $\boldsymbol{i}_{mr}$ with respect to the α axis is

$$p\alpha_\mu = \omega_r + \frac{R_r i_{sq}}{L_r i_{mr}} \tag{6.5}$$

and the magnetizing current equation in the field oriented reference frame, that is, in the d-q axes is

$$p i_{mr} = \frac{R_r}{L_r}(i_{sd} - i_{mr}) \tag{6.6}$$

where i_{mr} is the magnitude of $\boldsymbol{i}_{mr}$, i_{sd} and i_{sq} are the d-axis and the q-axis component of $\boldsymbol{i}_s^o$ in Section 4.3, respectively.

As shown in Chapter 4, the inverter switching is done by the vector approximation method which is a switching topology considering the vector approximation for the CSI drive induction motor. In a sixth of the period of $\boldsymbol{i}_s^o$, which is one of sectors shown in Fig.

4.3, assume i_{mr}, i_{sq}, i_s and α are constant, and then (6.3) becomes

$$\begin{aligned} u_{s\alpha} = \; & R_s i_s \cos\alpha_p - \omega_i \sigma L_s i_s \sin\alpha_p \\ & - \omega_i \frac{L_m^2}{L_r} i_{mr} \sin(\alpha_p - \alpha) + \sigma L_s \cos\alpha_p p i_s \\ & + \frac{L_m^2}{L_r} \cos(\alpha_p - \alpha) p i_{mr} \end{aligned} \tag{6.7}$$

where i_s is the magnitude of $\boldsymbol{i}_s$, α is the phase angle of $\boldsymbol{i}_s$ with respect to the d-axis, $\alpha_p = \alpha_\mu + \alpha$, and $\omega_i = p\alpha_p$ is the stator angular velocity. Phase voltages are given using the following phase transformation matrix:

$$\begin{bmatrix} u_{sU} \\ u_{sV} \\ u_{sW} \end{bmatrix} = \begin{bmatrix} 1 & 0 \\ -\frac{1}{2} & \frac{\sqrt{3}}{2} \\ -\frac{1}{2} & -\frac{\sqrt{3}}{2} \end{bmatrix} \begin{bmatrix} u_{s\alpha} \\ u_{s\beta} \end{bmatrix}$$

where $u_{sU} = u_{s\alpha}$, and the other phase voltages have phase differences $\frac{2}{3}\pi$ from u_{sU} and can be calculated as well as (6.7).

$$u_{sU} = u_{s\alpha} \tag{6.8}$$

$$\begin{aligned} u_{sV} = \; & R_s i_s \cos(\alpha_p - 2\pi/3) - \omega_i \sigma L_s i_s \sin(\alpha_p - 2\pi/3) \\ & - \omega_i \frac{L_m^2}{L_r} i_{mr} \sin(\alpha_p - \alpha - 2\pi/3) + \sigma L_s \cos(\alpha_p - 2\pi/3) p i_s \\ & + \frac{L_m^2}{L_r} \cos(\alpha_p - \alpha - 2\pi/3) p i_{mr} \end{aligned} \tag{6.9}$$

$$\begin{aligned} u_{sW} = \; & R_s i_s \cos(\alpha_p - 4\pi/3) - \omega_i \sigma L_s i_s \sin(\alpha_p - 4\pi/3) \\ & - \omega_i \frac{L_m^2}{L_r} i_{mr} \sin(\alpha_p - \alpha - 4\pi/3) + \sigma L_s \cos(\alpha_p - 4\pi/3) p i_s \\ & + \frac{L_m^2}{L_r} \cos(\alpha_p - \alpha - 4\pi/3) p i_{mr} \end{aligned} \tag{6.10}$$

In vector approximation method, the required current vector $\boldsymbol{i}_s^\circ$ is realized approximately by two realizable current vectors $\boldsymbol{i}_{s1}$ and $\boldsymbol{i}_{s2}$ which are applied by switching for Δt_1 and Δt_2 during one switching cycle Δt. From (4.19), $\boldsymbol{i}_s^\circ$ is expressed as follows:

$$\boldsymbol{i}_s^\circ = \left\{ \frac{\Delta t_1}{\Delta t} \frac{\boldsymbol{i}_{s1}}{|\boldsymbol{i}_{s1}|} + \frac{\Delta t_2}{\Delta t} \frac{\boldsymbol{i}_{s2}}{|\boldsymbol{i}_{s2}|} \right\} i_s \tag{6.11}$$

Assume $\boldsymbol{i}_{s1}$ and $\boldsymbol{i}_{s2}$ are applied on the phase UV and UW (i.e., the sector 0 in Fig. 4.3), respectively, for example. Then the average inverter input voltage V_{DC} is calculated:

$$V_{DC} = \frac{3}{\pi} \left\{ \int_{-\frac{\pi}{6}}^{\frac{\pi}{6}} \frac{\Delta t_1}{\Delta t} (u_{sU} - u_{sV}) d\alpha_p + \int_{-\frac{\pi}{6}}^{\frac{\pi}{6}} \frac{\Delta t_2}{\Delta t} (u_{sU} - u_{sW}) d\alpha_p \right\} \tag{6.12}$$

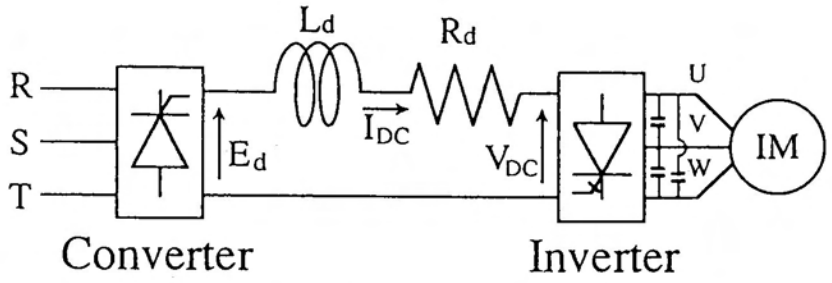

Fig. 6.1. CSI drive induction motor system.

Each firing time is expressed approximately as follows:

$$\frac{\Delta t_1}{\Delta t} = \frac{\sin\left(\frac{\pi}{3} - \alpha_p - \frac{\pi}{6}\right)}{\sin\left(\frac{\pi}{3} + \alpha_p + \frac{\pi}{6}\right)} \simeq \frac{1}{2} - \frac{3}{\pi}\alpha_p$$

$$\frac{\Delta t_2}{\Delta t} = 1 - \frac{\Delta t_1}{\Delta t} \simeq \frac{1}{2} + \frac{3}{\pi}\alpha_p$$

Substitute above equations and (6.7) into (6.12), and then (6.12) is calculated as

$$V_{DC} = \frac{9\sqrt{3}}{\pi^2} i_s R_s + \frac{9\sqrt{3}}{\pi^2}\frac{L_m^2}{L_r}\left(i_{mr}\omega_r + \frac{R_r}{L_r} i_{sq}\right)\sin\alpha \ . \tag{6.13}$$

Assuming continuous current in the dc link reactor shown in Fig. 6.1, and then dc link current I_{DC} can be considered to be determined by the averaged quantities V_{DC} and E_d. The differential equation of dc link circuit are expressed as

$$L_d \frac{dI_{DC}}{dt} + R_d I_{DC} = E_d - V_{DC} \tag{6.14}$$

where E_d is output voltage of the converter. The relation of currents are

$$i_s = \frac{i_{sq}}{\sin\alpha} = \frac{i_{sd}}{\cos\alpha} = \frac{2}{\sqrt{3}} I_{DC} \ . \tag{6.15}$$

From (6.13), (6.14) and (6.15), the differential equation of the dc link current are expressed as follows:

$$\begin{aligned} \frac{dI_{DC}}{dt} &= -\left(R_d + \frac{18}{\pi^2}R_s + \frac{18L_m^2 R_r}{\pi^2 L_r^2}\sin^2\alpha\right)\frac{I_{DC}}{L_d} \\ &\quad - \frac{9\sqrt{3}L_m^2}{\pi^2 L_r L_d} i_{mr}\omega_r \sin\alpha + \frac{E_d}{L_d} \end{aligned} \tag{6.16}$$

The instantaneous torque is

$$T_e = k_t i_{mr} i_s \sin\alpha, \ \ k_t = \frac{3}{2} P \frac{L_m^2}{L_r} \tag{6.17}$$

and the rotor angular velocity is related to the torque as

$$\frac{J}{P}\frac{d\omega_r}{dt} + \frac{f_v}{P}\omega_r = T_e - T_L \tag{6.18}$$

where ω_r is rotor angular velocity, P is the number of the pole-pairs, f_v is the viscous friction, and J is the moment of inertia. From (6.15), (6.17) and (6.18), the differential equation of the rotor angular velocity is expressed as follows:

$$\begin{aligned}\frac{d\omega_r}{dt} &= \frac{\sqrt{3}P^2L_m^2}{JL_r}i_{mr}I_{DC}\sin\alpha - \frac{f_v}{J}\omega_r - \frac{PT_L}{J} \\ &= \frac{3}{2}\frac{P^2L_m^2}{JL_r}i_{mr}I_{DC}\sqrt{\frac{4}{3} - \frac{i_{mr}^2}{I_{DC}^2}} - \mathcal{D}_v\omega_r - \frac{PT_L}{J}\end{aligned} \tag{6.19}$$

where $\mathcal{D}_v = f_v/J$.

6.3 Exact linearization

The nonlinear system with (6.16) and (6.19) are expressed by

$$\dot{\boldsymbol{x}} = f(\boldsymbol{x}) + g(\boldsymbol{x})u \tag{6.20}$$

where $(\dot{})$ denotes the differential operator, $\boldsymbol{x} = (\omega_r \quad I_{DC})^T$, $u = E_d$, and

$$f(\boldsymbol{x}) = \begin{pmatrix} D_c I_{DC}\sqrt{\frac{4}{3} - \frac{i_{mr}^2}{I_{DC}^2}} - \mathcal{D}_v\omega_r \\ A_c I_{DC} + \frac{B_c}{I_{DC}} + C_c\omega_r\sqrt{\frac{4}{3} - \frac{i_{mr}^2}{I_{DC}^2}} \end{pmatrix} \tag{6.21}$$

$$g(\boldsymbol{x}) = \begin{pmatrix} 0 \\ 1/L_d \end{pmatrix} \tag{6.22}$$

$$\begin{aligned} A_c &= -(R_d + \frac{18}{\pi^2}R_s + \frac{18L_m^2R_r}{\pi^2L_r^2})\frac{1}{L_d} \\ B_c &= \frac{27}{2\pi^2}\frac{L_m^2R_ri_{mr}^2}{L_r^2L_d} \\ C_c &= -\frac{27}{2\pi^2}\frac{L_m^2i_{mr}}{L_rL_d} \\ D_c &= \frac{3}{2}\frac{P^2L_m^2i_{mr}}{JL_r} \end{aligned}$$

Since the above system is so nonlinear, the controllable range may be limited with the conventional linearization method, the first order approximation of Taylor expansion, for example. Exact linearization [21][22] is a method to linearize the system without any approximation, and the controllable range is extended greatly. The system for exact linearization, however, must satisfy with the following theorem.

Theorem [21]. Consider the general case where (6.20) is a n-dimensional system. Then the necessary and sufficient conditions for the possibility of exact linearization are given as follows:

(a) $\{ad_f^0 g(0), \cdots, ad_f^{n-1} g(0)\}$ is independent lineally.

(b) $\{ad_f^0 g(\boldsymbol{x}), \cdots, ad_f^{n-2} g(\boldsymbol{x})\}$ is involutive.

where Lie bracket is defined as

$$[f, g](\boldsymbol{x}) = \frac{\partial g}{\partial \boldsymbol{x}^T} f(\boldsymbol{x}) - \frac{\partial f}{\partial \boldsymbol{x}^T} g(\boldsymbol{x}) \ , \tag{6.23}$$

and $ad_f^i g(\boldsymbol{x})$ calculates Lie bracket iteratively,

$$ad_f^0 g(\boldsymbol{x}) = g(0) \ , \quad ad_f^i g(\boldsymbol{x}) = [f, ad_f^{i-1} g](\boldsymbol{x}) \ . \tag{6.24}$$

□

If the above theorem is satisfied, then the function $\phi(\boldsymbol{x})$ exists with the following condition:

$$L_{ad_f^i g} \phi(\boldsymbol{x}) = 0 \ , \quad i = 0, 1, 2, \cdots, n-2 \tag{6.25}$$

where Lie derivative is defined as follows:

$$L_f \phi(\boldsymbol{x}) = \frac{\partial \phi}{\partial \boldsymbol{x}^T} f(\boldsymbol{x}) \ , \quad L_f^i \phi(\boldsymbol{x}) = L_f \{L_f^{i-1} \phi(\boldsymbol{x})\}$$

It is known that (6.20) can be transformed to the linear state equation, if the following state transformation and the input transformation are done:

$$\boldsymbol{\xi} = \begin{pmatrix} \xi_1 \\ \xi_2 \\ \vdots \\ \xi_n \end{pmatrix} = \begin{pmatrix} \phi(\boldsymbol{x}) \\ L_f \phi(\boldsymbol{x}) \\ \vdots \\ L_f^{n-1} \phi(\boldsymbol{x}) \end{pmatrix} \tag{6.26}$$

$$u = -\frac{L_f^n \phi(\boldsymbol{x})}{L_g L_f^{n-1} \phi(\boldsymbol{x})} + \frac{1}{L_g L_f^{n-1} \phi(\boldsymbol{x})} v \tag{6.27}$$

$$\dot{\boldsymbol{\xi}} = \begin{pmatrix} 0 & 1 & 0 & \dots & 0 \\ 0 & 0 & 1 & \ddots & \vdots \\ \vdots & \vdots & \ddots & \ddots & 0 \\ 0 & 0 & 0 & \dots & 1 \\ 0 & 0 & 0 & \dots & 0 \end{pmatrix} \boldsymbol{\xi} + \begin{pmatrix} 0 \\ 0 \\ \vdots \\ 0 \\ 1 \end{pmatrix} \tag{6.28}$$

In this case, the above theorem is satisfied, and the state transformation is found as follows:

$$\phi(\boldsymbol{x}) = \omega_r \tag{6.29}$$

$$\boldsymbol{\xi} = \begin{pmatrix} \xi_1 \\ \xi_2 \end{pmatrix} = \begin{pmatrix} \omega_r \\ D_c I_{DC} \sqrt{\frac{4}{3} - \frac{i_{mr}^2}{I_{DC}^2}} - \mathcal{D}_v \omega_r \end{pmatrix} \tag{6.30}$$

Since

$$\begin{aligned} L_f^1 \phi(\boldsymbol{x}) &= \frac{\partial \phi}{\partial \boldsymbol{x}} f(\boldsymbol{x}) \\ &= D_c I_{DC} \sqrt{\frac{4}{3} - \frac{i_{mr}^2}{I_{DC}^2}} - \mathcal{D}_v \omega_r \qquad (6.31) \\ L_f^2 \phi(\boldsymbol{x}) &= L_f \{ L_f \phi(\boldsymbol{x}) \} \\ &= f_3 f_1 - \mathcal{D}_v f_2 \qquad (6.32) \\ L_g L_f^1(\boldsymbol{x}) &= \frac{\partial L_f^1 \phi}{\partial \boldsymbol{x}} g(\boldsymbol{x}) = \frac{L_d}{f_3} , \qquad (6.33) \end{aligned}$$

from (6.27), the input transformation is given as follows:

$$u = -\frac{L_d}{f_3}(f_3 f_1 - \mathcal{D}_v f_2) + \frac{L_d}{f_3} v \tag{6.34}$$

where

$$\begin{aligned} f_1 &= A_c I_{DC} + \frac{B_c}{I_{DC}} + C_c \omega_r \sqrt{\frac{4}{3} - \frac{i_{mr}^2}{I_{DC}^2}} \\ f_2 &= D_c I_{DC} \sqrt{\frac{4}{3} - \frac{i_{mr}^2}{I_{DC}^2}} - \mathcal{D}_v \omega_r \\ f_3 &= D_c \sqrt{\frac{4}{3} - \frac{i_{mr}^2}{I_{DC}^2}} \left(\frac{i_{mr}^2}{I_{DC}^2 (\frac{4}{3} - \frac{i_{mr}^2}{I_{DC}^2})} + 1 \right) \end{aligned}$$

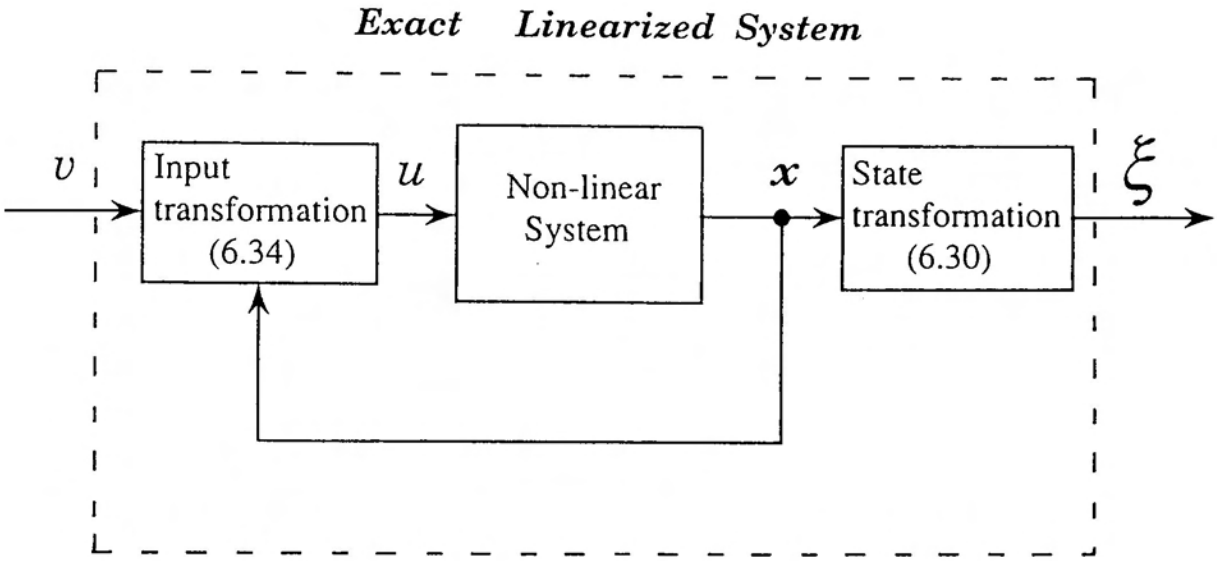

Fig. 6.2. Exact linearized system.

Then the exact linearized system are obtained as follows:

$$\dot{\xi} = \begin{pmatrix} 0 & 1 \\ 0 & 0 \end{pmatrix} \xi + \begin{pmatrix} 0 \\ 1 \end{pmatrix} v \tag{6.35}$$

$$y = \begin{pmatrix} 1 & 0 \end{pmatrix} \xi \tag{6.36}$$

The exact linearized system is shown in Fig. 6.2.

6.4 H_∞ control

This chapter treats the H_∞ control system with exact linearization for the CSI drive induction motor. The characteristic of the system considerably changes with the disturbances and the changes of parameters. The modelling and the exact linearization of the CSI drive induction motor are shown in the preceding sections. Then the H_∞ controller is designed for the obtained model, which is approximated lineally around an equilibrium point to be the current feedback system and the nonlinear compensator between the nonlinear model and the approximated model is constructed by the input transformation. Several experimental results show that the H_∞ control system with exact linearization is quite robust against disturbances and parameter changes as compared with both the PI control system and the H_∞ control system without exact linearization.

6.4.1 Design of the H_∞ controller

In this section, the H_∞ controller design of single input single output systems is shown; a control system is considered in Fig. 6.3, which is so-called the two block mixed sensitivity H_∞ design problem, where $G(s)$ is the control object, $W_s(s)$ and $W_t(s)$ are weighting functions for the sensitivity function S (i.e., $S = (I + GK)^{-1}$) and the complementary sensitivity function T (i.e., $T = GKS$) respectively. Denote that $w(s)$ is the disturbance vector; $u(s)$ is the control input vector; $z(s)$ is the controlled output vector; $y(s)$ is the measured output vector.

The H_∞ control problem is to choose a controller, $K(s)$, that makes the closed-loop system internally stable and minimizes the H_∞-norm of the transfer function from $w(s)$ to $z(s)$. In fact, the problem of the finding stabilizing $K(s)$ ($u = K(s)y$) such that

$$\|LFT(P_e, K)\|_\infty < \gamma_c \quad \gamma_c \in R^+ \tag{6.37}$$

where P_e is the transfer function of the generalized plant [23],

$$\begin{bmatrix} z \\ y \end{bmatrix} = P_e \begin{bmatrix} w \\ u \end{bmatrix} \tag{6.38}$$

$$\begin{aligned} P_e &= \begin{bmatrix} P_{11} & P_{12} \\ P_{21} & P_{22} \end{bmatrix} \\ &= \left[\begin{array}{c|c} W_s & -W_sG \\ 0 & W_tG \\ \hline I & -G \end{array}\right] \end{aligned} \tag{6.39}$$

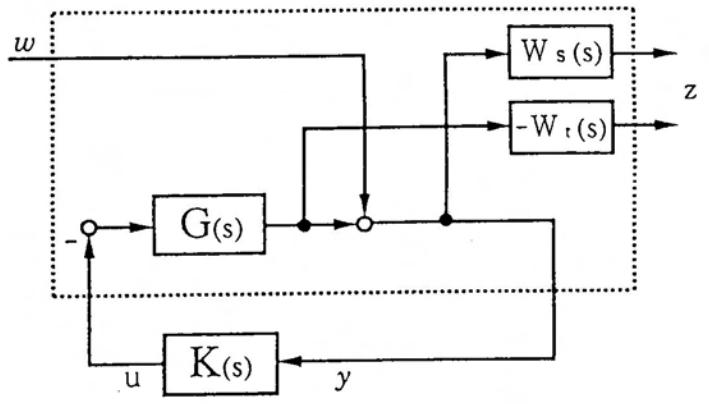

Fig. 6.3. Mixed sensitivity H_∞ problem.

and LFT is linear fractional transformation, then

$$\begin{aligned} LFT(P_e, K) &= \begin{bmatrix} W_s \\ 0 \end{bmatrix} + \begin{bmatrix} -W_s G \\ W_t G \end{bmatrix} K(I + GK)^{-1} I \\ &= \begin{bmatrix} W_s S \\ W_t T \end{bmatrix} . \end{aligned} \tag{6.40}$$

It should be noted that $-P_{22}(s)$ is the control object. So the internal stable problem is to choose a controller, $K(s)$, that makes the $G(s)$ internally stable. Since

$$S + T = 1 , \tag{6.41}$$

it cannot be satisfied simultaneously to make gains ($||S(j\omega)||$ and $||T(j\omega)||$) as low as possible together. Therefore, the suitable weighting functions $W_s(s)$ and $W_t(s)$ should be chosen separately to obtain the low sensitivity on the low frequency band and the robust stability on the high frequency band. If such a $K(s)$ exists, it is considered that the H_∞ problem is solvable. The state-space realizations of $G(s)$, $W_s(s)$ and $W_t(s)G(s)$ are denoted as

$$G(s) = \left[\begin{array}{c|c} A_p & B_p \\ \hline C_p & 0 \end{array}\right] \tag{6.42}$$

$$W_s(s) = \left[\begin{array}{c|c} A_s & B_s \\ \hline C_s & D_s \end{array}\right] \tag{6.43}$$

$$W_t(s)G(s) = \left[\begin{array}{c|c} A_p & B_p \\ \hline C_t & D_t \end{array}\right] \tag{6.44}$$

where $A_p \in R^{n_p \times n_p}$ and $A_s \in R^{n_s \times n_s}$, then the state-space representation [23] of the generalized plant $P_e(s)$ in (6.39) is

$$\begin{aligned} P_e(s) &= \left[\begin{array}{c|cc} A & B_1 & B_2 \\ \hline C_1 & D_{11} & D_{12} \\ C_2 & D_{21} & 0 \end{array}\right] \\ &= \left[\begin{array}{cc|cc} A_s & B_s C_p & B_s & 0 \\ 0 & A_p & 0 & -B_p \\ \hline C_s & D_s C_p & D_s & 0 \\ 0 & -C_t & 0 & D_t \\ 0 & C_p & I & 0 \end{array}\right] \end{aligned} \tag{6.45}$$

where $A \in R^{(n_s+n_p)\times(n_s+n_p)}$.

The following assumptions are made to ensure the existence of a controller [24].

A1. (A, B_2, B_3) is stabilizable and detectable.

A2. D_{12} has full column rank and D_{21} has full row rank.

A3. D_{12} and D_{21} are transformed into $D_{12} = \begin{bmatrix} 0 \\ I \end{bmatrix}$ and $D_{21} = \begin{bmatrix} 0 & I \end{bmatrix}$ by scaling of u and y, together with a unitary transformation w and z. D_{11} is partitioned compatible with D_{12} and D_{21} into $\begin{bmatrix} D_{1111} & D_{1112} \\ D_{1121} & D_{1122} \end{bmatrix}$.

A4. For all $\forall\, \omega \in R$, $\begin{bmatrix} A - j\omega I & B_2 \\ C_1 & D_{12} \end{bmatrix}$ has full column rank.

A5. For all $\forall\, \omega \in R$, $\begin{bmatrix} A - j\omega I & B_1 \\ C_2 & D_{21} \end{bmatrix}$ has full row rank.

Recently, a theory of optimal H_∞ control design has been widely developed. Among all tools available for such design, the method of Glover and Doyle [24] is widely accepted, which is called the standard H_∞ control design. In this section, "MATLAB", which is a tool for the design of control systems, is used.

Now the design of the H_∞ controller for the CSI drive induction motor is shown in the following. The nonlinear dynamical model of the rotor angular velocity and the dc link current were linearized by exact linearization in the preceding section. With the exactly linearized system, the control block diagram is considered as shown in Fig. 6.4, where the current feedback loop is still kept because the H_∞ controller to be designed is a speed controller and the current controller should be kept due to the current controlled type inverter drive. The control object is expressed by eliminating v from (6.34) and (6.35) as follows:

$$\dot{\xi} = \begin{bmatrix} \xi_2 \\ f_{p2}(\xi) \end{bmatrix} + \begin{bmatrix} 0 \\ g_{p2}(\xi) \end{bmatrix} E_d \tag{6.46}$$

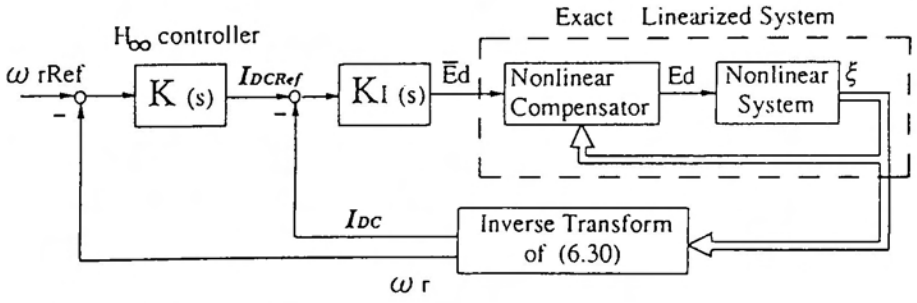

Fig. 6.4. Control block diagram.

where

$$\begin{aligned} f_{p2}(\boldsymbol{\xi}) &= -\mathcal{D}_v f_2 + f_3 f_1 \\ g_{p2}(\boldsymbol{\xi}) &= f_3 / L_d \ . \end{aligned}$$

The nonlinear model is approximated lineally by Taylor expansion around an equilibrium point ($\boldsymbol{\xi} = \boldsymbol{\xi}_0 + \bar{\boldsymbol{\xi}}$, $E_d = E_{d0} + \bar{E}_d$), then the approximated model is

$$\dot{\bar{\boldsymbol{\xi}}} = \begin{bmatrix} 0 & 1 \\ a_1 & a_2 \end{bmatrix} \bar{\boldsymbol{\xi}} + \begin{bmatrix} 0 \\ b_2 \end{bmatrix} \bar{E}_d \tag{6.47}$$

where

$$\begin{aligned} a_i &= \left. \frac{\partial f_{p2}(\boldsymbol{\xi})}{\partial \xi_i} \right|_{\boldsymbol{\xi}=\boldsymbol{\xi}_0} + \left. \frac{\partial g_{p2}(\boldsymbol{\xi})}{\partial \xi_i} \right|_{\boldsymbol{\xi}=\boldsymbol{\xi}_0} E_{d0} \qquad (i = 1, 2) \\ b_2 &= g_2(\boldsymbol{\xi}_0) \ . \end{aligned}$$

Thus, the nonlinear compensator between (6.46) and (6.47) is constructed as follows:

$$E_d = \frac{1}{g_{p2}(\boldsymbol{\xi})}(a_1 \bar{\xi}_1 + a_2 \bar{\xi}_2 + b_2 \bar{E}_d - f_{p2}(\boldsymbol{\xi})) \tag{6.48}$$

This compensation keeps the nonlinearity of the system in order to extend the controllable range, while the conventional linearized method has no such compensation.

An H_∞ controller is designed for the system shown above. The operating point of the system is set as follows: $I_{DC} = 10A$, $\omega_r = 120$ rpm, $E_{d0} = 22.37$ V. Then the coefficients a_1, a_2, and b_2 are calculated as follows: $a_1 = -13.47$, $a_2 = -13.88$, and $b_2 = 14.44$, where the nominal parameters shown in Fig. 4.1 are used, and the moment of inertia $J = 0.82$ kgm^2. The current controller $K_I(s)$ shown in Fig. 6.4 is treated as a part of the system, the transfer function of the system $G_e(s)$ including the current controller is given as follows: [34]

$$G_e(s) = \frac{61.53s + 473.32}{s^3 + 50.23s^2 + 317.56s + 187.99} \tag{6.49}$$

where $K_I(s)$ is set as

$$K_I(s) = \frac{0.03(s + 7.1994)}{s} \ . \tag{6.50}$$

Moreover, in order to include an integral controller, consider the extended system G_{ext}:

$$G_{ext}(s) = \frac{s + \xi}{s} G_e(s) \tag{6.51}$$

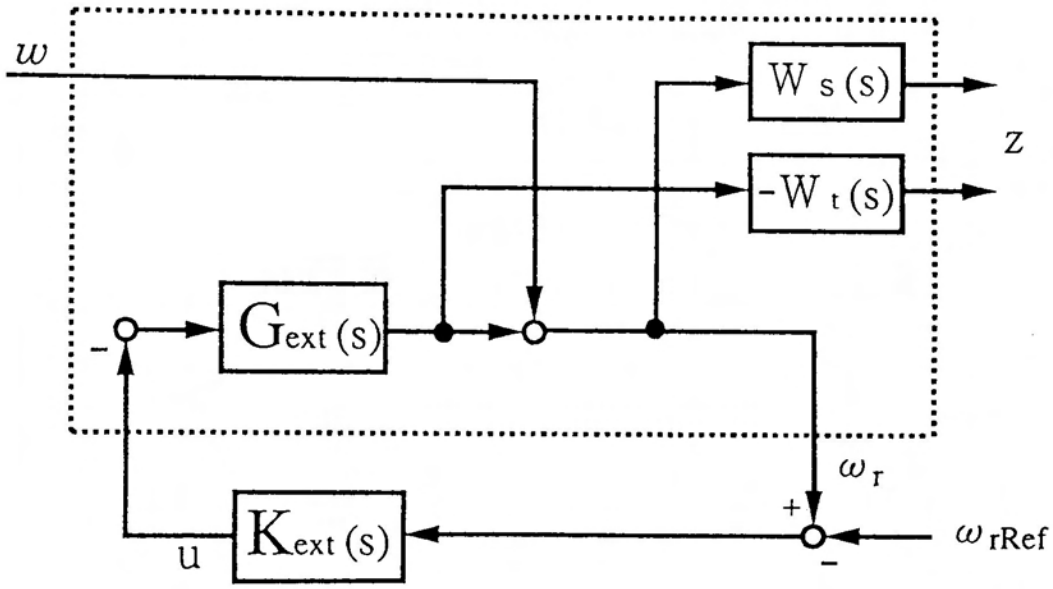

Fig. 6.5. Mixed sensitivity H_∞ problem in CSI drive induction motor system.

Fig. 6.5 indicates the mixed sensitivity H_∞ problem for this case, where the sensitivity function and the complementary sensitivity function are selected as follows:

$$W_s(s) = \frac{\rho}{s+\eta} \tag{6.52}$$

$$W_t(s) = \frac{(s+\alpha_t)^2}{\alpha_t^2 \beta_t} \tag{6.53}$$

where ρ, η, α_t, β_t, and ξ are parameters to be designed. In this augmented system, (6.37) is used as the performance index in the standard H_∞ control design. From (6.37) and (6.40), then (6.37) becomes

$$\left\| \begin{matrix} W_s S \\ W_t T \end{matrix} \right\|_\infty < \gamma_c \tag{6.54}$$

where $S(s)$ and $T(s)$ are expressed as follows:

$$S(s) = \frac{1}{1 + G_{ext}(s) K_{ext}(s)} \tag{6.55}$$

$$T(s) = \frac{G_{ext}(s) K_{ext}(s)}{1 + G_{ext}(s) K_{ext}(s)} \tag{6.56}$$

As a result of the design, if $\rho = 2$, $\eta = 1.2697$, $\alpha_t = 420$, $\beta_t = 15$, and $\xi = 10.91$, then the obtained H_∞ controller is

$$K_{ext}(s) = \frac{5.8989 \cdot 10^4 (s + 78.668)(s + 7.2285)}{s(s + 439.3 + j128.55)(s + 439.3 - j128.55)(s + 10.91)} . \tag{6.57}$$

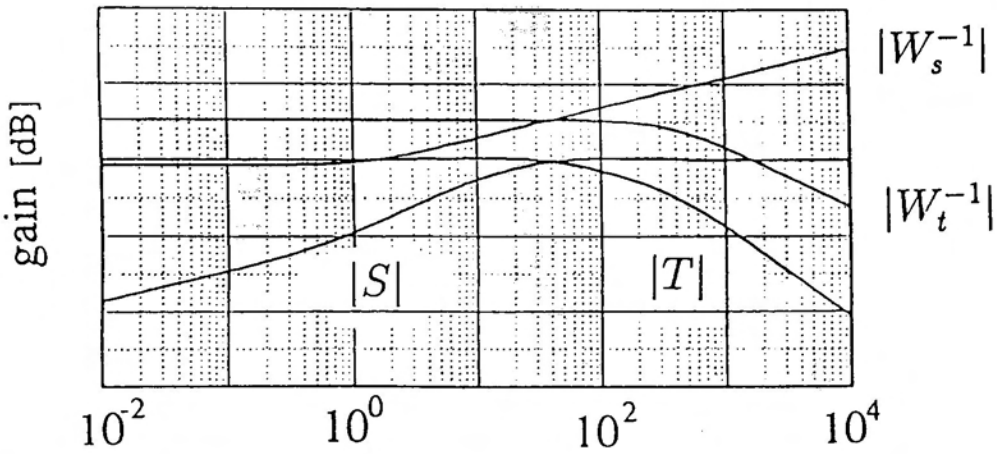

Fig. 6.6. Characteristics of $S(s)$ and $T(s)$.

Fig. 6.6 shows the characteristics of $S(s)$ and $T(s)$. In (6.51), the integral controller is considered, but the real system cannot include it; therefore, the controller should be included the integral controller. Finally, the designed H_∞ controller is shown as follows:

$$\begin{aligned} K(s) &= K_{ext}(s)\frac{s+\xi}{s} \\ &= \frac{5.8989 \cdot 10^4 (s+78.668)(s+7.2285)}{s(s+439.3+j128.55)(s+439.3-j128.55)} \end{aligned} \tag{6.58}$$

6.4.2 Verification of the H_∞ control

Fig. 6.7 shows the experimental system, where the nonlinear compensator is shown but it is taken out when the PI controller or the conventional H_∞ controller is used for the comparison. In order to verify the designed controller in the preceding section, the experimental tests are done with the PI controller, the H_∞ controller, and the H_∞ controller with exact linearization. In the experiments, the value of the speed reference is set to 120 rpm, where the load torque is changed suddenly with the increase of 200 % and 300 %, and the value of the rotor resistance set in the controller is increased more 16% than the nominal value at the steady state.

The sudden-load increase causes the drop of the speed and the increase of the current, that is, the operating point deviates from the initial equilibrium point, in order to confirm effectiveness of exact linearization.

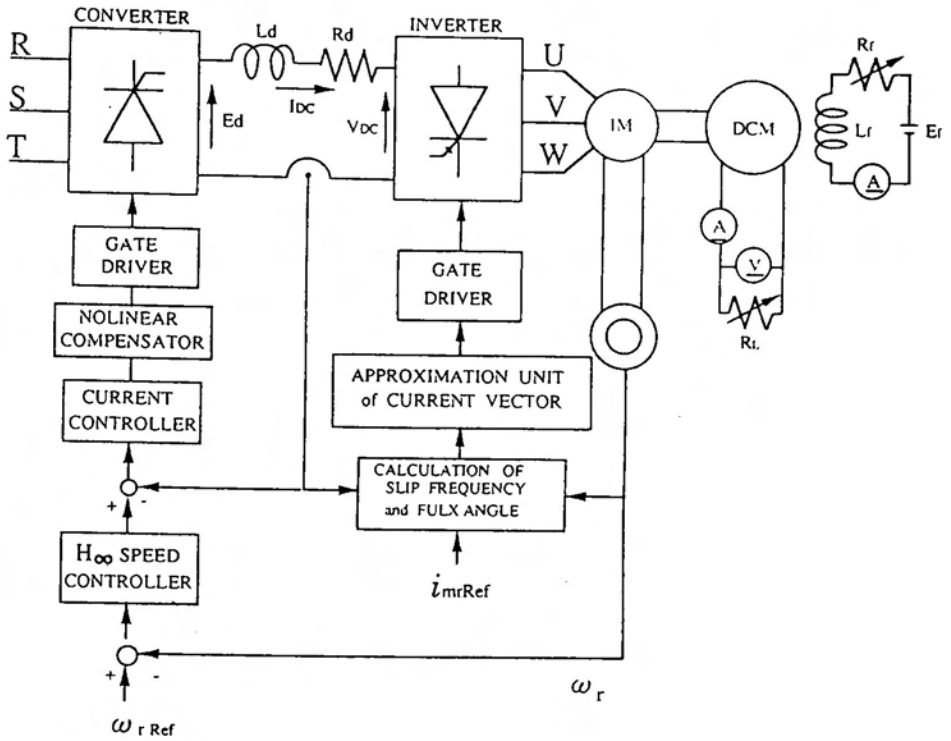

Fig. 6.7. Experimental system.

The artificial parameter change in the controller is done for checking the robustness of the H_∞ controller.

Fig. 6.8 shows the experimental results of the PI controller. At the sudden-load change of 200 %, the drop of speed against the reference is 2.53 %; at the sudden-load change of 300 %, the drop of speed against the reference is 5.06 %. Moreover, in the sudden-load change of 200 % and 300 % with the parameter increase of 16 % simultaneously, the drop of speed against the reference is 5.06 % and 6.32 % respectively. In Fig. 6.8, the recovering time of the speed controlled by the PI controller seems to be so long but for reducing the overshoot at the transient state the PI control gains are considered to be adequate.

Fig. 6.9 shows the experimental results of the H_∞ controller without exact linearization. From Fig. 6.9(a), the speed drop at the sudden-load change of 200 % was improved compared with the case of the PI controller; however, the speed drop at the sudden-load change of 300 % is 2.53 % against the reference,

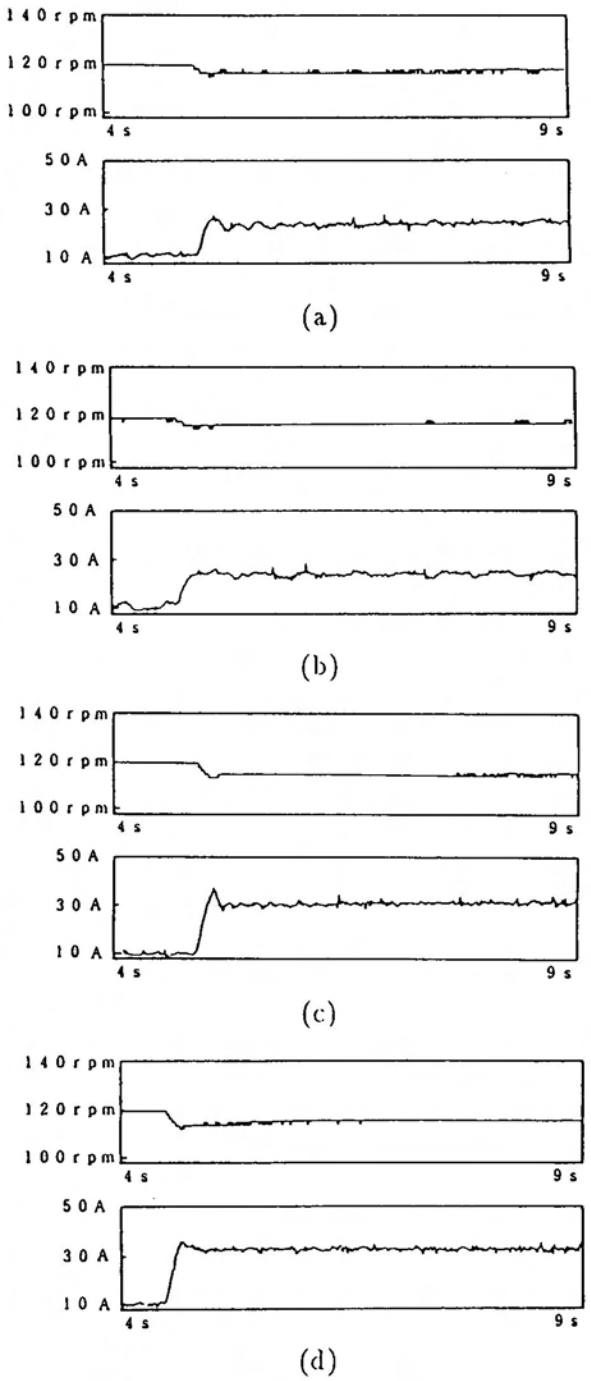

Fig. 6.8. Experimental results of the PI controller. (a) Test against the sudden-load change of 200 %. (b) Test against the sudden-load change of 200 % and the parameter increase of 16 %. (c) Test against the sudden-load change of 300 %. (d) Test against the sudden-load change of 300 % and the parameter increase of 16 %.

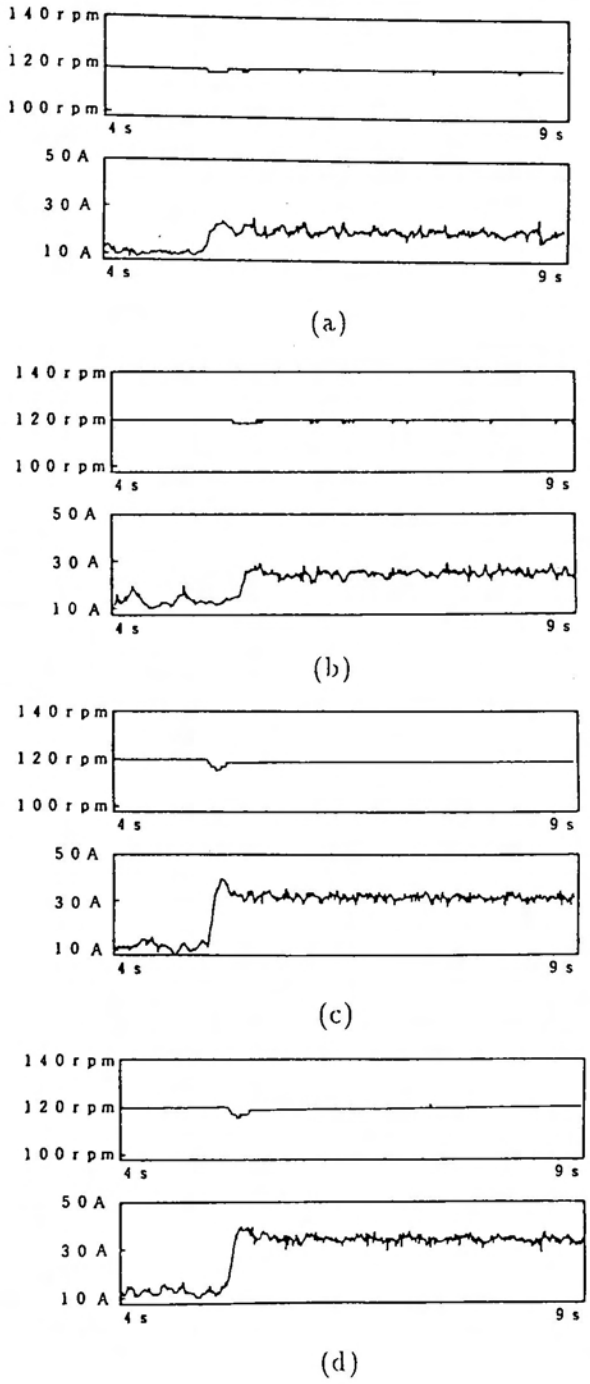

Fig. 6.9. Experimental results of the H_∞ controller. (a) Test against the sudden-load change of 200 %. (b) Test against the sudden-load change of 200 % and the parameter increase of 16 %. (c) Test against the sudden-load change of 300 %. (d) Test against the sudden-load change of 300 % and the parameter increase of 16 %.

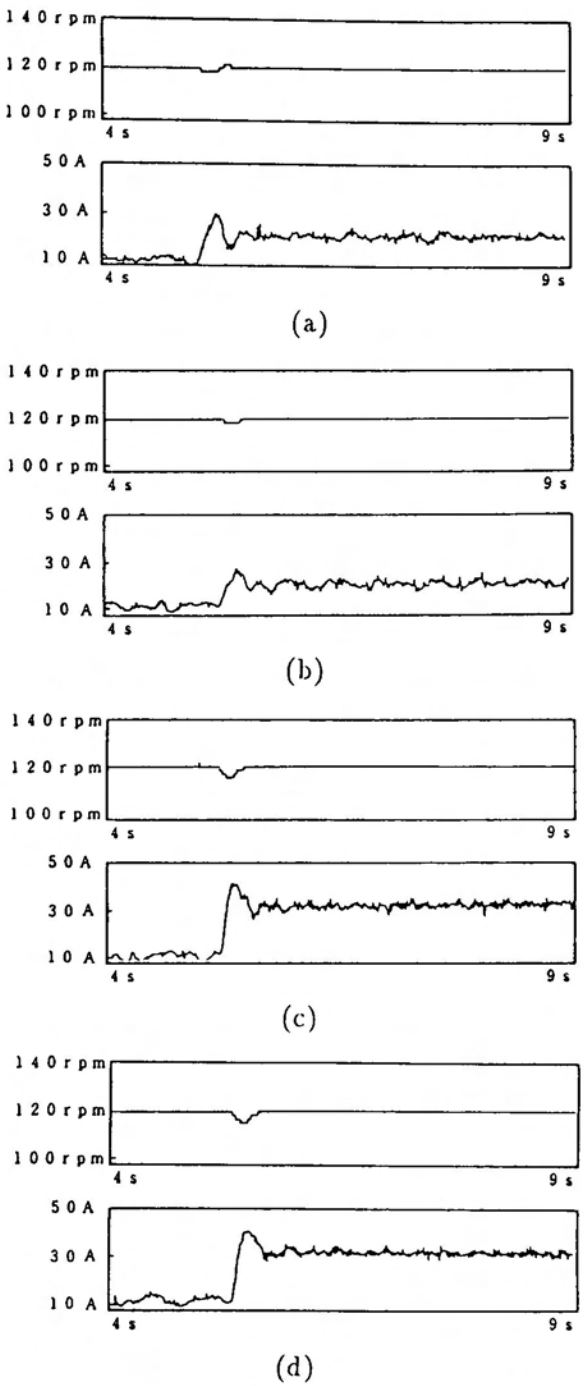

Fig. 6.10. Experimental results of the H_∞ controller with exact linearization. (a) Test against the sudden-load change of 200 %. (b) Test against the sudden-load change of 200 % and the parameter increase of 16 %. (c) Test against the sudden-load change of 300 %. (d) Test against the sudden-load change of 300 % and the parameter increase of 16 %.

and the speed drop at the sudden-load change of 300 % with the parameter increase of 16 % simultaneously is 5.06 %. This fact is understood that since the operating point of the system deviated far from the initial equilibrium point, even the H_∞ control could not cope with the sudden-load change.

On the other hand, Fig. 6.10 shows the experimental results of the H_∞ controller with exact linearization, where the good performance are shown; it could be seen that the designed controller can control the speed precisely in all of the test.

6.5 Simplified adaptive control

A simplified adaptive control (SAC) [25] has relatively simpler adaptive structure compared with that of model reference adaptive control, but also has the robust characteristics concerning disturbance and the effects of unmodeled dynamics. The SAC, however, can be originally applied to the linear system which should be limited to almost strictly positive real (ASPR) system. Since ac motor drives are so nonlinear system as shown in (6.16) and (6.19) that the SAC with the proof of the stability for ac motor drives have not been achieved. This chapter proposes the SAC for the nonlinear system by combining with exact linearization. The nonlinear dynamical model consisting of the rotor speed and the dc link current is exactly linearized in Section 6.3. The SAC system can be designed to the augmented system with parallel feedforward compensation which makes the exact linearized system ASPR. The proposed system can improve the fast tracking of the reference change without overshoot and the recovering time of speed at the sudden-load variations more than the conventional PI controller. From the practical point of view, the system has good features that the controller can be systematically designed. The effectiveness of the proposed method has been confirmed by the simulation and the experiment.

6.5.1 Design of the SAC

When the system to be controlled satisfies some condition, the adaptive control law can be simplified. Suppose that the system to be controlled and the chosen reference model are

given as follows:

$$\dot{\boldsymbol{x}}_p = A_p \boldsymbol{x}_p + b_p u_p \ , \quad y_p = C_p^T \boldsymbol{x}_p \tag{6.59}$$

$$\dot{\boldsymbol{x}}_m = A_m \boldsymbol{x}_m + b_m r_m \ , \quad y_m = C_m^T \boldsymbol{x}_m \tag{6.60}$$

If the following conditions,

(a) the control input u to realize the complete model matching $y = y_m$ exists,

(b) The closed loop transfer function by the output feedback with the gain $\tilde{K}_e$, $W(s) = C_p^T(sI - A_p - b_p \tilde{K}_e C_p^T)^{-1} b_p$, must be strictly positive real (SPR),

are satisfied, then by the adaptive control input,

$$\begin{aligned} u_p &= K^T \boldsymbol{z} \ , \\ \boldsymbol{z}^T &= (e, \boldsymbol{x}_m^T, r_m) \ , \quad e = y_p - y_m \ , \\ K^T &= (k_e, \boldsymbol{k}_x^T, k_r) \ , \end{aligned} \tag{6.61}$$

and the adaptive law,

$$K = K_P + K_I \ , \tag{6.62}$$

$$K_P = -\Gamma_p \boldsymbol{z} e, \tag{6.63}$$

$$\dot{K}_I = -\Gamma_I \boldsymbol{z} e \quad (\Gamma_P, \Gamma_I > 0) \ , \tag{6.64}$$

$\lim_{t \to \infty} e = 0$ is achieved [26].

The algorithm of the SAC shows that the number of integration in the controller is determined by only the input, output, and the order of the reference model, which is not concerned with the real system. Thus the controller is simplified with the low order reference model, and the proof of model matching is shown as "the command generator tracker theory" in [27].

In our case, the system to be controlled is (6.35) and (6.36), however, the transfer function is $G(s) = 1/s^2$ which is not satisfied with SPR condition. In such case, the parallel feedforward compensator $F(s)$ as shown in Fig. 6.11 is used, and the transfer function of the augmented system is

$$G_a(s) = G(s) + F(s) \tag{6.65}$$

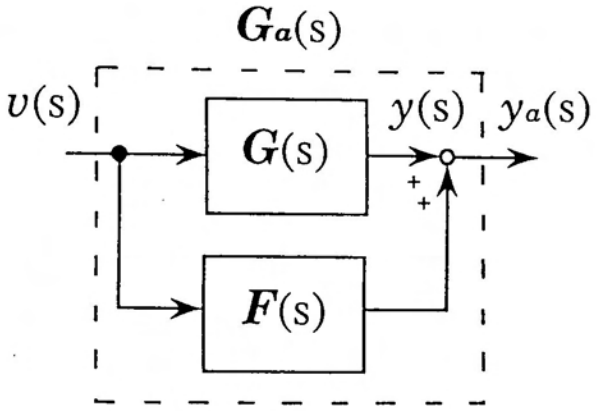

Fig. 6.11. Augmented system with parallel feedfoward compensator.

where $F(s) = \beta_f/(s + \alpha_f)$, and in Fig. 6.11, the output of the augmented system is defined as y_a. $F(s)$ must be determined to make the augmented system ASPR, that is, to satisfy the condition (b) for the SAC [27]. If the coefficient β_f is chosen to be sufficient small value, it can be considered as $G_a(s) \simeq G(s)$, and $y_a \simeq y$. From (6.35) and (6.36),

$$\dot{\boldsymbol{\xi}}_m = \begin{pmatrix} 0 & 1 \\ 0 & 0 \end{pmatrix} \boldsymbol{\xi}_m + \begin{pmatrix} 0 \\ 1 \end{pmatrix} v_m \quad , \quad y_m = (1 \quad 0)\, \boldsymbol{\xi}_m \, . \tag{6.66}$$

and put

$$v_m = \lambda_1(r_m - \xi_{m1}) - \lambda_2 \xi_{m2} \tag{6.67}$$

then

$$\dot{\boldsymbol{\xi}}_m = \begin{pmatrix} 0 & 1 \\ -\lambda_1 & -\lambda_2 \end{pmatrix} \boldsymbol{\xi}_m + \begin{pmatrix} 0 \\ \lambda_1 \end{pmatrix} r_m \, , \tag{6.68}$$

$$y_m = (1 \quad 0)\, \boldsymbol{\xi}_m \, . \tag{6.69}$$

The transfer function from r_m to y_m is expressed as

$$\frac{y_m}{r_m} = \frac{\omega_n^2}{s^2 + 2\zeta\omega_n s + \omega_n^2} \, . \tag{6.70}$$

where ζ is the damping factor and ω_n is the natural angular frequency, and λ_1 and λ_2 is determined as follows:

$$\begin{cases} \lambda_1 = \omega_n^2 \\ \lambda_2 = 2\zeta\omega_n \end{cases}$$

If $\zeta \geq 1$, then y_m has no overshoot, and ω_n controls the response of y_m.

Define the output error between the system and the reference model as $e_y = y_a - y_m$, and the input of the reference model as $r_m = \omega_{rRef}$, then the controller of the SAC is designed as follows:

$$v = K^T z + k_d \dot{e}_y \qquad (k_d < 0) \tag{6.71}$$

$$z^T = (e_y, \xi_m^T, r_m) \tag{6.72}$$

$$K^T = (k_e, k_\xi^T, k_r) \tag{6.73}$$

The adaptive gain K is determined as follows:

$$K = K_P + K_I \tag{6.74}$$

$$K_P = -\Gamma_p z e_y \tag{6.75}$$

$$\dot{K}_I = -\Gamma_I z e_y - \sigma K_I \tag{6.76}$$

$$\sigma = \sigma_1 e_y^2/(1 + e_y^2) + \sigma_2 \qquad (\sigma_1, \sigma_2 > 0) \tag{6.77}$$

The block diagram of the SAC is shown in Fig. 6.12.

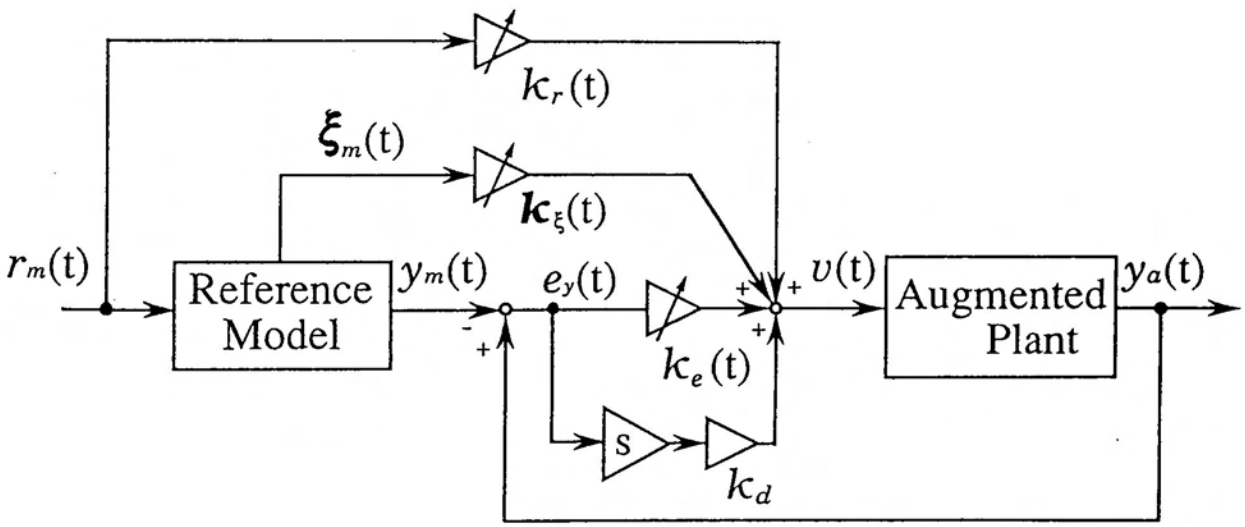

Fig. 6.12. Block diagram of the SAC.

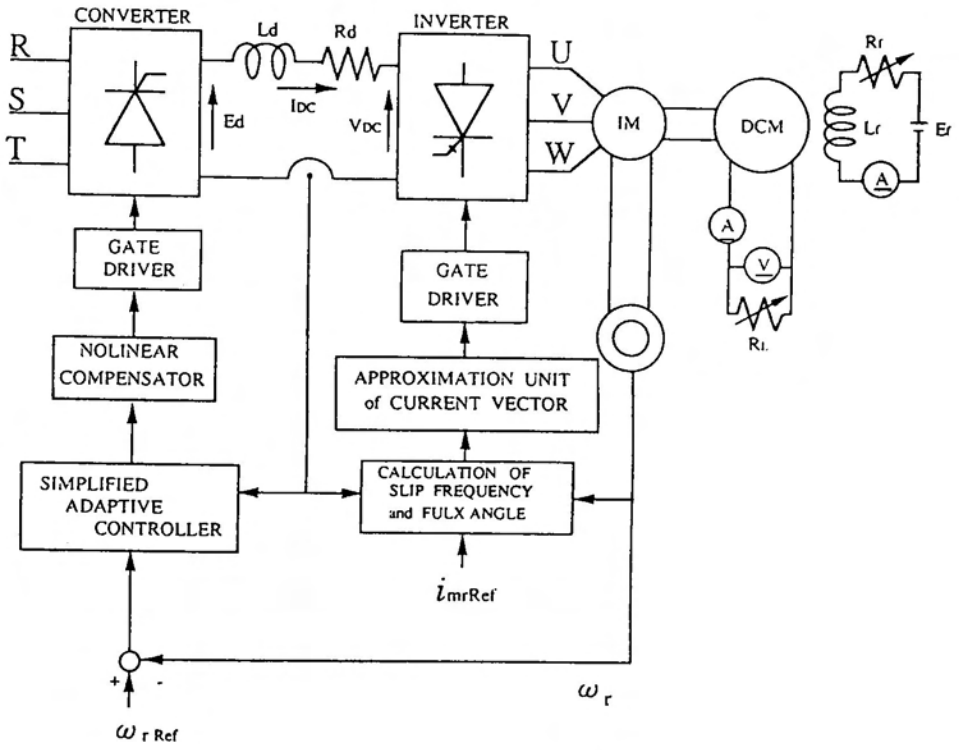

Fig. 6.13. Experimental system.

6.5.2 Verification of the SAC

Fig. 6.13 shows the experimental system. The speed controller consists of the SAC and the nonlinear compensator that is the state feedback (6.34). The firing angle for the converter is controlled by the reference input voltage calculated by the SAC. The inverter is controlled by the vector approximation method in Chapter 4.

This section shows the simulation and the experimental results to confirm the effectiveness of the proposed system. Fig. 6.14 shows the step tracking characteristics, where three conditions are tested, that is, ω_n are i): 10.0 (rad/sec), ii): 3.0 (rad/sec), and iii): 2.0 (rad/sec), respectively, at $\zeta = 1.0$. The output of reference model ξ_{m1} is indicated by the dashed line, and the actual rotor angular velocity ω_r is indicated by the solid line. The actual rotor angular velocity ω_r converges to ξ_{m1}. Next, the modelling error is assumed in (6.34), that is, u_{Ref} is defined as $u_{Ref} = a_e u$. The coefficient (a_e) indicates the modelling error. Fig. 6.15 and 6.16 show the step tracking characteristics when $a_e = 1.2$ and 0.8 in the

same condition with Fig. 6.14 i). These results show the robustness against the modelling error.

The step load regulation characteristics are shown in Fig. 6.17. The load torque has increased from 5.0 to 15.0 Nm. Fig. 6.17(a) and (b) show the responses of the rotor angular velocity using the PI speed controller and the SAC system respectively. The recovering time of the velocity in Fig. 6.17(b) was about 0.08 sec, while the velocity in Fig. 6.17(a) has not been recovered yet within 0.3 sec. Because the integral gain of the PI controller has been selected to relatively small value, the recovering time is so long. However, if the integral gain were increased in order to keep the fast recovering time, the overshoot at the step response would be large. These are confirmed in Figs. 6.18 and 6.19, where the speed controlled by the SAC is indicated by the dashed line and the speed controlled by the PI controller is indicated by the solid line.

Fig. 6.18 shows the simulation results when the integral gain of the PI controller is increased, the recovering time of speed controlled by the PI controller is reduced. In Fig. 6.19, however, as the step tracking characteristics is shown when the speed increases from 120 to 130 rpm, the overshoot of speed controlled by the PI controller becomes so large, even the overshoot is somewhat limited due to the current limiter. On the other hand, there is no overshoot when the SAC is applied. The usual PI controller could not be contented to realize no overshoot and the fast recovering time.

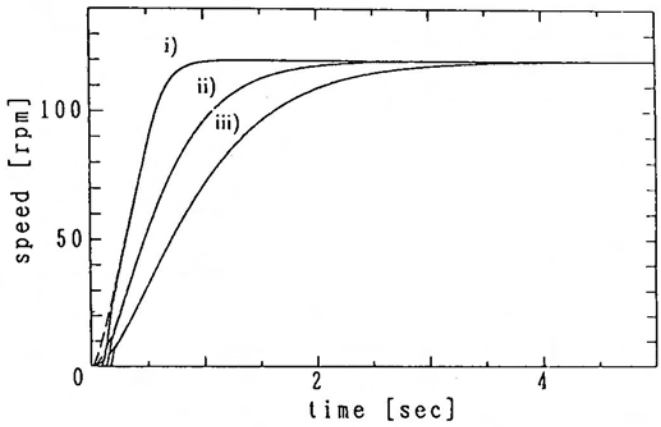

Fig. 6.14. Step tracking characteristics: ω_n i): 10 (rad/sec), ii): 3 (rad/sec), iii): 2 (rad/sec).

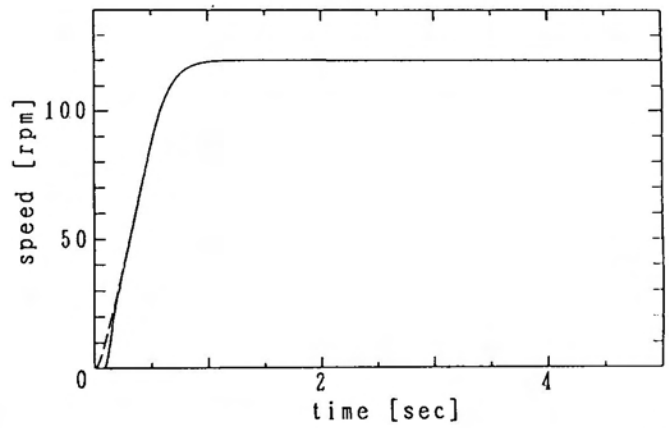

Fig. 6.15. Step tracking characteristics with the modelling error a_c=1.2.

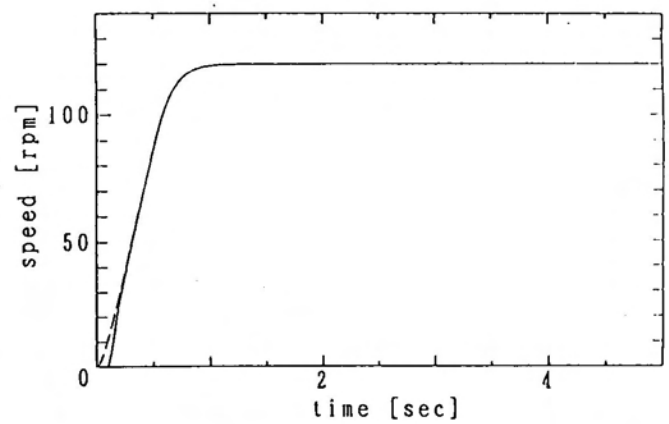

Fig. 6.16. Step tracking characteristics with the modelling error a_c=0.8.

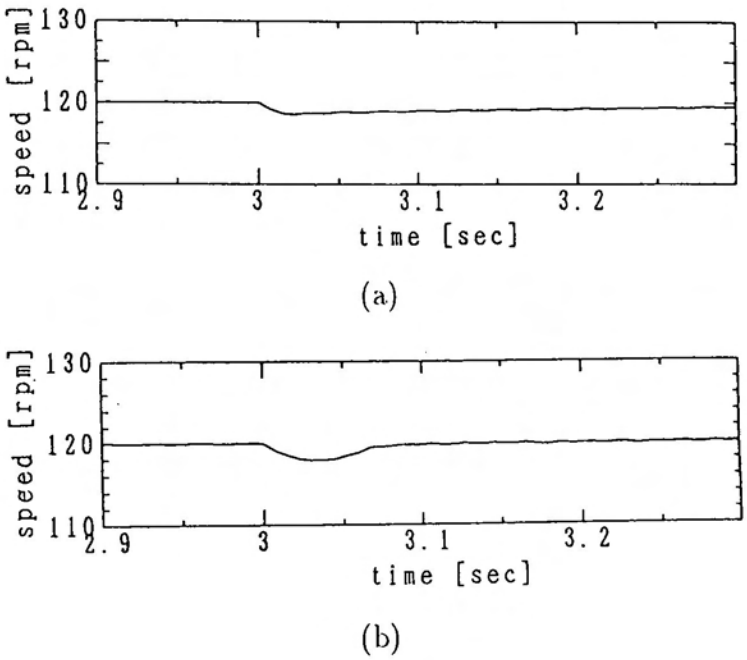

Fig. 6.17. Responses of the rotor angular speed at the sudden-load variation: (a) PI controller; (b) SAC.

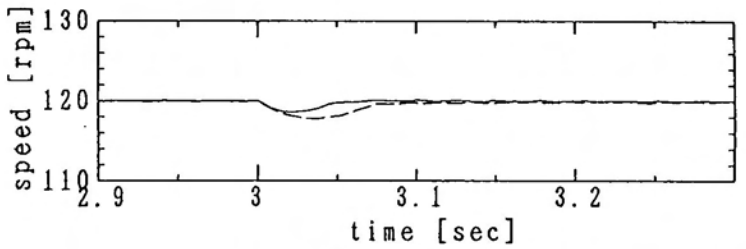

Fig. 6.18. Responses of the rotor angular speed at the sudden-load variation.

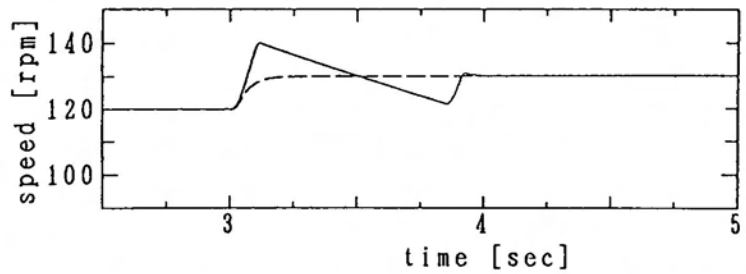

Fig. 6.19. Step tracking characteristics when the speed command increases from 120 to 130 rpm.

Figs. 6.20 and 6.21 show the experimental results, where the step tracking is achieved as the simulation. In the experiment, the control parameters are set as follows:

$$\begin{aligned}
\Gamma_P &= diag(0.2, 0.01, 0.01, 0.01), \\
\Gamma_I &= diag(2.88 \times 10^6, 577, 577, 577), \\
\sigma_1 &= 0.001, \quad \sigma_2 = 1.0 \times 10^{-7}, \\
\alpha_f &= 25, \quad \beta_f = 0.9 \times 10^{-4}, \quad k_d = -500
\end{aligned}$$

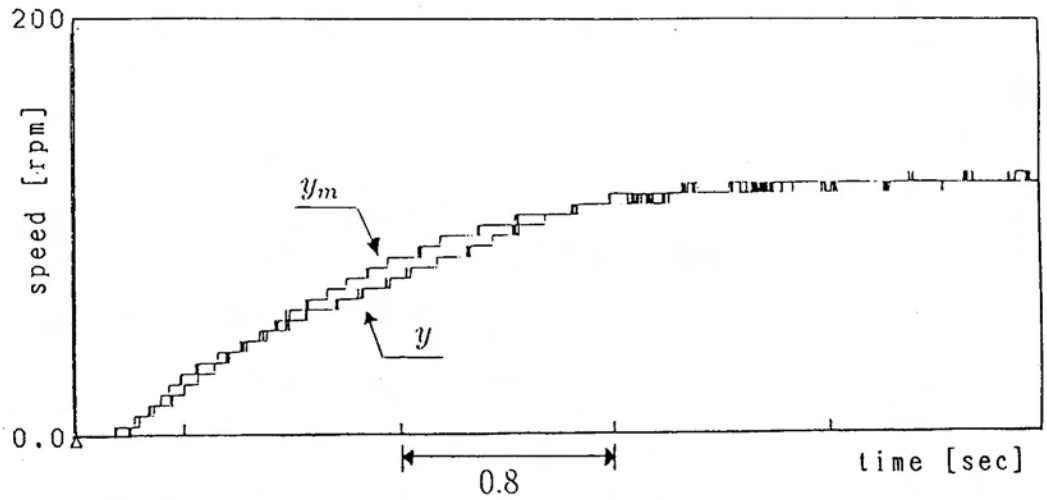

Fig. 6.20. Step tracking characteristics in the experiment: $\omega_n = 3$ (rad/sec).

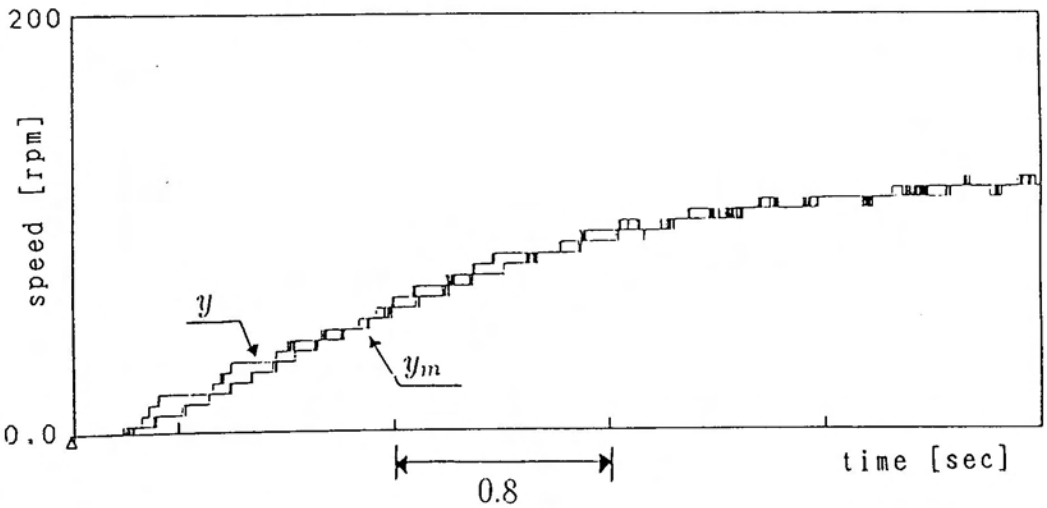

Fig. 6.21. Step tracking characteristics in the experiment: $\omega_n = 2$ (rad/sec).

With the real system, the dc link current must be limited during the transient condition for keeping the feature of the CSI as the protecting tendency for power semiconductor devices. In order to limit the dc link current, we set $u_{max} = K_{lim}(I_{DClim} - I_{DC})$ with $K_{lim} > 0$ and u is limited such that if $u > u_{max}$, then $u = u_{max}$, where K_{lim} is determined empirically.

6.6 Conclusion

For the robust control of speed, two different approaches, that is, the applications of the H_∞ control and the SAC with exact linearization have been shown in this chapter. When the operating point of the system deviates from the initial equilibrium point, the effectiveness of exact linearization could be confirmed obviously. The robustness nature of the system with the H_∞ controller and the SAC have been confirmed in the comparison with the PI controller by the simulation and the experimental results. The structure of the designed H_∞ controller is simpler than that of the designed SAC, but the SAC has wider allowable ranges of parameter changes than the H_∞ control.

Chapter 7

Conclusions

In this dissertation, the microcomputer–controlled CSI drive induction motor by vector approximation has been discussed in order to solve the problems in the field oriented control of ac machines. Such problems are unreliable assumptions of the ideal stator current, the constant parameters in the linear equivalent circuit, and so on.

Due to the semiconductor switching inverter, the torque pulsations occur because the stator current vector is not rotating smoothly, while the rotor magnetizing current is rotating smoothly. The vector approximation has been proposed in order to solve this problem.

On the other hand, in order to solve the parameter variation problems, the parameter adaptation has been proposed. Moreover, the robust speed control against the sudden-load change, the nonlinearity and modelling error of the system, has been proposed in this dissertation.

This dissertation is summarized as follows:

- In Chapter 2, the dynamic model of the induction machine using space vectors have been reviewed, and the mathematical model of the induction machine has been shown. The foundation of every control design is explained by the mathematical model of the plant.
- Chapter 3 has shown the principle of the field oriented control. In order to estimate the rotor flux, four kinds of flux estimation models have been reviewed, and after the

comparison of these models the best model has been selected.

- Chapter 4 has shown the vector approximation method. The principle and algorithm of the vector approximation have been described. The system configuration for the implement has been shown. The performance of vector approximation has been verified by the simulation and the experiments. It has been shown theoretically that the direct torque control would be possible by this method, and the torque ripple could be decreased.

- Chapter 5 has shown the parameter adaptation and torque control technique for CSI drive induction motor with the vector approximation. The parameter adaptation with the saturation model has been shown to estimate the rotor resistance and the torque correctly at each different flux level, by the simulations and the experiments. As mentioned in Section 3.2, the complete decoupled control of i_{sd} and i_{sq} of the stator currents like the separately excited dc machine is said to be difficult by the field oriented control in the CSI drive system. However, the direct torque control with the proposed method could force to realize the precise torque control, which would be effective as well as the decoupled control.

- Chapter 6 has shown the applications of robust control. Conventional linear control methods such as PI control have been widely used in industry electrical drives; however, dynamic performance of the control system is often limited due to the conflict between overshoot and long setting time of the system response. The conventional linear control methods have inadequate rejections against external disturbance as well as the sensitivity in performance to the system parameter variation and nonlinearity. Thus, robust stable drive systems are required for any applications. For the robust control of speed, the different approaches, that is, the H_∞ control and SAC with exact linearization have been shown in this chapter. The robustness of these systems compared with the PI control system have been verified by the simulation and the experiments. The structure of the designed H_∞ controller is simpler than that of the designed SAC, but the SAC has wider allowable ranges of parameter changes than the H_∞ control.

The proposed method in this dissertation are not so complicated to implement and are

adequate for the precise torque and speed control for medium and large-size drives with low speed.

References

[1] B. K. Bose, "Power Electronics & AC Drives," Englewood Cliffs, NJ: Prentice-Hall, 1986.

[2] T. Tsuji, J. Sakakibara and S. Naka, "CSI drive induction motor by vector approximation," *IEEE Trans. Ind. Applicat.*, vol. IA-27, no. 4, p. 715, July/Aug. 1991.

[3] S. Nonaka and Y. Neba, "New GTO current source inverter with pulsewidth modulation control techniques," *IEEE Trans. Ind. Applicat.*, vol. IA-22, no.4, p. 666, July/Aug. 1986.

[4] L. Walker and P. Espelager, "A high performance controlled current inverter drive," *IEEE Trans. Ind. Applicat.*, vol. IA-16, no.2, p. 193, Mar./Apr. 1980.

[5] W. Leonhard, "Control of Electrical Drives," Berlin: Springer-Verlag, 1985.

[6] C. Wang, D. W. Novotny and T. A. Lipo, "An automated rotor time constant measurement system for indirect field oriented drives," *IEEE Trans. Ind. Applicat.*, vol. IA- 24, no.1, p. 151, Jan./Feb. 1988.

[7] L. J. Garces, "Parameter adaption for the speed controlled static ac drive with a squirrel-cage induction motor," *IEEE Trans. Ind. Applicat.*, vol. IA-16, no.2, p. 173, Mar./Apr. 1980.

[8] R. D. Lorenz, D. B. Lawson, "A simplified approach to continuous on-line tuning of field-oriented induction machine drives," *IEEE Trans. Ind. Applicat.*, vol. IA-26, no. 3, p. 420, Mar./June 1990.

[9] H. Sugimoto and S. Tamai, "Secondary resistance identification of an induction-motor applied model reference adaptive system and its characteristics," *IEEE Trans. Ind. Applicat.*, vol. IA-23, no. 2, p. 296, Mar./Apr. 1987.

[10] F. M. H. Khater, R. D. Lorenz, D. W. Novotny and K. Tang, "Selection of flux level in field-oriented induction machine controllers with consideration of magnetic saturation effects," *IEEE Trans. Ind. Applicat.*, vol. IA-23, no. 2, p. 276, Mar./Apr. 1987.

[11] V. Vuckovic, N. Tesla, E. Levi and N. Sad, "Rotor flux calculator for saturated induction machines with field-oriented control," *in Proc. European Conf. Power Electron. and Applicat.*, EPE Aachen, Germany, 1989, p. 505.

[12] P. Vas and M. Alakula, "Field-oriented control of saturated induction machines," *IEEE Trans. Energy Conversion*, vol. 5, no. 1, p. 218, 1990.

[13] G. Heinemann and W. Leonhard, "Self-tuning field-oriented control of an induction motor drive," *in Proc. Int. Power Electron. Conf. IPEC* Tokyo, Japan, p. 465, 1990.

[14] P. Krause, "Method of multiple reference frames applied to the analysis of symmetrical induction machinery," *IEEE Trans. Power App. and Syst.*, vol. PAS-87, no. 1, p. 218, 1968.

[15] H. Sugimoto and S. Kawasaki, "Secondary resistance identification of induction motor based on MRAS with torque sensor," *Trans. IEE Japan*, vol. 111-D, no. 9, p. 802, 1991.

[16] I. D. Landau, "Adaptive control-The Model Reference Approach. New York: Marcel Dekker, 1979.

[17] C. Schauder, "Adaptive speed identification for vector control of induction motors without rotational transducers," *in Proc. IEEE Ind. Applicat. Annu. Meeting*, 1989, p. 493.

[18] D.Y. Ohm and J. R. Kimzey, "Rotor time constant adaptation method for induction motors using dc link power measurement," *in Proc. of IEEE Ind. Applicat. Annu. Meeting*, 1989, p. 588.

[19] E. P. Cornell and T. A. Lipo, "Modeling and design of controlled current induction motor drive systems," *IEEE Trans. Ind. Applicat.*, vol. IA-13, no. 4, p. 321, July/Aug. 1977.

[20] S. Nonaka and Y. Neba, "Quick regulation of sinusoidal output current in PWM converter-inverter system," *IEEE Trans. Ind. Applicat.*, vol. IA-27, no. 6, p. 1055, Nov./Dec. 1991.

[21] R. Su, "On the linear equivalents of nonlinear systems," *Syst. and Cont. Letters*, vol. 2, no. 1, p. 48, 1982.

[22] M. Sanpei, "Design method of state feedback and observer for nonlinear control systems," *Syst. Cont. and Informat.*, vol. 37, no. 4, p. 247, 1993.

[23] S. Hara, "Servo system design by H_∞ control," *Record of SICE Basic Tutorial Course*, Japan, 1992, p. 63.

[24] K. Glover and J. C. Doyle, "State-space formulae for all stabilizing controllers that satisfy an H_∞-norm bound and relations to risk sensitivity," *Syst. and Cont. Letters*, vol. 11, p. 167, 1988.

[25] Z. Iwai and I. Mizumoto, "Robust and simple adaptive control systems," *Int. J. Cont.*, vol. 55, no. 6, p. 167, 1992.

[26] K. Sobel, H. Kaufman and L. Mabius,"Implicit adaptive control for a class of MIMO systems," *IEEE Trans. Aerospace and Electron. Syst.*, vol. AES-18, no. 5, p. 576, 1982.

[27] I. Bar-Kana, "Global stability and performance of a simplified adaptive algorithm," *Int. J. Cont.*, vol. 42, no. 6, p. 1491, 1985.

[28] P. Vas, "Vector Control of AC Machines," , New York: Oxford University Press, 1990.

[29] T. Tsuji, K. Ide and A. Hirata, "Vector approximation and identification in CSI drive induction motor," *in Proc. Symp. Power Electron. Electric. Drives SPEEDAM*, Positano, Italy, 1992, vol. 1, p. 139.

[30] K. Ide, Z. G. Bai, Z. J. Yang and T. Tsuji, "Vector approximation with the secondary parameters compensation of IM," *in Proc. IEEE Power Electron. Special. Conf. PESC'94*, Taipei, Taiwan, 1992, vol. 1, p. 139.

[31] K. Ide, Z. G. Bai, Z. J. Yang and T. Tsuji, "Vector approximation method with parameter adaptation and torque control of CSI-fed induction motor," *in Proc. IEEE Ind. Applicat. Annu. Meeting*, 1994, vol. 1, p. 711.

[32] K. Ide, Z. G. Bai, Z. J. Yang and T. Tsuji, "Torque control of induction machine by vector approximation with parameter adaptation based on MRAS," *in Proc. Int. Conf. Ind. Electron. Cont. and Instru. IECON'94*, Bologna, Italy, 1994, vol. 1, p. 711.

[33] K. Ide, Z. G. Bai, Z. J. Yang and T. Tsuji, "Vector approximation method with parameter adaptation and torque control of CSI-fed induction motor," *IEEE Trans. Ind. Applicat.*, vol. 31, no. 4, p. 830, July/Aug. 1995.

[34] Z. G. Bai, K. Ide, Z. J. Yang and T. Tsuji, "H_∞ control with exact linearization for ac drive system with CSI," *in Proc. Asian Cont. Conf. ASCC*, Tokyo, Japan, 1994, vol. 2, p. 617.

[35] Z. G. Bai, K. Ide, Z. J. Yang and T. Tsuji, "H_∞ control with exact linearization for ac drive system with CSI," *Trans. IEE Japan*, vol. 114-D, no. 12, p. 1242, 1994.

[36] K. Ide, T. Tanaka, Z. J. Yang and T. Tsuji, "Simple adaptive control with exact linearization for CSI-fed induction motor," *in Proc. Int. Conf. Ind. Electron. Cont. and Instru. IECON'95*, Florida, USA, 1995, vol. 1, p. 317.